

Protein Profiling of Primary Human Samples for Pathway Analysis and Patient Stratification

Dissertation

der Mathematisch-Naturwissenschaftlichen Fakultät
der Eberhard Karls Universität Tübingen
zur Erlangung des Grades eines
Doktors der Naturwissenschaften
(Dr. rer. nat.)

vorgelegt von

M.Sc. Felix Günther Christian Schäfer-Ruoff
aus Tübingen

Tübingen

2022

Gedruckt mit Genehmigung der Mathematisch-Naturwissenschaftlichen Fakultät der Eberhard Karls Universität Tübingen.

Tag der mündlichen Qualifikation:

21.11.2022

Dekan:

Prof. Dr. Thilo Stehle

1. Berichterstatter/-in:

Prof. Dr. Katja Schenke-Layland

2. Berichterstatter/-in:

Prof. Dr. Dieter Stoll

Table of Contents

Abstract	I
Zusammenfassung	III
Abbreviations	V
List of Figures	VII
List of Publications	VIII
Contributions	XI
1 Introduction	1
1.1. Multiplexed Protein Analysis of Complex Human Samples	1
1.1.1. Microsphere Based Multiplexed Western Blotting – the DigiWest	3
1.1.2. Novel Data Analysis Tools for DigiWest	5
1.2. Protein Analysis of Primary Human Sample Material	6
1.2.1. Protein Analysis of Blood Samples	6
1.2.2. Protein Analysis of Formalin-Fixed and Paraffin-Embedded Tissue	9
1.2.3. Protein Analysis of Cryo-Preserved Tissue	11
1.3. Current Topics Requiring Multiplexed Protein Analysis in Biomedical Research	12
1.3.1. Serological Monitoring of SARS-CoV-2 Antibody Response	12
1.3.2. Treatment Alternatives for Cervical Intraepithelial Neoplasia	14
1.3.3. Stratification and Risk Assessment of Breast Cancer Patients	15
2 Objectives of the Thesis	21
3 Results I: Multiplexed Serum Antibody Screening	25
3.1. Detection of Serum Antibodies Utilizing DigiWest	26
3.2. Detecting Serum Antibodies Recognizing Different Human Coronaviridae	27
3.3. Evaluation of Assay Characteristics	28
3.4. Multiplexed Immunoglobulin Detection Against Different Coronaviridae	29
4 Results II: Multiplexed Protein Expression Analysis of Treated FFPE Tissue	33
4.1. Evaluation of Treatment Response Through Protein Analysis of Cervical Punch Biopsies after NIPP Treatment	34
4.2. Protein Expression Changes Following In Vivo and In Vitro NIPP Treatment	35
5 Results III: Protein Profiling of Fresh Frozen Breast Carcinomas	41
5.1. Quality Assessment of Enrolled Patient Samples	42
5.2. Targeted Protein Expression Analysis by DigiWest	43

5.2.1. Assessment of Immune Cell Infiltration by DigiWest for Patient Stratification	44
5.3. Detailed Protein Expression Evaluation of Hot and Cold Carcinomas	45
5.3.1. Increased Proliferative Activity and a More Competitive Phenotype is Observed in Hot Carcinomas	46
5.3.2. Hot Carcinomas Display Higher Apoptotic Activity and Expression of Tumour-Suppressive Markers	46
5.3.3. Cold Carcinomas Display Increased Expression of Immune-Suppressing Factors	47
6 General Discussion and Conclusion	51
6.1. Multiplexed Serum Antibody Screening by DigiWest	53
6.2. Treatment Evaluation by Protein Analysis of FFPE Fixed Samples	55
6.3. Protein Profiling of Fresh Frozen Resectates and Assessment of Immune Cell Infiltration	57
6.4. Conclusion	59
References	61
Acknowledgements	78
Declaration	79
Appendix	80

Abstract

In recent years, scientific progress has led to the advancement of precision medicine, a novel therapeutic strategy. For this purpose, molecular investigation of patient-derived samples is a necessity. Genetic analysis has been the gold standard in this field for years. However, in a cell, proteins and their posttranslational modifications lead to differences in genotype and phenotype. Therefore, the use of genetic information as basis for treatment decisions does not always translate into therapeutic benefits. The integration of proteomic approaches to further elucidate pathophysiological mechanisms is essential. Protein analysis methods need to be flexible to be used in different sample types and provide high sensitivity as well as throughput to complement these novel therapeutic approaches. The recently emerging DigiWest technology allows for detection of numerous proteins and protein variants from a single sample. Here, the DigiWest workflow was adapted and modified for protein analysis from clinically relevant sample types, such as formalin-fixed or fresh frozen tissue extracts and blood samples. A novel serum-screening platform was designed and established. Through the integration of authentic antigens, the parallel detection of immunoglobulins against different pathogenic strains of coronaviruses was achieved. Furthermore, multiplexed protein analysis from minuscule formalin-fixed and paraffin-embedded cervical punch biopsies by DigiWest was established. In vivo treatment effects of non-invasive-physical plasma, a novel therapeutic approach for treatment of cervical intraepithelial neoplasia, were evaluated and upon comparing results to in vitro cell culture experiments, general trends in treatment response could be confirmed. However, differences in protein expression profiles emphasize the need for molecular investigation of treatment effects in vivo. The potential of protein analysis of fresh frozen samples was explored by referencing snap frozen breast cancer biopsies. The multiplexed detection of several infiltrating immune cell markers by DigiWest as prognostic factor was established. A subset of co-expressed immune cell markers, revealing a positive influence on patient outcome was identified and induced changes in several pathways were detected. Overall, sample preparation, assay strategies

and analysis tools were adapted to the multiplexed protein analysis of different human sample types via DigiWest and the unique potential of this approach was demonstrated.

Zusammenfassung

In den letzten Jahren hat der wissenschaftliche Fortschritt zur Entwicklung der Präzisionsmedizin, eines neuen therapeutischen Ansatzes, geführt. Für diesen Ansatz ist eine molekulare Untersuchung von Patientenproben unabdingbar. Genetische Untersuchungen sind seit Jahren der Goldstandard in diesem Bereich. Jedoch führen Proteine und ihre posttranslationalen Modifizierungen zu Unterschieden im Genotyp und Phänotyp einer Zelle. Daher führt die Verwendung genetischer Informationen als Grundlage für Behandlungsentscheidungen nicht immer zu therapeutischen Erfolgen. Die Integration von proteomischen Ansätzen zur weiteren Aufklärung pathophysiologischer Mechanismen ist daher von wesentlicher Bedeutung. Die hierzu verwendeten Proteinanalysemethoden sollten flexibel in der Anwendung an verschiedenen Probenotypen sein und eine hohe Empfindlichkeit sowie einen hohen Durchsatz bieten, um diesen neuen therapeutischen Ansatz zu ergänzen. Die kürzlich entwickelte DigiWest-Technologie ermöglicht den parallelen Nachweis zahlreicher Proteine und Proteinvarianten aus einer einzigen Probe. In dieser Arbeit wurde der DigiWest-Arbeitsablauf für die Proteinanalyse aus klinisch relevanten Probenotypen, wie Formalin-fixierten oder frisch gefrorenen Gewebeextrakten sowie Blutproben, angepasst und modifiziert. Eine neuartige Serum-Screening-Plattform wurde entwickelt und etabliert. Durch die Integration authentischer Antigene wurde der multiplexe Nachweis von Immunglobulinen gegen verschiedene pathogene Stämme von Coronaviren erreicht. Darüber hinaus wurde eine multiplexe Proteinanalyse von kleinen Formalin-fixierten und paraffineingebetteten Stanzbiopsien des Gebärmutterhalses durch den DigiWest etabliert. Die in vivo Behandlungseffekte von nicht-invasivem physikalischem Plasma, einem neuartigen therapeutischen Ansatz zur Behandlung der intraepithelialen Neoplasie des Gebärmutterhalses, wurden ausgewertet, und beim Vergleich der Ergebnisse mit in vitro Zellkulturexperimenten konnten allgemeine Trends beim Ansprechen auf die Behandlung bestätigt werden. Die Unterschiede in den Proteinexpressionsprofilen zwischen Gewebeproben und Zellkultur unterstreichen jedoch die Notwendigkeit einer molekularen Untersuchung der Behandlungs-

effekte in vivo. Das Potenzial der Proteinanalyse von frisch gefrorenen Proben wurde anhand von Brustkrebsresektaten untersucht. Der multiplexe Nachweis mehrerer infiltrierender Immunzellmarker durch den DigiWest wurde etabliert. Dadurch konnte eine Untergruppe von ko-exprimierten Immunzellmarkern identifiziert werden, die einen positiven Einfluss auf das ereignisfreie Überleben haben, sowie induzierte Veränderungen in mehreren Signalwegen festgestellt werden. Insgesamt wurden die Probenvorbereitung, Assay-Strategien und Analysewerkzeuge an die Multiplex-Proteinanalyse verschiedener menschlicher Probentypen mittels DigiWest angepasst. Somit konnte das besondere Potenzial dieses Ansatzes gezeigt werden.

Abbreviations

ADE	antibody-dependent enhancement
AFI	average fluorescents intensity
Akt	protein kinase B
CD	cluster of differentiation
CDK	cyclin-dependent kinase
CI	confidence interval
CIN	cervical intraepithelial neoplasia
CK	cytokeratin
c-RAF	RAF proto-oncogene serine/threonine- protein kinase
CSCC	cervical squamous cell carcinoma-derived cell line
DC	dendritic cell
DC1	myeloid dendritic cells
DC2	plasmacytoid dendritic cells
DCIS	ductal carcinoma in situ
E	envelope-protein
EDTA	ethylenediaminetetraacetic acid
EFS	event-free survival
ELISA	enzyme-linked immunosorbent assay
ER	estrogen receptor
FFPE	formalin-fixed and paraffin-embedded
FoxP3	forkhead-box-protein P3
H&E	haematoxylin and eosin
hCoV	human infecting coronavirus
Her2	human epidermal growth factor receptor 2
HF	high frequency
HIAR	heat induced antigen retrieval
HSIL	high-grade squamous intraepithelial lesions
IDC	invasive ductal carcinoma
IHC	immunohistochemistry
Jak	janus kinase
LSIL	low-grade squamous intraepithelial lesions
M	membrane-protein
M1	classically activated macrophages
M2	alternatively activated macrophages
mAb	monoclonal antibody
MAPK	mitogen-activated protein kinase
MEK1	dual specificity mitogen- activated protein kinase kinase 1
MOB1	DBF2 kinase activator protein
MS	mass spectrometry
N	nucleocapsid-protein
N1	N1 phenotypical neutrophils
N2	N2 phenotypical neutrophils
NIPP	non-invasive physical plasma

NK	natural killer cells
NKT	natural t-killer cells
OCT	optimal cutting temperature compound
p21	cyclin dependent kinase inhibitor 1
p38	p38 mitogen-activated protein kinases
PCR	polymerase chain reaction
PD1	programmed cell death 1 protein
PE	phycoerythrin
PI3K	phosphoinositid-3-Kinase
PPAR γ	Peroxisome proliferator-activated receptor gamma
PR	progesterone receptor
PTM	posttranslational modification
PVDF	polyvinylidene fluoride
RBD	receptor-binding domain
RNS	reactive nitrogen species
ROS	reactive oxygen species
RPPA	reverse phase protein array
S	spike glycoprotein
SARS-CoV	severe acute respiratory syndrome corona virus
SDS-PAGE	sodium dodecyl sulfate polyacrylamide gel electrophoresis
Src	proto-oncogene tyrosine-protein kinase Src
STAT	signal transducer and activator of transcription
Th2	Th2 t-helper cells
Th17	Th17 t-helper cells
TIL	tumour-infiltrating lymphocytes
TIME	tumour immune microenvironment
TME	tumor microenvironment
TNBC	triple-negative breast cancer
Treg	regulatory t-cell
Wnt	proto-oncogene int-1 homolog
α -CoV	alpha-coronavirus
β -CoV	beta-coronavirus

List of Figures

Figure 1. Experimental design and workflow of DigiWest experiments.	4
Figure 2. Schematic overview of direct binding and competitive immunoassays.	9
Figure 3. Chemical reaction of protein crosslinking through formaldehyde.	10
Figure 4. Schematic representation of the structure of coronaviridae.	13
Figure 5. Overview of breast cancer molecular subtypes and treatment options.	15
Figure 6. Schematic overview of breast cancer infiltrating immune cells and their contribution to tumor development.	17
Figure 7. Schematic overview of the developed serum-screening assay.	26
Figure 8. Schematic illustration of non-invasive physical plasma application and overview of the expression analysis workflow.	34
Figure 9. Schematic illustration of study workflow.	42

List of Publications

Accepted Manuscripts

1. Simon Fink*, **Felix Ruoff***, Aaron Stahl, Matthias Becker, Philipp Kaiser, Bjoern Traenkle, Daniel Junker, Frank Weise, Natalia Ruetalo, Sebastian Hörber, Andreas Peter, Annika Nelde, Juliane Walz, Gérard Krause, Armin Baillot, Katja Schenke-Layland, Thomas O. Joos, Ulrich Rothbauer, Nicole Schneiderhan-Marra, Michael Schindler, and Markus F. Templin. *Multiplexed Serum Antibody Screening Platform Using Virus Extracts from Endemic Coronaviridae and SARS-CoV-2*. ACS Infectious Diseases; 7, (6), 1596-1606 (2021).

<https://doi.org/10.1021/acsinfecdis.0c00725>

*authors contributed equally

2. **Felix Ruoff**, Melanie Henes, Markus F. Templin, Markus Enderle, Hans Bösmüller, Diethelm Wallwiener, Sara Y. Brucker, Katja Schenke-Layland, and Martin Weiss. *Targeted Protein Profiling of In Vivo NIPP-Treated Tissues Using DigiWest Technology*. Applied Sciences; 11, (23), 11238 (2021).

<https://doi.org/10.3390/app112311238>

3. Natalia Ruetalo, Ramona Businger, Karina Althaus, Simon Fink, **Felix Ruoff**, Michaela Pogoda, Angelika Iftner, Tina Ganzenmüller, Klaus Hamprecht, Bertram Flehmig, Tamam Bakchoul, Markus F. Templin, and Michael Schindler. *Antibody Response against SARS-CoV-2 and Seasonal Coronaviruses in Nonhospitalized COVID-19 Patients*. mSphere; 6, (1), 2379-5042 (2021).

<https://doi.org/10.1128/mSphere.01145-20>

4. Matthias Becker, Monika Strengert, Daniel Junker, Philipp D. Kaiser, Tobias Kerrinnes, Bjoern Traenkle, Heiko Dinter, Julia Häring, Stéphane Ghozzi, Anne Zeck, Frank Weise, Andreas Peter, Sebastian Hörber, Simon Fink, **Felix Ruoff**, Alex Dulovic, Tamam Bakchoul, Armin Baillot, Stefan Lohse, Markus Cornberg, Thomas Illig, Jens Gottlieb, Sigrun Smola, André Karch, Klaus Berger, Hans-Georg Rammensee, Katja Schenke-Layland, Annika Nelde, Melanie Märklin, Jonas S. Heitmann, Juliane S. Walz, Markus F. Templin, Thomas O. Joos, Ulrich Rothbauer, Gérard Krause and Nicole Schneiderhan-Marra. *Exploring Beyond Clinical Routine SARS-CoV-2 Serology Using MultiCoV-Ab to Evaluate Endemic Coronavirus Cross-Reactivity*. Nature Communications; 12, 1152 (2021).
<https://doi.org/10.1038/s41467-021-20973-3>

5. Julia Marzi*, Matthias B. Stope*, Melanie Henes, André Koch, Thomas Wenzel, Myriam Holl, Shannon L. Layland, Felix Neis, Hans Bösmüller, **Felix Ruoff**, Markus F. Templin, Bernhard Krämer, Annette Staebler, Jakob Barz, Daniel A. Carvajal Berrio, Markus Enderle, Peter M. Loskill, Sara Y. Brucker, Katja Schenke-Layland, and Martin Weiss. *Noninvasive Physical Plasma as Innovative and Tissue-Preserving Therapy for Women Positive for Cervical Intraepithelial Neoplasia*. Cancers; 14, (8), 1933 (2022).
<https://doi.org/10.3390/cancers14081933>

*authors contributed equally

6. Myriam Holl, Marie-Lena Rasch, Lucas Becker, Anna-Lena Keller, Laura Schultze-Rhonhof, **Felix Ruoff**, Markus Templin, Silke Keller, Felix Neis, Franziska Keßler, Jürgen Andress, Cornelia Bachmann, Bernhard Krämer, Katja Schenke-Layland, Sara Y. Brucker, Julia Marzi, and Martin Weiss. *Cell Type-Specific Anti-Adhesion Properties of Peritoneal Cell Treatment with Plasma-Activated Media (PAM)*. Biomedicines; 10, (4), 927 (2022).
<https://doi.org/10.3390/biomedicines10040927>

7. **Felix Ruoff**, Nicolas Kersten, Nicole Anderle, Sandra Jerbi, Aaron Stahl, André Koch, Annette Staebler, Andreas Hartkopf, Sara Y. Brucker, Markus Hahn, Katja Schenke-Layland, Christian Schmees, and Markus F. Templin. *Protein Profiling of Breast Carcinomas Reveals Expression of Immune-Suppressive Factors and Signatures Relevant for Patient Outcome*. *Cancers*; 14, (8), 4542 (2022).

<https://doi.org/10.3390/cancers14184542>.

8. Cécile Cumin, Yen-Lin Huang, Charlotte Rossdam, **Felix Ruoff**, Susana Posada Céspedes, Ching-Yeu Liang, Flavio C. Lombardo, Ricardo Coelho, Natalie Rimmer, Martina Konantz, Mónica Núñez López, Shahidul Alam, Alexander Schmidt, Diego Calabrese, Andre Fedier, Tatjana Vlajnic, Mark von Itzstein, Markus F. Templin, Falk F. R. Buettner, Arun Everest-Dass, Viola Heinzelmann-Schwarz, and Francis Jacob. *Glycosphingolipids are Mediators of Cancer Plasticity Through Independent Signaling Pathways*. *Cell Reports*; 40, (7), 111181 (2022).

<https://doi.org/10.1016/j.celrep.2022.111181>

9. Jeanesse Scerri, Christian Scerri, **Felix Schäfer-Ruoff**, Simon Fink, Markus F. Templin, and Godfrey Grech. *PKC-Mediated Phosphorylation and Activation of the MEK/ERK Pathway as a Mechanism of Acquired Trastuzumab Resistance in HER2-Positive Breast Cancer*. *Frontiers in Endocrinology*; 13:1010092 (2022).

<https://doi.org/10.3389/fendo.2022.1010092>.

Contributions

No.	Accepted	Number of authors	Postion of the candidate in the list of author	Scientific ideas by candidate (%)	Data generation by candidate (%)	Intepretation and analysis by candidate (%)	Paper writing by candidate (%)
1	yes	21	1*	25	40	25	25
2	yes	9	1	45	75	65	45
3	yes	36	15	5	5	5	3
4	yes	13	5	5	10	10	5
5	yes	21	8	5	10	5	5
6	yes	20	6	10	15	15	5
7	yes	13	1	50	60	65	45
8	yes	22	4	5	5	5	5
9	yes	6	3	10	10	20	10

*authors contributed equally

Chapter 1

Introduction

1 Introduction

1.1. Multiplexed Protein Analysis of Complex Human Samples

In recent years, scientific progress has elucidated the molecular mechanism of many pathological processes and diseases, laying the foundation for precision medicine, a novel therapeutic strategy ^{1,2}. Yet practical implementation of precision medicine is still at the very beginning. Clinical studies mostly focus on genome-based strategies ^{3,4} where somatic and genetic alterations are identified by applying advanced technologies like next generation sequencing, in an approach termed “genomic-precision medicine” ⁵. Numerous mutations are recognizable, but knowledge about this genetic information frequently does not translate into a therapeutic benefit ⁶, a discrepancy essentially attributable to the difference of genotype and phenotype. Through post-translational control and modification of proteins, altered genes do not always have an impact on cellular mechanisms. It has been shown that changes in genetic information poorly translate into changes in protein expression ^{7,8}. Thus, to understand pathological processes and their pathophysiological origins, it is crucial to integrate proteomic approaches as well. For this purpose, extensive data on abundance as well as modifications of proteins in human cells are needed. Given the fact that they provide high throughput and good sensitivity, modern protein analysis methods hold great potential to enhance these stratified therapeutic approaches.

Modern immunological or genetic examination of human material allows for identification of pathological processes. Yet histopathological examination is still the gold standard for investigation of clinical specimen. Besides histological approaches, novel analysis methods gain more and more importance in diagnosis, choice of therapy and monitoring of therapeutic effects on a molecular basis. Global analysis techniques like next generation sequencing or protein identification by mass spectrometry (MS) enable elucidation of pathophysiological mechanisms and the understanding of pathological interrelationships ⁹.

Post-translationally modified proteins are key components of cellular signal transduction ¹⁰. They represent the phenotypical and pathological features of

malignant cells in particular, and many diseases are characterized by specifically altered protein expression profiles ^{11,12}.

Therefore, the detection and quantification of such posttranslational modifications from human sample material is of great interest. Classical protein detection methods such as enzyme-linked immunosorbent assay (ELISA) and Western blotting are limited in terms of throughput and sensitivity. Mass spectrometry approaches allow for detailed analysis of large amounts of proteins, however, the high amount of sample needed to identify protein modifications and the overwhelming amount of data generated has made it difficult to translate this technique into clinical applications ¹³. To date, it has been used in several case studies only ^{14,15}.

Multiplexed immunoassays for parallel detection of numerous proteins from a single specimen have become a valuable tool in biomedical research and clinical trials. The parallel detection of several hundred proteins is extremely time and cost efficient. In addition, such assays require less sample material, which can be crucial in a clinical setting ¹⁶. Miniaturized and parallelized array based immunoassay systems, like reverse phase protein microarrays (RPPA), are able to sensitively identify hundreds of proteins and protein modifications from minuscule amounts of sample material. Here, proteins are spotted onto microchips and subsequent reverse phase immuno-detection allows for identification of protein expression in large patient cohorts as well as for comprehensive analysis of signal transduction ^{9,17}. However, crucial information about the molecular weight properties of analytes is lost.

The DigiWest technology, a recently emerging protein analysis method ¹⁸, allows for identification of numerous proteins and protein variants from minimal sample amount as well. It is possible to identify and semi-quantitatively analyse hundreds of proteins in one sample in a parallelized and reproducible manner. This approach yields the potential for multiplexed investigation of changes in intracellular signal transduction, which therefore exemplifies an excellent tool for the analysis of human derived specimen. However, the complexity of multiplexed immunoassays and diverse sample types that have to be analysed in biomedical applications, make consideration of pre-analytical requirements as well as extensive validation and testing of analytical performance a necessity to secure accuracy and reliability of results ^{16,19}.

1.1.1. Microsphere Based Multiplexed Western Blotting – the DigiWest

The complexity of challenges in life sciences is ever increasing, hence demands on assay systems are as well, making high-throughput and multiplexed assessment of parameters more crucial than ever. The DigiWest, a high throughput multiplexed variant of the Western blot, was invented and patented by the assay development department at the NMI in Reutlingen ¹⁸. Since its publication in 2016, it has been constantly improved and used in a multitude of applications ²⁰⁻²³.

In general, the DigiWest procedure is separated in two main segments, namely the sample preparation that includes the coupling of proteins on microspheres (Figure 1, 1-6) and the immunoassay itself (Figure 1, 7-9). For coupling of proteins, lysates are separated by applying sodium dodecyl sulfate polyacrylamide gel electrophoreses (SDS-PAGE) and blotted onto a polyvinylidene fluoride (PVDF) membrane. To enable coupling of the proteins on microspheres, the proteins are biotinylated on the membrane. Subsequently the sample is fractionated by cutting the protein lanes into 96 horizontal strips, where each strip constitutes for a distinct molecular weight fraction of the original blot. After cutting, proteins are eluted into a 96-well plate with membrane strips sorted from highest to lowest molecular weight. Therefore, each well only contains a defined molecular weight fraction of the original sample. The biotinylated proteins are then coupled onto neutravidin-coated color-coded microspheres, with each molecular weight fraction represented by a specific microsphere ID. To recreate the original western blot lane, all microspheres are pooled. For antibody-based protein detection, an aliquot of the microsphere mix is incubated with an antibody specific to a protein of interest, followed by incubation with a phycoerythrin- (PE-) labelled species-specific secondary antibody. Finally, readout is performed by utilizing a Luminex Flexmap 3D.

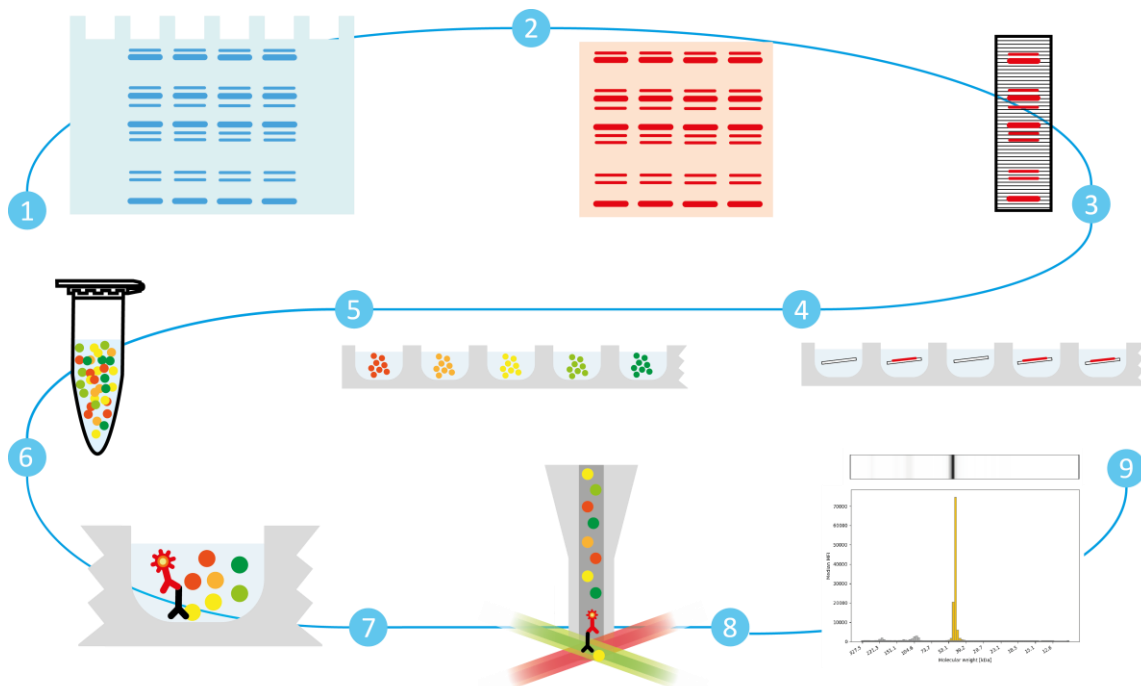


Figure 1. Experimental design and workflow of DigiWest experiments. Schematically depiction of the DigiWest workflow. Proteins are separated via SDS-PAGE (1) and transferred onto a PVDF membrane (2). Protein lanes are cut into 96 strips corresponding to 96 molecular weight fractions (3). Membrane strips are sorted into a 96 well plate according to the molecular weight and proteins are eluted (4). Biotinylated proteins are coupled onto distinct neutravidin-coated magnetic microspheres (5) and subsequently pooled to recreate the original protein lane (6). A small aliquot of the microsphere pool is used for the immunoassay and incubated with an analyte-specific primary antibody before incubation with PE-labeled species specific secondary antibody (7). The readout is performed utilizing a Luminex FlexMap 3D (8). The initial lane is reconstituted, and data analysis is performed (9) (adapted from Treindl et al. ¹⁸).

By transferring proteins onto a microsphere-based microarray platform, the robustness of Western blotting and the high-throughput as well as the multiplexing capabilities of microsphere-based assay systems are combined. Due to the miniaturization of the assay system, sensitivity as well as the dynamic range are increased ²⁴. This leads to reduced amount of sample being required for parallel detection of hundreds of proteins and protein variants (e.g. phosphorylated proteins), while maintaining information about the molecular weight properties. For that reason, the DigiWest is a valid alternative to RPPA or MS-based approaches, especially for the analysis of primary human material, where phosphoproteomics and limitation of sample material are of high concern.

1.1.2. Novel Data Analysis Tools for DigiWest

The ever-increasing amount and complexity of data in biomedical research also requires improvement of analytical and evaluation tools. Over the last decade several analysis programs and algorithms have been developed and upgraded, that enable the development of multi-omics pipelines, meta-analysis workflows and comprehensive databases ²⁵.

The established approach of DigiWest analysis originally is an Excel-macro-based data evaluation. The generated fluorescent signals for each molecular weight fragment are plotted against the calculated molecular weight of this fragment, resulting in a chromatogram-like depiction of peak signals ¹⁸. By integrating the area under the peak, a semi-quantitative value is generated for each peak of interest. However, due to the inherent nature of the analysis template only up to four samples of one microsphere mix can be analysed in the original template. For every additional sample mix, a new template must be generated and analysed separately. Additionally, sorting of raw output data and information about used antibodies by hand is time-consuming and may lead to unnoticed errors. Hence, the Excel-based analysis is a bottleneck for DigiWest studies, especially when large sample numbers are concerned as is often the case for biomedical investigations. Therefore, an automated integrative analysis tool for DigiWest-derived data that can process hundreds of samples and analytes simultaneously is of real need. Vital requirements for an analysis and evaluation pipeline are the automation of the most time consuming steps in DigiWest analysis, while maintaining full surveillance by the user. Key features of an analysis tool must include a unified analysis of multiple samples, improved efficiency and reproducibility, modular adaption of analysis designs and, most importantly, a unified data structure for export. Additionally, the integrative data analysis of DigiWest output and additional meta-data should be implemented. Therefore, routinely executed data evaluation steps like normalisation, cluster-analysis, differential expression, pathway enrichment and meta-data analysis (e.g. feature enrichment or survival analysis), that are conventionally executed with several external software programs, should be integrated and automated. Challenges for this type of analysis package are the combination and evaluation of structured

data (e.g. omics-data) and unstructured-data (medical imaging, economic factors, and clinical features). The importance of the interface of generated omics-data, databases and meta-data is ever increasing. Hence, generated output must be unified and has to support a common data structure to enable access, understanding and utilization by the scientific community ²⁶. Therefore, it is essential that the generated data format of a novel analysis and evaluation pipeline is commonly available and accessible. To accomplish this a software pipeline improving analysis and evaluation of DigiWest results was designed and developed. However, integration and extensive testing of the software pipeline is still ongoing and a publication of this work is in preparation ²⁷.

1.2. Protein Analysis of Primary Human Sample Material

The most relevant source of information for investigation and detection of pathological processes, as well as for therapeutic decisions are human tissue extracts and bio fluids. Over the last decades, multiple methods of sample preservation as well as protein extraction and analysis have been developed, each tailored towards specific sample types to answer various biomedical questions.

1.2.1. Protein Analysis of Blood Samples

Liquid biological samples, such as blood samples or cerebrospinal fluids are an important sample type for biomedical investigations. Blood samples are the favourable specimen in cases where sample collection has to be performed frequently. This is due to the lowly invasive extraction form and sample handling, compared to extraction of cerebrospinal fluids, tissue biopsies or resectates. In general, blood is investigated either in form of plasma or serum and is a suitable representation of the global biochemistry at the time of sample extraction ^{28,29}.

Blood consists of cellular components, such as erythrocytes, leucocytes and thrombocytes, as well as plasma. On the one hand, the cellular components, also called haematocrit, represent approximately 45% of the total volume, whereas the rest is composed of liquid intercellular substances. Plasma on the other hand consists of app. 90% water; the rest is composed of app. 7% proteins and 2% electrolytes (Na⁺, Cl⁻, K, Ca²⁺, Mg²⁺, bicarbonate, phosphate), nutrients (e.g.

glucose, lipids), organic acids (lactate, pyruvate, citrate, ketone), metabolic products (e.g. creatinine, urea) and hormones respectively signal molecules ³⁰. The most abundant proteins are albumin and α 1-, α 2-, β -, γ -globulin. The γ -globulins, also called immunoglobulins or antibodies are the most prominent representatives of the globulin protein family ^{31,32}. Another notable plasma protein is the coagulant fibrinogen. Fibrinogen is cleaved by thrombin to form fibrin, a crucial factor for coagulation ³³. Through coagulation, plasma is transformed into serum. For analytical purposes, serum is commonly prepared by centrifuging the coagulated blood, after resting the sample for 1 hour and collecting the supernatant above the clot ^{34,35}. Coagulation can be blocked for analytical purposes by adding clotting-preventing agents also called anticoagulants, with citrate, heparin or ethylenediaminetetraacetic acid (EDTA) most frequently used. By centrifugation, the cellular components are separated from the lighter liquid components. In contrast to serum samples, the supernatant of plasma samples additionally contains fibrinogen and other coagulation factors.

In terms of bioanalytical investigations, serum and plasma are practically identical ²⁸. However, some differences can occur in protein concentrations, enzyme activity and other components, mainly attributable to differences in handling and processing before and during centrifugation ³⁶. Overall, total protein concentration in serum samples is lower than in plasma samples ³⁷⁻³⁹. Proteins necessary for clotting, such as glucose and fibrinogen are reduced in serum samples, whereas substances that are released during coagulation, such as lactate and phosphate are increased. Plasma extraction is much faster and it more accurately represents the physiological situation. However, it contains anticoagulant agents, which may interfere with different analytical methods. For example, heparin forms a complex with antithrombin which binds and suppresses proteolytic degradation of clotting factors. It also binds positively charged troponin and reduces antigenicity for some antibodies against troponin, thus limiting the use of heparinized blood for troponin detection ⁴⁰.

Additionally, some protein biomarkers appear to be differently concentrated in serum or plasma samples depending on the characteristics of the proteins. For example vascular endothelial growth factor A, epidermal growth factor, vascular cell adhesion molecule 1 and resistin are higher concentrated in serum samples, whereas matrix metalloproteinase 1 is higher concentrated in plasma samples ⁴¹.

Therefore, serum and plasma samples cannot always be used interchangeably and the differences in sample matrices should be contemplated in preanalytical considerations. Examination of pre-analytical influences on biomarker assays is crucial, especially when incorporated into large clinical investigations, where differences in sample handling and processing can directly affect results of an ongoing study.

An important type of protein biomarkers in blood samples are immunoglobulins (IgG, IgA, IgM, IgE, IgD). Immunoglobulins are an ideal analytical reagent, since a single diagnostic principle, the antigen-antibody reaction, can be used for a multitude of assays. Thus, immunoglobulins can be utilized to monitor a variety of disease and help to support diagnosis, for instance autoimmune disorders by measuring autoantibodies ⁴², or infectious diseases by measuring the frequency of specific antibodies against pathogens in a population, also called seroprevalence ⁴³. The concentration of immunoglobulins (e.g. IgG, IgM and IgA) is higher in serum than in uncoagulated samples. However, this difference seems to have no influence on the detection of antibodies in serum or plasma samples and thus can be used interchangeably for the detection of immunoglobulins ⁴¹. Immunoglobulins are most commonly detected by direct binding assays or competitive binding assays. For the former, antigens are immobilized on a solid phase in form of peptides or whole proteins and a labelled species-specific secondary antibody detects binding of antigen specific immunoglobulins (Figure 2a).

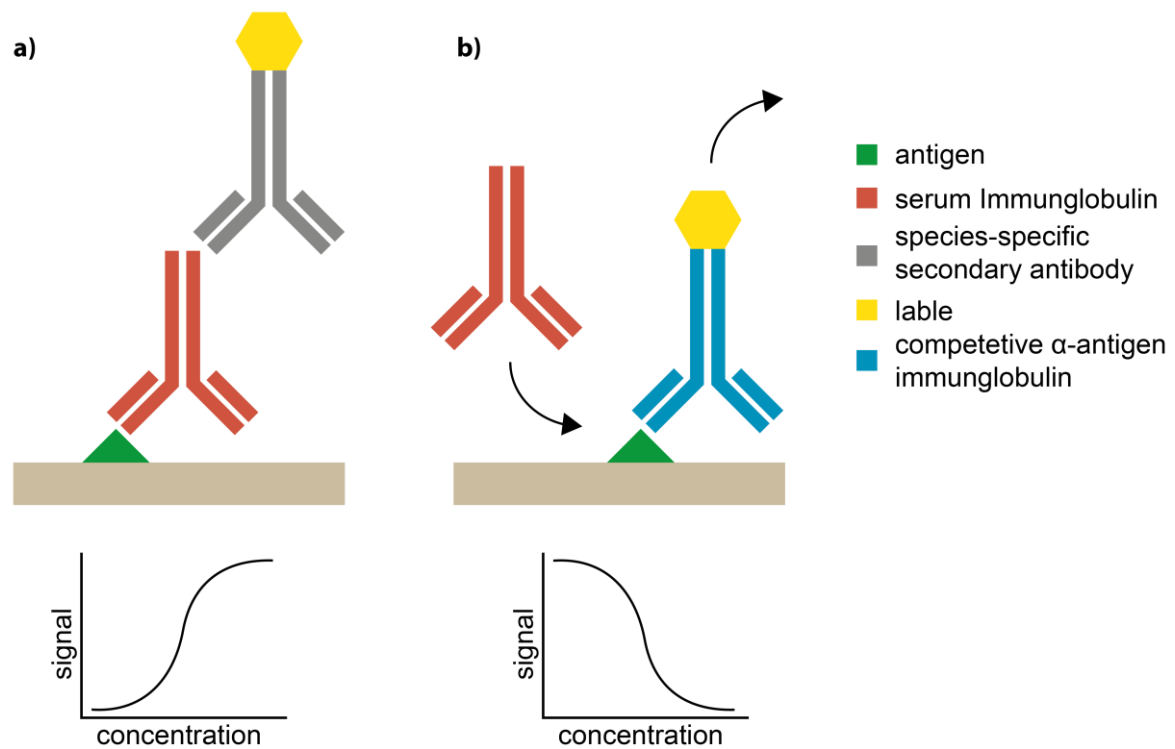


Figure 2. Schematic overview of direct binding and competitive immunoassays. In direct binding assays binding of target immunoglobulins to immobilized antigens are detected by a labelled secondary antibody. Detected signal is proportional to the concentration of immunoglobulins in the sample (a). In competitive assays labelled antibodies are replaced with competing immunoglobulins in the sample. The detected signal is reciprocal to the concentration of immunoglobulins in the sample (b).

For this purpose, antigens can be produced in recombinant form or isolated from authentic pathogens. In this assay format, the generated signal is proportional to immunoglobulins present in the sample. In competition assays (Figure 2b), the binding of a labelled immunoglobulin to the target protein in presence of competing serum antibodies is detected. Therefore, generated signal is reciprocal to the number of present immunoglobulins in the sample.

1.2.2. Protein Analysis of Formalin-Fixed and Paraffin-Embedded Tissue

For tissue extracts, the most important preservation methods are cryo-preservation and formalin-fixation. Despite being ideal for research purposes, fresh-frozen tissue is not always available and for clinical investigation, histological approaches are still the gold standard. For histological examination, it is crucial that the morphological structure of the tissue is conserved. To ensure this,

collected samples are routinely fixed in formalin. For subsequent preparation of histological slides, the tissue is also embedded in paraffin wax. Samples prepared in this fashion can be stored long-term, even at room temperature without protein degradation^{44,45}. Hence, formalin-fixed and paraffin-embedded (FFPE) samples, attached with meta-data, are widely available and are a valuable resource for prospective as well as retrospective biomedical studies⁴⁶⁻⁴⁸.

Formalin consists of 37-40% (w/w) formaldehyde and 10% methanol as a stabilizer in water⁴⁹. Amino acids react with the formaldehyde, forming highly reactive methylene and methylol-adducts at aminogroups of lysine, asparagin, arginine, histidine, and glutamine⁵⁰. Subsequently, dehydration of methyl-compounds initiates nucleophilic attacks by nearby amino acids, including arginine, asparagine, glutamine, histidine, tryptophan and tyrosine, leading to a connection of two proteins by methylene carbon bridges^{47,51} (Figure 3). These inter- and intra-protein methylene carbon cross-links form a protein grid that prevents protein degradation and conserves the morphological structure of the tissue.

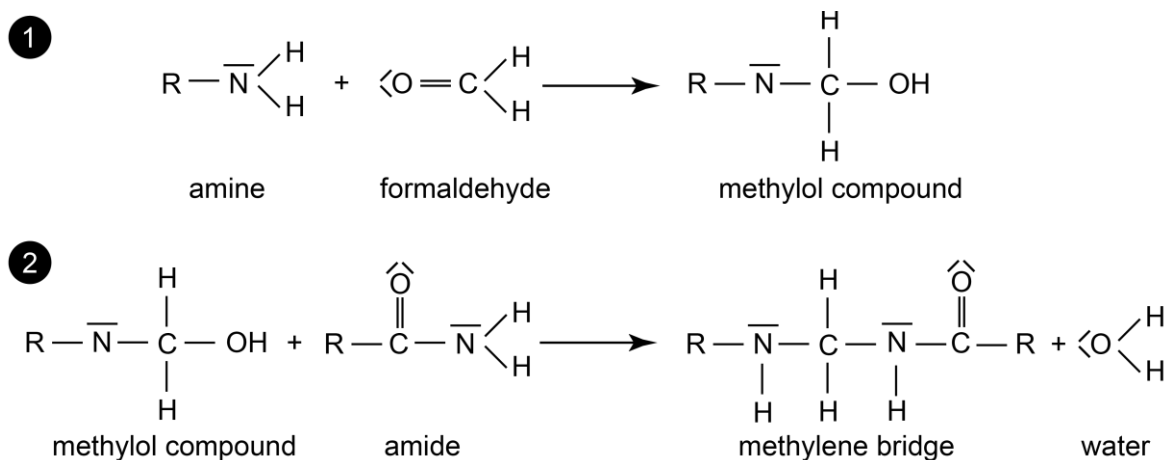


Figure 3. Chemical reaction of protein crosslinking through formaldehyde. In the first step of the reaction, a primary amine of a Protein reacts with formaldehyde to form an methylol compound. Next, the methylol compound reacts with a nearby amide group of another Protein and forms methylene bridges thereby releasing water.

Extraction from FFPE material and subsequent analysis of DNA and RNA is a well established procedure ⁵². However, protein extraction is more challenging since the generated crosslinks disturb many downstream analysis methods, especially concerning methods that separate proteins according to their molecular size ⁵³. The induced chemical structural changes and contamination with embedding medium also interfere with peptide-based approaches like mass spectrometry ⁵⁴. Therefore, several protocols for protein extraction from formalin-fixed samples have been developed and improved ⁵⁵⁻⁵⁹. In general extraction buffers with high concentrations of tensides and reducing agents are used in combination with high temperatures (80-100°C), which is comparable to heat induced antigen retrieval (HIAR) developed for immunohistochemical staining. HIAR induces renaturation of formalin-fixed proteins and a thermal partial hydrolysis of methylene bridges, retrieving the antigenic residues of proteins ⁶⁰. Extracted protein amount and antigenicity depends on several factors like formalin fixation-, storage- and heating time. It has been demonstrated that the DigiWest is a useful tool for protein analysis of FFPE samples with minimal protein amount available, and several antibodies have been validated for reliable use in FFPE material ^{20,61}.

1.2.3. Protein Analysis of Cryo-Preserved Tissue

Effects on proteins induced by fixation with formalin, as described above, make fresh frozen samples the preferred alternative for molecular investigations. Fresh frozen samples are most commonly prepared by snap freezing tissue in liquid nitrogen or a mixture of dry ice and alcohol.

Despite the lack of chemical modification, the snap freezing process bears other difficulties. The rapid freezing induces alterations of tissue structure. Factors influencing quality of the frozen sample are the choice of freezing medium, the pace of freezing, moisture in the sample and the freezing temperature itself ^{62,63}. Furthermore, the time between sample collection and freezing needs to be minimized, in order to avoid protein alteration or degradation. A maximum of 30 minutes is regarded as optimal, however is not always achievable. A delay of up to 2 hours is tolerable but should be noted. Therefore, it is important to install a standardized infrastructure of tissue collection, handling and storage ⁶⁴. For subsequent histological examination, the tissue can be embedded in optimal

cutting temperature compound (OCT) before freezing, to facilitate cutting with a cryotome. OCT primarily consists of polyvinyl alcohol and polyethylene glycol and preserves the tissue without penetrating it. However, it will cause ion suppression in mass spectrometry. Hence its limiting the dynamic detection range of the protein of interest and therefore will interfere with mass spectrometric assays ⁶⁵. Additionally, abundant OCT can interfere with protein separation by SDS-PAGE. Therefore, it should be removed prior or during protein extraction. Since OCT does not penetrate the tissue, it will not induce any chemical changes in the specimen and will not interfere with analysis of protein expression or phosphorylation if removed thoroughly ^{66,67}. Several OCT removal protocols have been established during the last decade ^{65,68,69}. Most commonly, the specimen is washed with ethanol or in a combination of cold ethanol and chloroform. OCT can also be removed by carefully scraping it off prior to sample collection. The fast and cost-effective way of analysing proteins and protein modifications via DigiWest, is a great alternative approach for protein investigation in fresh-frozen and OCT-embedded tissue samples. The minimal protein amount required for analysis is especially favourable in studies where sample material is limited or samples are not reproducible, as is often the case in clinical studies.

1.3. Current Topics Requiring Multiplexed Protein Analysis in Biomedical Research

The field of biomedical research is rapidly advancing, and proteomic analysis of tissue extracts and bio fluids is a valuable source of information for improving diagnosis and treatment of diseases ⁷⁰. The following chapter shall highlight some of the latest topics of biomedical research in which protein expression analysis is applied to elucidate urgent issues.

1.3.1. Serological Monitoring of SARS-CoV-2 Antibody Response

In late 2019, the severe acute respiratory syndrome corona virus 2 (SARS-CoV-2) began to spread all over the globe and has meanwhile reached a pandemic status ⁷¹. The social and economic consequences have been tremendous ⁷². The family of human infecting coronaviruses (hCoV) is branched in alpha- (α -CoV) and beta-

coronaviruses (β -CoV). In contrast to SARS-CoV-2 (β -CoV), NL63 and 229E, belonging to the α -CoV, as well as OC43 and HKU1, belonging to the β -hCoV, only cause mild symptoms and are also known as common cold or endemic coronaviruses⁷³⁻⁷⁵. Yet, key features of molecular structure in the hCoV family are highly conserved⁷⁶. All coronaviruses express the surface spike (S) glycoprotein and the nucleocapsid core-protein (Figure 4). The S-protein plays a critical role for viral entry through binding of the angiotensin converting enzyme 2 expressed by host cells^{77,78}. Hence, the S-protein has been the target of many vaccines and therapeutic approaches against SARS-CoV-2 infections.

The structural nucleocapsid protein is associated with the viral single stranded RNA and is important for genome packaging and viral assembly⁷⁹.

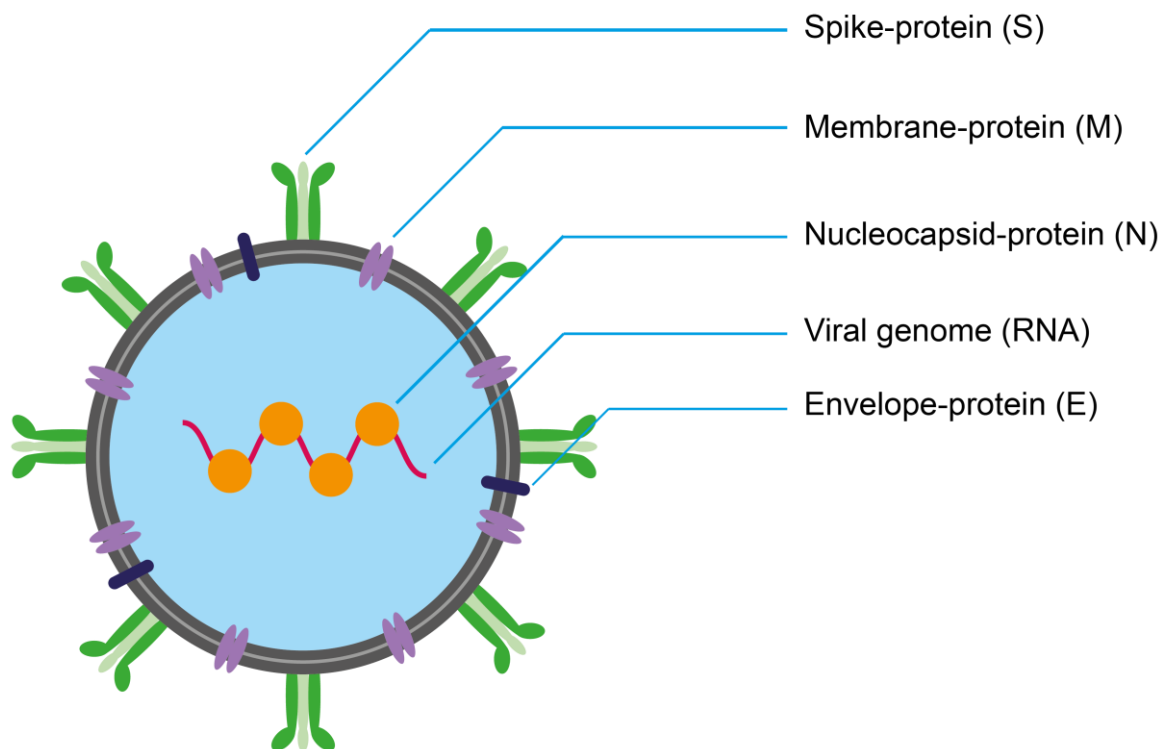


Figure 4. Schematic representation of the structure of coronaviridae. Members of the coronaviridae family express the viral surface proteins spike-glycoprotein (S), envelope-protein (E) and membrane-protein (M) and integrate them in a lipid bilayer. The structural nucleocapsid-protein (N) is associated with the viral genome (RNA).

A new light has been shed on the role of serological testing of seroprevalence and antibody response since the outbreak of the pandemic. Serological assays are a crucial tool for testing and monitoring antibody response not only to viral infection, but to novel vaccine candidates as well. Most commercially available assays

measure antibodies against a specific type of coronavirus or a mutational variant and use recombinant proteins or peptides as antigens. These antigens lack posttranslational modifications and may not thoroughly represent the authentic virus. Multiplexed sero-assays capable of detecting antibody response against different coronaviruses, utilizing antigens from infectious virus particles, can help elucidating the dynamic development of infectious diseases in serological investigations.

1.3.2. Treatment Alternatives for Cervical Intraepithelial Neoplasia

Cervical intraepithelial neoplasia (CIN) is a common precancerous lesion in young women. CIN entails abnormal growth of the cervical epithelial cells. Thus, it has the potential to transform into cervical cancer, which is still a major cause of cancer-related death in women with app. 270 000 cancer-related deaths per year⁸⁰⁻⁸². CIN is classified into low- and high-grade squamous intraepithelial lesions (LSIL and HSIL) by the Bethesda system⁸³. HSIL encompasses moderate and severe dysplasia, whereas LSIL only involves mild dysplasia. The current guidelines for treatment of CIN recommend local excision procedures, which can be executed by invasive loop excision procedure, or thermal,- and cryo-ablation⁸⁴. However, these procedures are either time-consuming or invasive, associated with general or local anaesthesia, and present serious long or short-term effects, most notably an increased risk of pregnancy complications⁸⁵⁻⁸⁷. Taking into account that only 20% of HSIL become invasive and young women are affected most commonly, overtreatment of CIN is a major problem for both patients and the overall health economy^{88,89}. Thus, there is a critical need for alternative treatment options. Non-invasive physical plasma (NIPP) has recently emerged as a non-invasive treatment alternative for CIN⁹⁰. Physical plasma is generated by ionizing gas and is known as the fourth state of matter. Interactions of NIPP with ambient atmosphere leads to the formation of reactive oxygen and nitrogen species (ROS and RNS), which are responsible for pro-therapeutic effects through devitalization of pre-cancerous and cancerous cells while preserving the integrity of deeper tissue⁹¹⁻⁹⁵. However, most of the knowledge on NIPP-induced effects originates from in vitro experiments, and there are only a few individual case reports on NIPP

treatment in patients ⁹⁶. To gain more insight into the mode of action of this innovative treatment approach direct effects within treated human tissue need to be investigated in detail on proteomic level.

1.3.3. Stratification and Risk Assessment of Breast Cancer Patients

Female breast cancer is the most diagnosed cancer worldwide, and still the 5th most common cause of cancer-related death ⁹⁷. Mamma carcinomas arise from the epithelial cells of the ducts or lobules in the breast glandular tissue. Histologically, breast cancers are classified as pre-invasive ductal carcinomas in situ (DCIS) and lobular carcinomas in situ ⁹⁸. These premalignant cells in situ can progress into invasive ductal carcinomas (IDC) or invasive lobular carcinomas over time, yielding a high metastatic potential. On a molecular level, breast cancers are classified by their respective similarity to the basal or luminal cells of the ductus, from which they originate (Figure 5a, b).

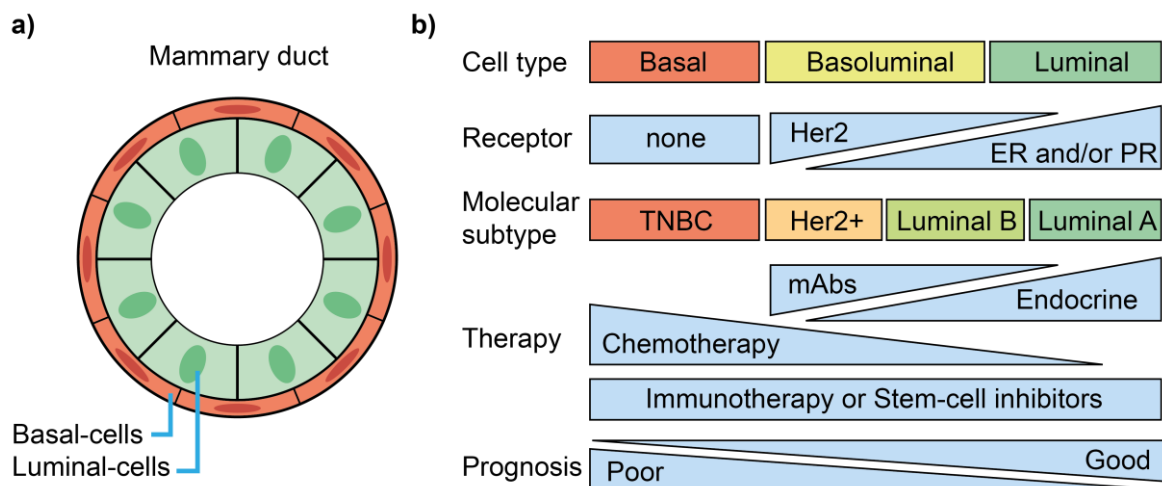


Figure 5. Overview of breast cancer molecular subtypes and treatment options. (a) Schematic overview of the mammary duct, specifying the epithelial (luminal) and myoepithelial (basal) cells. (b) Model of cell types of which breast cancer originates, expressed receptors, the molecular subtypes and their influence on administrated treatment as well as on prognosis (adapted from Hergueta-Redondo et al; and Sims et al. ^{99,100}).

Based on the cellular analogies four primary molecular subtypes are differentiated. Luminal A and B breast cancers are characterized by a high similarity to luminal cells of the ductus and expression of estrogen receptor (ER) and/or progesterone receptor (PR) ^{99,101}. The human epidermal growth factor receptor 2 (Her2) positive or Her2neu subtype is characterised by an intermediate basoluminal phenotype

and the expression of Her2^{99,102}. Triple negative breast cancers (TNBCs) are phenotypically similar to cells of the basal layer and are characterized by a lack of hormone receptor or Her2 expression^{99,103}. They display the highest grade of cell differentiation among all molecular subtypes.

A pertinent treatment can be highly effective in early stages of the disease. Therefore, administration of the right treatment regime early on is crucial. Treatment most commonly consists of a combination of surgical removal, adjuvant medication or radiation therapy. Treatment decision and prognosis are exceedingly based on the molecular subtype and expression of receptor type (Figure 5b)¹⁰⁰. Breast cancers classified as Luminal A have a lower grade of cell differentiation, better prognosis and may be treated with endocrine therapies that target hormone receptors, such as Tamoxifen¹⁰⁴. Her2 expressing cancers can be treated with Trastuzumab, a monoclonal antibody that specifically targets the Her2 receptor¹⁰⁵. TNBCs generally have a poor prognosis, since they lack specific targets on the cell surface leaving only radical chemotherapy as a medication option.

The molecular subtype is routinely assessed by histological and imaged-based examination. These methods are time consuming, have a limited number of assessed parameters and need a trained pathologist for evaluation. All patients with a respective diagnosis are treated with medication according to clinical guidelines ("one-fits-all-principle"). In case of cancer progression or relapse, therapy can be replaced by second or even third line medication according to the guidelines. Yet, breast cancer is a highly dynamic disease, and many patients do not respond to clinical guideline therapies or develop recidives.

Several predictive tests, like MammaPrint, Oncotype DX and PAM50-based Prosignia, utilizing state-of-the art methodologies, have recently been developed to support clinical decision making and prognosis¹⁰⁶⁻¹⁰⁸. However, most of these tests focus on the analysis of gene expression. Thus, it is important to also integrate protein-based approaches as well as auxiliary factors to support treatment decisions and prognosis.

The assessment of the tumour immune microenvironment (TIME) is a novel factor for clinical evaluation and further patient stratification¹⁰⁹⁻¹¹². Bulk gene expression studies showed that the presence of different infiltrating immune cells is

associated with a reduced risk of relapse ^{113,114}. On the one hand, several studies investigating protein markers of infiltrating immune cells, such as cluster of differentiation 8 (CD8), utilizing image-based methods have linked certain cell types to beneficial patient outcome ¹¹⁵⁻¹¹⁷. On the other hand, certain immune cells, as alternatively activated macrophages are linked to tumour progression (Figure 6) ^{118,119}.

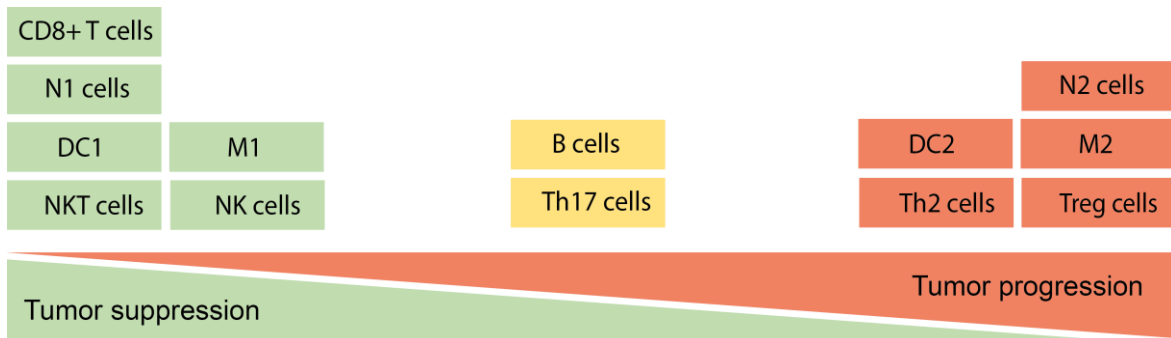


Figure 6. Schematic overview of breast cancer infiltrating immune cells and their contribution to tumor development. Antitumorigenic classically activated macrophages (M1), cytotoxic T cells (CD8+), myeloid dendritic cells (DC1), natural t-killer cells (NKT), natural killer cells (NK), N1 phenotypical neutrophils (N1) as well as protumorigenic alternatively activated macrophages (M2), regulatory and Th2 t-helper cells (Treg, Th2), plasmacytoid dendritic cells (DC2) and N2 phenotypical neutrophils (N2) are shown. The role of B-lymphocytes (B cells) and Th17 t-helper cells (Th17) is still controversial (adapted from Salgado et al. ¹¹⁸).

Yet, the detailed immunological landscape of breast cancers and its influence on patient outcome remains to be further elucidated by studying protein expression signatures of immune cell infiltration in complex human tumour samples.

Chapter 2

Objectives of the Thesis

2 Objectives of the Thesis

Due to its high throughput and multiplex nature, the DigiWest holds great potential for the investigation of molecular processes in human derived samples. Nevertheless, building on established workflows and analysis tools, the suitability of the DigiWest technique was examined. Analysis tools, as well as assay strategies, were adapted and improved for the investigation of the most important clinical sample materials. To accomplish this the DigiWest workflow was streamlined and thereby adapted for the analysis of protein expression and protein modifications in different studies, encompassing serum samples, fresh-frozen as well as FFPE tissue extracts.

The scope of the first study was to develop a multiplexed serum-screening assay utilizing the DigiWest platform. Especially achieving high throughput analysis from small microgram amounts of authentic antigens was taken as aim. Seroreactivity, for different coronaviruses, was detected in a multiplexed fashion to demonstrate the potential of serum screening via DigiWest. The developed immunoassay was characterized in detail and compared with commercially available immunoassays to illustrate the capabilities of the novel assay system.

The second study focused on the feasibility of multiplexed protein analysis from minuscule FFPE punch biopsies, utilizing the DigiWest workflow. This was exemplarily shown on CIN before and after treatment with NIPP. For this purpose, macro dissection of small FFPE cervical punch biopsies and subsequent protein expression analysis was performed. Molecular effects of NIPP treatment were investigated, and differences in protein expression were compared to in vitro NIPP-treated human malignant cervical cells.

Protein expression analysis of fresh frozen tissue was addressed in the third study. The goal was the preparation and analysis of fresh frozen breast cancer resectates in a retrospective study. Auxiliary factors for prognosis and prediction of treatment outcome were reviewed. Therefore, DigiWest was applied to detect infiltrating immune cells and protein expression changes in the tissue. The resulting expression profiles were compared between responder groups and baseline samples. For evaluation of clinical metadata, a newly designed DigiWest analysis and evaluation pipeline was integrated and tested.

2 Objectives of the Thesis

The insights gained from this work will help to enhance and expedite protein expression studies of human sample material by DigiWest in the future.

Chapter 3

Results I: Multiplexed Serum Antibody Screening

The contents of this chapter are based on:

Simon Fink*, **Felix Ruoff***, Aaron Stahl, Matthias Becker, Philipp Kaiser, Bjoern Traenkle, Daniel Junker, Frank Weise, Natalia Ruetalo, Sebastian Hörber, Andreas Peter, Annika Nelde, Juliane Walz, Gérard Krause, Armin Baillot, Katja Schenke-Layland, Thomas O. Joos, Ulrich Rothbauer, Nicole Schneiderhan-Marra, Michael Schindler, and Markus F. Templin. *Multiplexed Serum Antibody Screening Platform Using Virus Extracts from Endemic Coronaviridae and SARS-CoV-2*. ACS Infectious Diseases; 7, (6), 1596-1606 (2021).

<https://doi.org/10.1021/acsinfecdis.0c00725>

*authors contributed equally

In this work, I developed and prepared virus-specific detection reagents and performed experiments for the detection of virus proteins together with Simon Fink (PhD student, NMI Natural and Medical Sciences Institute at the University of Tübingen, Reutlingen). I performed all experiments using the test sample set for calculation of the fundamental assay characteristics, such as sensitivity, specificity, and dynamic range, independently. All experiments for validation of detected peaks and definition of cut-off values were performed by Simon Fink. I analysed, interpreted the data, prepared figures, and wrote the manuscript together with Simon Fink and Markus Templin. Parts of the results presented here will also be described in the PhD-thesis of Simon Fink.

3 Results I: Multiplexed Serum Antibody Screening

The adaptive immune response is highly specific for pathogens. A major part of the adaptive immune response is the humoral response, in which protective antibodies against pathogens are generated and are present in patient sera. These antibodies are aimed to label pathogens for the degradation by phagocytes, also called opsonization. Furthermore, Antigen-Antibody complexes activate the complement system and trigger the release of chemokines thereby attracting immune cells. Additionally, antibodies can bind receptors of a pathogen and thus inactivating its pathogenic activity. However, a phenomenon termed antibody-dependent enhancement (ADE) might be the reason for a sometimes overreacting immune system and a fatal course of diseases. ADE occurs through already existing cross-reacting and non-neutralizing antibodies and is a concern for the development of vaccines or immunoglobulin-based therapies¹²⁰⁻¹²². Multiplexed monitoring of immunoglobulins in patient sera or plasma may help to elucidate the role of existing antibodies during infections.

There are various methods for detection of immunoglobulins against viral infection in serum or plasma samples. Many of these systems use recombinant antigens for antibody detection. Despite being economical and making the generation of large numbers of assays feasible, this approach may not detect antibodies against protein modifications and additional proteins present in the authentic pathogen^{123,124}. Thus, an assay system measuring antibodies against the whole viral proteome as well as protein modifications would be valuable. The DigiWest can be used as a tool for the detection of multiple antibodies present in patient sera or plasma at the same time¹⁸. However, several adaptations to the workflow must be performed to facilitate the use of human sera or plasma as specimen.

This study aimed to develop a multiplexed screening platform for the detection of antibodies against SARS-CoV-2 and other endemic coronaviridae, such as OC43, 229E, and NL63 in parallel from patient sera (Figure 7). Therefore, the DigiWest procedure was adapted utilizing whole virus lysates as authentic antigens to develop a multiplexed direct binding immunoassay. Assay parameters and performance were deeply characterized and compared to commercially available assay systems.

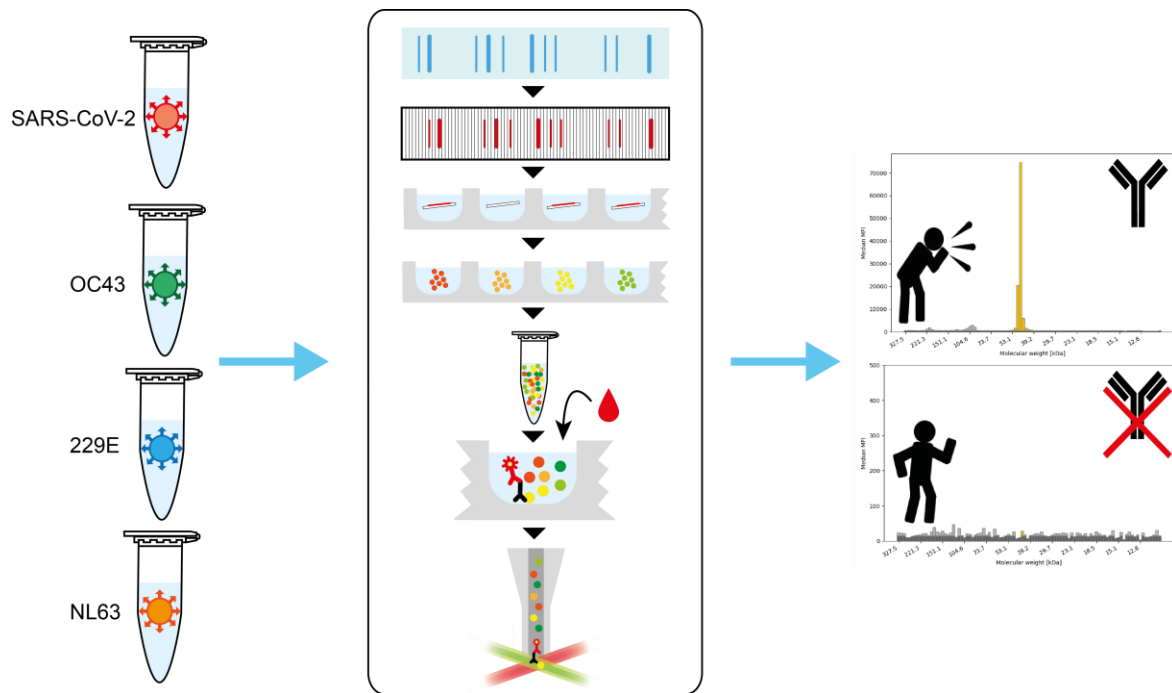


Figure 7. Schematic overview of the developed serum-screening assay. Whole virus lysates of SARS-CoV2, OC43, 229E and NL63 were fractionated and immobilized on microspheres. Microsphere mixes were pooled for the parallel detection of immunoglobulins against the different virus strains. Human patient sera were added and signal against the different viral proteins was detected (adapted from Fink & Ruoff et al. ¹²⁵).

3.1. Detection of Serum Antibodies Utilizing DigiWest

In a first step, DigiWest was performed by immobilizing lysates from infectious SARS-CoV-2 virus particles on microspheres (Fink & Ruoff et. al, **Appendix 1**, Fig. 1). Virus lysates were prepared by collecting the supernatant of infected Caco-2 cells, and subsequent lysis in lithium dodecyl sulfate sample buffer. Thus, the lysates represented the complete viral proteome. DigiWest microsphere mixes were generated by utilizing 0.5 μg of the viral lysate. To investigate the quality of the generated microsphere mix, total protein detection, as well as incubation with commercially available antibodies generated against SARS-CoV-2 nucleocapsid and SARS-CoV-2 spike protein, were performed. Total protein detection revealed a characteristic protein band pattern for the SARS-CoV-2 lysate (Fink & Ruoff et. al, **Appendix 1**, Fig. 2a). Incubation with the anti nucleocapsid antibody revealed a prominent peak at 47.2 kDa, while incubation with the anti-spike protein antibody showed a peak at 141 kDa, which is in agreement with the expected molecular weight of the proteins (Fink & Ruoff et. al, **Appendix 1**, Fig. 2b, c).

As a next step, the detection of antibodies specific for viral proteins from patient sera was investigated. Human sera were prepared by collecting the supernatant after a clotting time of 1h and centrifugation at 16.000 rpm. Human SARS-CoV-2 positive sera were diluted 1:200 in a modified serum assay buffer and used for detection on the generated microsphere mixes. The main peak of reactivity for positive sera was mostly seen at 47 kDa, which is the size of the SARS-CoV-2 nucleocapsid protein (Fink & Ruoff et. al, **Appendix 1**, Fig. 2e). At the same time, SARS-CoV-2 negative sera obtained no or very low signal (Fink & Ruoff et. al, **Appendix 1**, Fig. 2d). The observed assay background showed sample-specific fluctuations. Since calculated values are based on the peak area, and are corrected for local background, reliable values are generated using the DigiWest evaluation macro ¹⁸. These results demonstrated that reactivity against viral nucleocapsid protein was consistently detected in convalescent sera.

3.2. Detecting Serum Antibodies Recognizing Different Human Coronaviridae

Next the serum-screening assay was expanded to cover reactivity against additional endemic coronaviruses. Accordingly, lysates from two α -hCoV (229E, NL63) and from a β -hCoV (OC43) were produced. DigiWest assays were established, and microsphere mixes were combined into one assay by pooling different virus derived microsphere mixes. Serum screening of SARS-CoV-2 negative individuals displayed seroreactivity for endemic viral nucleocapsid protein in most samples indicating prior contact with the viruses. Since, no information about previous infections with endemic coronaviruses was available, the detected reactivity had to be validated as recognizing nucleocapsid protein of the different coronaviruses. In order to do so recombinant nucleocapsid of SARS-CoV2, OC43, 229E and NL63 were produced in *E. coli* and subsequently purified. A DigiWest experiment using the recombinant nucleocapsid proteins as antigens was performed utilizing a subset of 12 patient sera. Obtained results were compared to those generated with whole virus lysates. The detected peaks for SARS-CoV2, OC43, 229E and NL63 nucleocapsid protein were found at 47.2 kDa (calculated 45.6 kDa), 53.1 kDa (calculated 49.3 kDa), 45.4 kDa (calculated 43.5 kDa) and 42.1 (calculated 42.3 kDa) correspondingly (Fink & Ruoff et. al, **Appendix 1**,

Fig. 3a). The detected molecular weights corresponded to the expected molecular weights. By using the same sera on recombinant proteins, molecular weights of target proteins were confirmed (Fink & Ruoff et. al, **Appendix 1**, Fig. 3b). These results proved that the parallel-detected immunoglobulins are directed against nucleocapsid proteins of SARS-CoV2, OC43, 229E and NL63.

3.3. Evaluation of Assay Characteristics

To define assay parameters for the anti-SARS-CoV-2 nucleocapsid immunoglobulin detection, the multiplexed serum-screening platform comprising SARS-CoV-2, 229E, OC43 and NL63, was used to analyse a training set of previously well-characterized samples¹²⁶. The training set consisted of 68 negative sera, of which 49 were pre-pandemic and 19 self-reported negative and 195 sera, which were polymerase chain reaction (PCR)-positive for SARS-CoV-2. Cut-off for seropositivity was defined by employing the pre-pandemic not infected samples and all PCR positive sera. Highest average fluorescence intensity (AFI) value in the pre-pandemic sera was found to be 1295. The lowest AFI value above this value, in the PCR positive sample set was defined as seropositive, and was found to be 1968 AFI. To define cut-off for seroconversion the mean of these values was calculated (1632 AFI).

As a next step, specificity and sensitivity were calculated, by applying the previously defined cut-off. Therefore, a test set comprising 53 PCR negative and 31 positive sera were screened. Utilizing this sample set a specificity of 98.1 % (confidence interval (CI) 94.5-100%) and a sensitivity of 90.3 % (CI 79.9-100%) was achieved. Furthermore, positive and negative predictive values for the assay were calculated and found to be 0.966 (CI 0.899-1.0) and 0.945 (CI 0.855-1.0) respectively. In order to determine the dynamic range of the developed immunoassay, SARS-CoV-2 positive sera (n=3) were serially diluted in a negative sample. Dilution was performed in 13 steps, and dilution factors ranged from 1:25 to 1:1131 (Fink & Ruoff et. al, **Appendix 1**, Fig. 4). By utilizing a sigmoidal fit and 4-parametric regression, logistic regression was performed, which revealed a hill slope of -0.88, -0.96, and -0.92 as well as an IC50 of 0.53, 1.472, and -0.04 for samples one, two, and three respectively. The obtained results demonstrated

good signal linearity and seropositivity was detected up to a dilution of 1:5000. The evaluation of assay characteristics yielded comparable values to commercially available SARS-CoV-2 immunoassays^{127,128}.

For further validation, the whole sample set was reanalysed using the commercially available SARS-CoV-2 assays Elecsys® (Roche Diagnostics), ADVIA Centaur SARS-CoV-2 (Siemens Healthcare Diagnostics), EUROIMMUN SARS-CoV-2 IgG as well as IgA ELISA test systems (Euroimmun). All results of the utilized assays, including the DigiWest SARS-CoV-2 serum-screening platform, were compared and concordance (Cohen's κ) and correlation analyses (Spearman's r) were performed (Fink & Ruoff et. al, **Appendix 1**, Fig. 5a, b, c). A strong concordance of the DigiWest assay with the assays of Roche, Siemens and Euroimmun IgG (borderline results considered positive) was found (Cohen's $\kappa > 0.9$). However, concordance of DigiWest compared to Euroimmun IgA (borderline results considered positive) was found to be weaker (Cohen's $\kappa = 0.75$; 95% CI: 0.67-0.83). Spearman's correlation analysis demonstrated a positive correlation of all investigated assays (Fink & Ruoff et. al, **Appendix 1**, Fig. 5d). The strongest correlation for the DigiWest assay was found with the Roche system (Spearman's $r = 0.91$; 95% CI; 0.89-0.93). The results demonstrate that all of the investigated assays showed a good concordance and correlation, except for the Euroimmun IgA assay, and will give comparable results.

3.4. Multiplexed Immunoglobulin Detection Against Different Coronaviridae

Finally, the full sample set was analysed utilizing the DigiWest assay integrating virus lysates from SARS-CoV-2, 229E, OC43, and NL63. The analysis revealed that immunoglobulins against all endemic coronaviruses were detected frequently in most investigated sera. In SARS-CoV-2 PCR negative samples no signal for SARS-CoV-2 nucleocapsid was found, despite the high frequency of antibodies against the endemic coronaviridae, indicating a high specificity for SARS-CoV-2 nucleocapsid protein of the assay. However, correlation analysis of all detected coronaviruses, utilizing the cut-off for SARS-CoV-2 (1632 AFI) as a provisional cut-off for the endemic coronaviridae, revealed moderate to weak correlations of observed signals, with Spearman's r ranging from 0.03 to 0.75 (Fink & Ruoff et. al,

Appendix 1, Fig. 6). These results indicate that cross-reactivity of antibodies directed against nucleocapsid proteins of endemic coronaviruses does not play a critical role in SARS-CoV-2 infections.

Overall, it has been demonstrated that the fast setup of an assay for immunoglobulin detection from human sera against authentic antigens is achievable by utilizing the DigiWest technology. This makes this an attractive approach for immunoglobulin detection from human blood samples utilizing complex mixtures of antigens from various kind of sources.

Chapter 4

Results II: Multiplexed Protein Expression Analysis of Human FFPE Tissue

The contents of this chapter are based on:

Felix Ruoff, Melanie Henes, Markus F. Templin, Markus Enderle, Hans Bösmüller, Diethelm Wallwiener, Sara Y. Brucker, Katja Schenke-Layland, and Martin Weiss. *Targeted Protein Profiling of In Vivo NIPP-Treated Tissues Using DigiWest Technology*. *Applied Sciences*; 11, (23), 11238 (2021).

<https://doi.org/10.3390/app112311238>

In this work, I performed selection, evaluation, and macro dissection of FFPE tissue sections, preparation of assay reagents and assays for pathway analysis independently. Additionally, I generated and evaluated a panel of antibodies suitable for the protein expression analysis of FFPE cervical punch biopsies. I curated, investigated, and analysed the data, prepared figures and wrote the manuscript together with Martin Weiss.

4 Results II: Multiplexed Protein Expression Analysis of Treated FFPE Tissue

Overtreatment of CIN in young women, which is a disease that may lead to cervical cancer, is a considerable problem. High invasiveness and the need for local or general anaesthesia lead to serious short- and long-term adverse events, including a higher risk of pregnancy complications^{85,86}. Therefore, innovative and non-invasive treatment alternatives are an urgent need, for affected women as well as the general health economy. The application of NIPP is such a treatment procedure. NIPP has shown promising anti-neoplastic effects on a broad array of oncological and medical issues^{90,93-96,129}. Recently, NIPP has been characterized as a procedure for CIN treatment⁹⁰. NIPP, a highly energized gas, induces the generation of ROS and RNS, by the interaction with the atmosphere, fluids, and organic surfaces¹³⁰ (Figure 8a). ROS and RNS induce distinct cellular effects, including anti-proliferative and apoptotic signaling in the treated cell layers, while sparing deeper tissue areas^{91,92}. However, most of the insights about NIPP-induced effects in human cells originate from cell culture experiments. For further elucidation of the mode of action and conceivable medical applications of this treatment approach, it is crucial to investigate induced molecular effects on protein level within patient material such as cervical punch biopsies. Yet, cervical punch biopsies are defined by limited sample size and are routinely fixed in formalin, both being factors which complicate protein analysis. For this purpose, methods for multiplexed detection of protein expression changes from such complex human samples are required.

The goal of this study was to establish a workflow for multiplexed protein analysis from minuscule FFPE cervical punch biopsies and to characterize analytes that are detectable by this approach, in order to obtain valuable insights in protein expression changes induced after NIPP treatment. Therefore, sample preparation and DigiWest workflow were improved and adapted (Figure 8b). To validate generated results and investigate the differences of in vitro and in vivo effects, protein profiles of human FFPE tissue samples were compared to NIPP-treated cell culture samples as well.

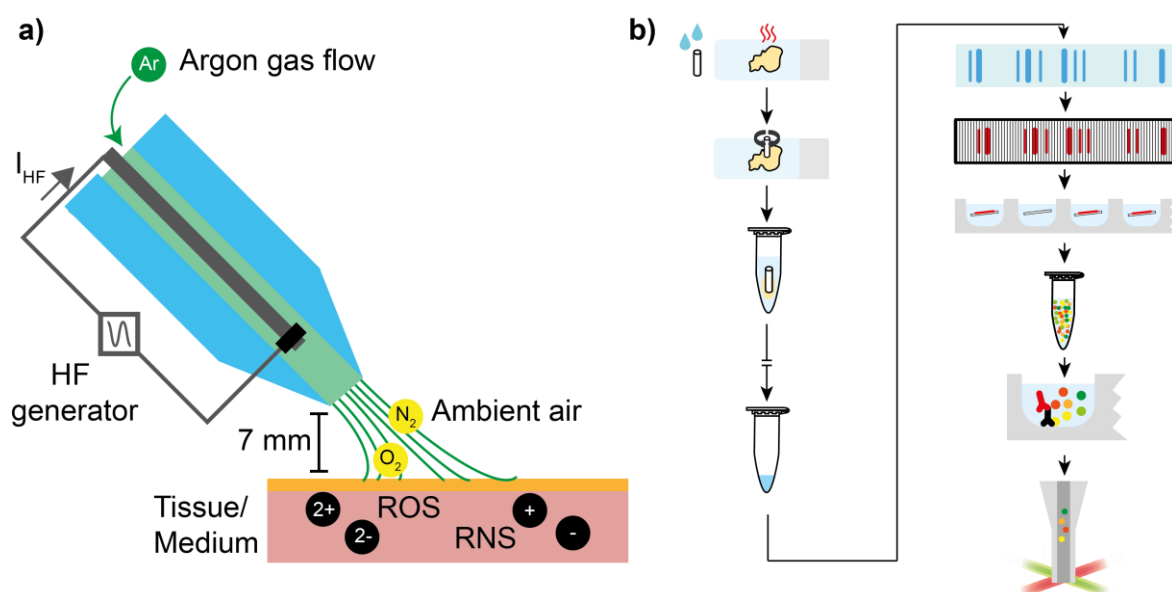


Figure 8. Schematic illustration of non-invasive physical plasma application and overview of the expression analysis workflow. (a) Physical plasma is generated through ionization of gas. In order to do so, a current (I_{HF}) is applied to an argon gas (Ar) flow through a high frequency (HF) generator. Through interaction with the atmosphere (O_2 , N_2) reactive species (ROS, RNS) are generated. These species are the active treatment components in the tissue or medium (adapted from Weiss et al. ¹³¹). (b) Pre-heated FFPE slides are macro-dissected utilizing pre-wetted tissue picks. Subsequently picked samples are transferred into a reaction tube and protein extraction is performed. Protein expression of resulting lysates is analysed via DigiWest as described earlier (adapted from Ruoff et al. ¹³²)

4.1. Evaluation of Treatment Response Through Protein Analysis of Cervical Punch Biopsies after NIPP Treatment

For sample preparation, cervical punch biopsies were collected and mounted on slides for histopathological assessment before ($n = 5$ patients), directly after (0 h; $n = 3$ patients), and 24 h after in vivo NIPP treatment for 30 seconds. After preparing slides for haematoxylin and eosin (H&E) staining, 4-6 sections with tissue areas ranging from 10 mm^2 to 400 mm^2 in total were mounted on slides for macro dissection. The H&E stained master slide, on which CIN areas were marked by a pathologist were used as a template for macro dissection. After heptane-based deparaffinization and protein extraction, proteins were concentrated by volume reduction in a vacuum concentrator. For protein detection, the DigiWest was applied. Initially, 69 proteins of interest, covering apoptosis, DNA damage response, and cell cycle control were analyzed. Twenty-nine of the used antibodies delivered a detectable signal in all investigated samples. The resulting AFI values were compared among the control group (untreated) as well

as 0 h and 24 h after treatment. Hierarchical cluster linkage analysis (complete linkage, Euclidean distance) of median centred and log₂ transformed AFI values revealed that all pre-NIPP samples (control) displayed a similar protein expression pattern and that most of the samples 0 h and 24 h post-NIPP treatment had a similar protein expression (Ruoff et al., **Appendix 2**, Fig. 2). These results indicate a sufficient protein yield and a sample quality that enables multiplexed protein measurement from cervical punch biopsies.

4.2. Protein Expression Changes Following In Vivo and In Vitro NIPP Treatment

A variety of biological effects is induced through NIPP treatment, including antineoplastic efficacy⁹⁶. For further elucidation of these effects, the overall antineoplastic properties of NIPP treatment were investigated, by comparing treatment of a human malignant cervical squamous cell carcinoma-derived cell line (CSCC) in vitro, and treatment of patients with histologically confirmed CIN lesions in vivo.

In a first step cell pellets of NIPP-treated CSCC cell culture (n = 6) were analysed, and compared to argon gas treated control samples (n = 6) harvested after 24 h. 132 proteins, again covering apoptosis, DNA damage response and cell cycle control were analysed. Forty-four analytes were matching with the previous FFPE analysis (Ruoff et al., **Appendix 2**, Fig. 3a, 4a). In general, the differences in protein expression of the cell culture sample set were comparatively lower, since only one analyte displayed a log₂ foldchange larger than 1 or -1 by comparing median signals of in vitro NIPP treated cells with the control group (Ruoff et al., **Appendix 2**, Fig. 3b). Overall, higher differences in protein expression changes were detected by comparing median AFI values of FFPE untreated samples and 24 h after treatment. Thereby, eight analytes showed a noticeable change in protein expression, indicated by a log₂ fold change larger than 1 or -1 (Ruoff et al., **Appendix 2**, Fig. 4b).

Primarily, NIPP-treated CSCC cells showed a significantly reduced expression of several factors associated with cell growth and proliferation when compared to the untreated control group (Ruoff et al., **Appendix 2**, Fig. 3c). Especially the mitogen-activated protein kinase (MAPK) pathway was targeted by the treatment. This was

indicated by a significant decrease in expression of p38 mitogen-activated protein kinases (p38), the RAF proto-oncogene serine/threonine- protein kinase (c-Raf), which is known to be a kinase cascade initiator ¹³³, and the dual specificity mitogen- activated protein kinase kinase 1 (MEK1). The latter is a dual threonine and tyrosine recognition kinase and important for MAPK phosphorylation and activation ¹³⁴. All of these factors are crucial for cell growth, as well as regulation of apoptosis, and when deregulated can act as oncogenes. Another central kinase, the proto-oncogene tyrosine-protein kinase Src (Src) was also significantly lower expressed after treatment, yet phosphorylation of Src (pTyr527) showed a slight increase. Src is an important regulator of cell survival, proliferation, and invasion and has been linked to interaction with various signaling proteins, such as MAPK/MEK/RAF, protein kinase B (Akt) ¹³⁵ as well as the signal transducer and activator of transcription-3 (STAT3) ^{135,136}. STAT3, which plays a critical role in cell growth and apoptosis ¹³⁷, was significantly lower expressed after NIPP treatment. In addition the cyclin dependent kinase inhibitor 1, also known as p21, which is linked to inhibition of cyclin-dependent kinase 2 (CDK2) ^{138,139}, was found to be downregulated. Accordingly, phosphorylation of CDK2 (pTyr160) was increased after NIPP treatment. Overall NIPP treatment induced inhibition of cell growth and cell cycle regulation factors in CSCC cell culture.

Protein expression analysis from in vivo NIPP-treated CIN tissue extracts revealed similar results. Protein expression of untreated control samples was compared to NIPP-treated tissues 24h post-treatment. Repeatedly, NIPP treatment of patient tissue induced a decrease of Src expression and phosphorylation (pTyr527). However, the expression of other pro-proliferative proteins, such as p38, c-Raf, MEK1, STAT3, and p21, were not significantly changed. In common with the NIPP-treated CSCC cells, in vivo NIPP-treated CIN tissue showed a noticeable increase in expression of CDK2, yet this difference was not statistically significant (Ruoff et al., **Appendix 2**, Fig. 4c). These findings demonstrate that results generated from in vivo treated tissue can differ from cell culture experiments, yet expose analogous trends.

Finally, protein expression directly after in vivo NIPP treatment (0 h) was compared to the untreated control (pre-NIPP). A significant increase of cytokeratin (CK) 8 and 18 was shown after treatment (Ruoff et al., **Appendix 2**, Fig. S2). Interestingly this effect was inversed 24 h after treatment. CK18 and the

complementary partner CK8 play an important role in maintaining the physiological cell function and are associated with the cell cycle and apoptosis¹⁴⁰⁻¹⁴². Moreover, a significant decrease in Akt expression 0 h and 24 h after NIPP treatment was detected. Among other functions, Akt is a regulator of the CDK inhibitor p21 as well as Src and plays a critical role in apoptotic mechanisms and cell cycle control^{143,144}.

This study demonstrated that multiplexed protein analysis from minuscule FFPE cervical punch biopsies is feasible by adapting the DigiWest workflow. The generated results agree to prevailing knowledge. Further, it has been presented that effects observed by in vitro studies do not always translate to effects observed in human tissue and that treatment effects need to be studied more frequently in vivo. Therefore, this approach can add valuable information to knowledge generated from traditional cell culture experiments.

Chapter 5

Results III: Protein Profiling of Fresh Frozen Breast Carcinomas

The contents of this chapter are based on:

Felix Ruoff, Nicolas Kersten, Nicole Anderle, Sandra Jerbi, Aaron Stahl, André Koch, Annette Staebler, Andreas Hartkopf, Sara Y. Brucker, Markus Hahn, Katja Schenke-Layland, Christian Schmees, and Markus F. Templin. *Protein Profiling of Breast Carcinomas Reveals Expression of Immune-Suppressive Factors and Signatures Relevant for Patient Outcome*. *Cancers*; 14, (8), 4542 (2022).

<https://doi.org/10.3390/cancers14184542>.

In this work, I prepared layered cuts of fresh frozen tissues and performed haematoxylin and eosin staining together with Sandra Jerbi. I evaluated and selected analytes for detailed protein expression analysis, prepared assay reagents and performed assays for pathway analysis and immune marker detection, immunohistochemistry of immune cell markers, analysed, interpreted the total data, and prepared figures independently. I wrote the manuscript together with Markus Templin.

5 Results III: Protein Profiling of Fresh Frozen Breast Carcinomas

A multitude of treatment options for breast cancer is currently available, including surgery, chemo-, hormonal- and biological therapy ¹⁴⁵. Nevertheless, overdiagnosis and long-term therapy resistance still pose a problem. Hence, more personalized treatment approaches have become a focus of current research ¹⁴⁶. With the advancement of immunotherapies, the role of cancer-infiltrating immune cells in disease progression and treatment has been emphasized ^{147,148}. For instance, assessment of tumour-infiltrating lymphocytes (TILs) has been established as a novel prognostic factor. Moreover, insight into interaction of tumour cells and tumor immune microenvironment (TIME) have rendered an understanding of reasons accounting for treatment failure ¹⁰⁹. Most studies that link protein expression of certain immune cells to risk of relapse assess general TIL density by H&E staining or immune cell marker expression via immunohistochemistry (IHC) ^{117,119,149}.

However, such image-based methods can be time-consuming, require evaluation by trained pathologists and quantification can be difficult. Therefore, there is an urgent need in the clinical setting for novel approaches to investigate immune cells in patient tissue, especially fresh frozen biopsies or resectates ^{150,151}.

In this study, sample preparation was adapted to fresh frozen resectates from breast cancer patients and comparative protein expression analysis was performed by DigiWest. The activation state of central signalling pathways was monitored, and the multiplexed assessment of several immune cell markers was established in fresh frozen tissue. To do so, relevant immune cell markers had to be identified and verified by IHC staining. Additionally, a novel analysis software pipeline enabling simultaneous analysis of numerous samples and subsequent inclusion of clinically relevant metadata ²⁷ was utilized and tested. The sample-set was stratified according to the established immune cell markers and differences in event-free survival (EFS, time from definitive surgery until disease recurrence/metastases or death from any cause) as well as the activation state of different pathways were investigated.

5.1. Quality Assessment of Enrolled Patient Samples

A set of 159 retrospective fresh frozen resectates (after primary surgery with no neo-adjuvant treatment) was provided by the central bio bank at the university clinic Tübingen. Samples were classified based on response to primary surgery. In case of distant metastases or local relapse within 10 years, samples were assigned to the poor responder group. If however no distant metastases or local relapse occurred within 10 years and no contralateral carcinoma occurred within 5 years samples were labelled as good responders (Ruoff et al., **Appendix 3**, Fig. S1). None of the enrolled patients had any known metastases before surgery. Before protein expression analysis the tumour content of each sample was assessed. H&E stained layered cuts of resectates were prepared (Ruoff et al., **Appendix 3**, Fig. 1a) and two layers were stained per sample, while the intermediate tissue (100 μm) was collected for protein expression analysis (Figure 9). A pathologist (Annette Stabler, Department of Women's Health, University of Tübingen, Tübingen, Germany) assessed the tumour content of each layer, yielding an estimated average tumour content for each sample.

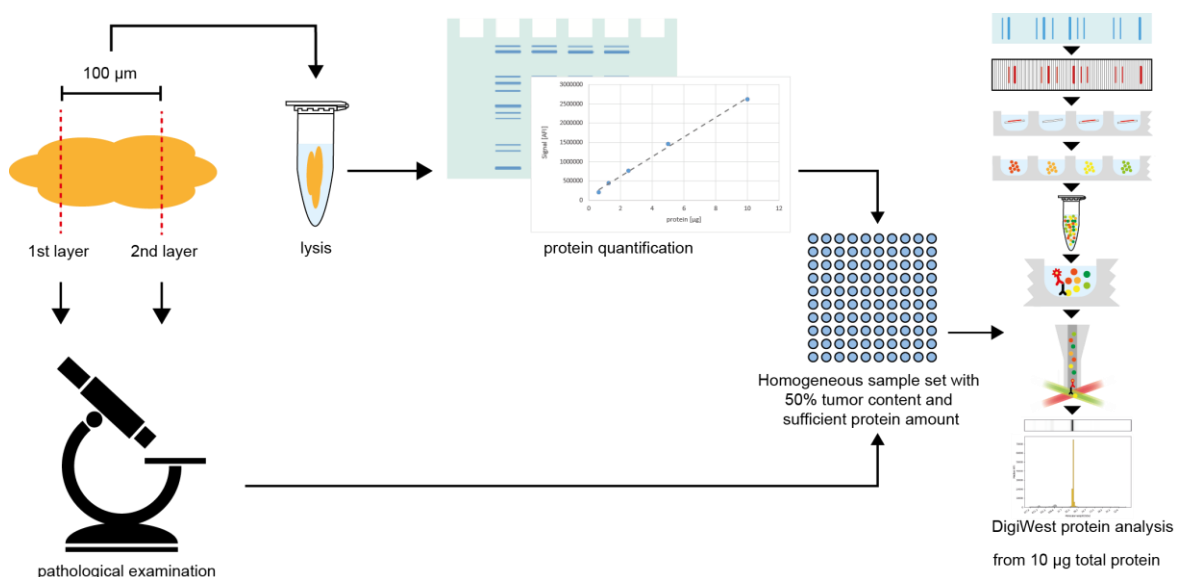


Figure 9. Schematic illustration of study workflow. Layered cuts of tumour resectates were generated and intermediate tissue (100 μm) was collected. Tumour content in first and second layer was assessed by a pathologist. Collected sample material was lysed and protein quantification was performed. A set of samples with at least 50% tumour content and sufficient protein amount was selected for protein analysis via DigiWest (adapted from Ruoff et al. ¹⁵²)

In total, 90% (n=144) of the enrolled samples were categorized as IDC, while 2.5% (n=4) were categorized as normal tissue, 5.0 % (n=8) as DCIS and 1.9% (n=3) as necrotic tissue (Ruoff et al., **Appendix 3**, Fig. 1b). Of all samples 60.4 % (n=96) displayed a tumour content of at least 50 %. To standardize the analysis sample set, only samples with tumour content of 50% or higher as well as sufficient protein concentration were selected for analysis (n=84). As a control, a baseline sample set was used consisting of samples with a tumour content of 10% or less. DigiWest analysis of common tumour markers Ki67, CK8/18, CK8 (pS23) and CK6 demonstrated a significant difference ($p < 0.05$, Wilcoxon Rank-Sum test) in expression between analysis- and baseline samples confirming the cooperatively higher tumour content in the analysis set (Ruoff et al., **Appendix 3**, Fig. S3a).

Furthermore, DigiWest results were set against previous pathological classification. To do so, expression of hormone receptors (ER and PR) as well as Her2 was measured and compared to pathological receptor status (assessed through IHC in compliance to the standard procedure at the pathological institute at the University of Tübingen). Samples pathologically categorized as ER/PR-Her2- (corresponding to TNBC subtype), displayed low to no expression of the respective receptors. While ER/PR+ Her2- samples (corresponding to luminal subtype) displayed increased expression of ER and PR but not Her2, whereas in ER/PR +/- Her2+ samples (corresponding to Her2+ subtype) an increase in Her2 expression was observed (Ruoff et al., **Appendix 3**, Fig. 1c, d).

Overall, measurements of receptor status by DigiWest complied with the receptor status established by the pathology confirming good quality of the enrolled analysis sample set.

5.2. Targeted Protein Expression Analysis by DigiWest

To investigate differences in signal transduction between good or poorly responding breast carcinoma samples, 150 proteins and protein variants, 41 of which were phosphorylated proteins, were measured by DigiWest. The analysis covered cell cycle control, apoptosis, janus kinase (Jak)/Stat-, MAPK-, phosphoinositid-3-Kinase (Pi3K)/Akt-, proto-oncogene Int-1 homolog- (Wnt-) and

autophagic signalling as well as general tumour markers and immune cell markers. PANTHER pathway enrichment analysis revealed that Jak/Stat signalling displayed the greatest distinction between the two groups (highest $-\log_2$ Q-value) (Ruoff et al., **Appendix 3**, Fig. 2a). Additionally, a significant difference in expression of several members of the Jak/Stat pathway and immune cell markers was found, indicating a discrepancy in immune cell infiltration and related signalling (Ruoff et al., **Appendix 3**, Fig. 2b). Therefore, immune cell infiltration and the connection to patient response was investigated in detail.

5.2.1. Assessment of Immune Cell Infiltration by DigiWest for Patient Stratification

For evaluation of immune cell infiltration, the expression of selected immune cell markers (CD8 α , CD4, CD68, CD11c, CD16, CD56, CD25, CD163) was evaluated in detail. Spearman's correlation analysis revealed that CD8, CD68, CD11c and CD16 expression displayed the highest correlation among the immune-cell related analytes (Spearman's $r < 0.55$, Ruoff et al., **Appendix 3**, Fig. 3a, Table S1). These results suggest a co-occurrence of immune cells representative for these markers. Therefore, they served as a stratification criterion for the sample set for unsupervised hierarchical cluster linkage analysis (Euclidean distance, complete linkage). Two distinct groups with higher ($n=27$) and lower ($n=57$) expression of these immune cell marker were revealed (Ruoff et al., **Appendix 3**, Fig. 3b, c). From now on, the higher infiltrated group will be referred to as hot carcinomas, whereas the lower infiltrated group will be referred to as cold carcinomas. To validate DigiWest results, IHC staining of CD8a, CD68, CD11c and CD16 was performed selectively on matching FFPE slides and the mean pixel intensity per slide was calculated. A significant difference between the two groups stratified by DigiWest was found for all four markers (Ruoff et al., **Appendix 3**, Fig. 3d, e; Mann-Whitney- U test, $p < 0.05$). When comparing different clinical variables among hot and cold carcinomas, the responder status was the only criterion that displayed a significant difference between the two groups (Ruoff et al., **Appendix 3**, Fig. 3f; Table 1; chi-square test, $p < 0.05$). When looking at the 10 year EFS rate, the higher infiltrated subgroup displayed a significant better outcome (Ruoff et al., **Appendix 3**, Fig. 3g; log-rank test, $p = 0.03$). Comparison of EFS rates among hot

and cold samples, categorized by pathological hormone and Her2 receptor status, revealed that higher infiltrated samples had a better outcome in tendency, which was found to be significant for ER+ and PR+ samples (Ruoff et al., **Appendix 3**, Fig. S5). Additionally, univariate Cox regression of immune cell infiltration status assessed by DigiWest demonstrated a significant prediction for clinical outcome ($p=0.04$).

Taken together, these results indicate that the selected immune cell markers assessed by DigiWest in fresh frozen carcinomas could be used for patient stratification.

5.3. Detailed Protein Expression Evaluation of Hot and Cold Carcinomas

To identify factors contributing to the immune cell infiltration status, a detailed evaluation of protein expression was performed comparing hot and cold carcinomas. A set of 30 proteins and protein variants displayed a significant difference (Mann-Whitney- U test; FDR Benjamini-Hochberg; corrected $p<0.05$) and a \log_2 fold change of at least $\frac{2}{3}$ or $-\frac{2}{3}$ (Ruoff et al, **Appendix 3**, Fig. 4A, B, D).

CD163, a marker for M2 macrophages ¹⁵³, CD56, a marker for human natural killer cells ¹⁵⁴ and CD25, a marker for regulatory t-cells (Tregs) ¹⁵⁵ and activated cytotoxic t-cells displayed elevated expression levels in the hot carcinoma group. Interestingly, forkhead-box-protein P3 (Foxp3), a marker for Tregs linked to immunosuppression ^{156,157} was higher expressed in the cold subgroup (Ruoff et al, **Appendix 3**, Fig. 4C).

Again, various members of the Jak/Stat pathway displayed significant expression changes, i.e. Jak 2, STAT4, STAT1 and its active phospho-variant (Tyr701), which are all important mediators of cytokine response and immune cell activity ¹⁵⁸⁻¹⁶⁰, displayed increased expression in hot carcinomas (Ruoff et al, **Appendix 3**, Fig. 4C). Additionally, the programmed cell death 1 protein (PD1), a marker of immune cell activity ¹⁶¹, was enriched in the hot subgroup. Overall, these results indicate a higher immunological activity in the subgroup classified as hot carcinomas, supporting the previously established classification.

5.3.1. Increased Proliferative Activity and a More Competitive Phenotype is Observed in Hot Carcinomas

Samples in the hot subgroup generally displayed a more competitive phenotype. This was indicated by elevated expression levels of Src, calcium channel flower (FLOWER; C9orf7), hepatocyte growth factor receptor (c-Met) and forkhead box C1 (FoxC1), which are all factors linked to competitive growth and cancer invasiveness¹⁶²⁻¹⁶⁵. This was accompanied by lower expression of vascular endothelial cadherin (VE-cadherin), an adhesion molecule that is lost during late phases of mesenchymal-to-epithelial transition and is therefore considered as a marker for metastases formation¹⁶⁶. Additionally, higher expression of important cell cycle regulators (Cyclin B1, CDK1)¹⁶⁷ as well as phosphorylation of Histone H3 at Serine 10, an indication of mitosis¹⁶⁸, was observed in the hot subgroup. Appositely, expression of cell growth repressor E2F-4¹⁶⁹ was found to be decreased. Taken together, the data suggest that the expression of invasive-, competitive- and proliferative-markers facilitates the recognition of cancer cells by immune cells and contributes to higher infiltration rates.

5.3.2. Hot Carcinomas Display Higher Apoptotic Activity and Expression of Tumour-Suppressive Markers

DigiWest data showed that hot carcinomas displayed an increase in tumour-suppressive factors compared to cold carcinomas. This was indicated by increased phosphorylation of the tumour suppressors p53 (pSer20) and DBF2 kinase activator protein (MOB1; pThr35) as well as higher expression of tumorigenesis factor isocitrat-dehydrogenase 1 (IDH1)¹⁷⁰⁻¹⁷². Moreover, higher expression of cleaved Caspase 6 and 9, both promoting apoptosis^{173,174}, as well as pro-apoptosis factor Bax¹⁷⁵ was observed in hot carcinomas (Ruoff et al, **Appendix 3**, Fig. 4c, d). These results indicate that higher infiltration with immune cells induces tumour-suppressive signalling and leads to more apoptotic activity, which may contribute beneficially to patient outcome.

5.3.3. Cold Carcinomas Display Increased Expression of Immune-Suppressing Factors

The tumour co-marker PR, which was previously linked to an immunosuppressed tumor microenvironment (TME) ^{176,177}, showed the most notably increased expression in cold carcinomas (Ruoff et al., **Appendix 3**, Fig. 4b, c, Fig. 5c). Peroxisome proliferator-activated receptor gamma (PPAR γ), which is associated with immunosuppression ¹⁷⁸⁻¹⁸⁰ is also worth pointing out. Interestingly, phosphorylation of PPAR γ (Ser112) positively correlated with PR expression (Pearson's $r=0.45$, $P<0.0001$; Ruoff et al, **Appendix 3**, Fig. 5b), suggesting a co-expression of these factors. IHC staining of CD8, PR, PPAR γ and PPAR γ -pSer112 validated the predominant expression of PPAR γ -pSer112 by cancer cells in cold carcinomas (Ruoff et al, **Appendix 3**, Fig. 5a). To investigate the influence of PPAR γ -pSer112 on immune cell infiltration status the sample set was divided in elevated (greater than median) and decreased (lower than median) PPAR γ -pSer112 expression. Crucially, samples classified as cold carcinomas were significantly enriched in the group with elevated PPAR γ -pSer112 levels (Ruoff et al, **Appendix 3**, Fig. 5d; Fishers exact test, $p=0.0046$). Taken together, these data suggest that phosphorylation of PPAR γ might be involved in a mechanism of immune cell repulsion by breast cancer cells.

This study demonstrated that multiplexed immune cell marker assessment from fresh frozen resectates by DigiWest is feasible and that protein profiling of this sample type can provide functional signalling data valuable for patient stratification. Additionally, peak integration and several downstream analyses such as survival analysis as well as PANTHER pathway-, and clinical feature-enrichment were conducted by applying the novel DigiWest-Analyser and Evaluator software packages ²⁷. It was shown that the novel software pipeline facilitates data handling and integration of metadata, thus overcoming a bottleneck in the DigiWest workflow.

Chapter 6

General Discussion and Conclusion

6 General Discussion and Conclusion

With the advancement of precision medicine, molecular investigation of clinically relevant and disease-related samples for companion diagnostics and treatment evaluation is becoming more and more crucial in biomedical research¹⁸¹⁻¹⁸³. Gene and mRNA analysis methods like next generation sequencing and NanoString are state of the art in the field of precision medicine^{5,184}. Despite high sensitivity, throughput and robustness, technologies like NanoString require complex probe design and extensive data processing¹⁸⁴. These approaches can give valuable information about the origin of diseases. Yet, genetic information does not always translate into clinical practice. Hence, benefit for patients is often limited. This gap is largely attributable to the differences in genotype and phenotype^{185,186}. Therefore, methods able to investigate mechanisms of diseases on the protein level are of great need.

For a long time, imaged-based approaches like immunohistochemistry have been the gold standard for protein investigation in the clinical setting¹⁸⁷. These approaches can give valuable information about the spatial relationship of cells or proteins¹⁸⁸. However, these techniques are limited in throughput and number of investigated analytes. Even with the development of multiplexed immunohistochemistry and immunofluorescence, imaged based analysis is restricted to several analytes from one sample¹⁸⁹. Additionally, they require trained pathologists for evaluation and display high inter-observer variance, which is why quantification can be difficult¹⁸⁹.

State of the art methods for proteomic investigations are MS approaches^{190,191}. By analysing the mass to charge ratio (m/z) versus signal intensity, MS-based approaches are able to identify thousands of proteins, and generate protein profiles from human samples, to detect protein expression changes indicating diseases or treatment effects¹⁹⁰. Yet, MS analysis is expensive and demands large amounts of sample material. Analysis time and sensitivity, both crucial factors in the clinical setting, still require concessions in MS-based protein investigations¹⁹², making its implementation into routine biomedical use difficult¹³. Besides mass spectrometric approaches multiplexed immunoassays have become valuable tools in biomedical investigations. However, the linear dynamic

range of MS approaches and many multiplexed immunoassays is limited ^{193,194}. This plays a critical role in parallel detection of analytes from complex samples like human sera or tissue extracts, where high- and low-abundant proteins have to be measured in parallel. For example, concentrations of serum proteins can vary from the 1 g/L range for albumin or immunoglobulins to under 1 ng/L for signalling molecules such as cytokines ²⁹. Especially the enormous concentration range of proteins carrying post-translational modifications (PTM) like phosphorylation, can be challenging for the parallel detection in a single sample, and requires vast amount of material as well as specialised protocols. Yet, these PTMs are crucial to understand pathological mechanisms, since they indicate malfunctioning processes within cells ^{195,196}. The DigiWest is a multiplexed immunoassay, hence is limited by the availability and quality of supplied antibodies. However, the high dynamic range of the DigiWest approach ¹⁸ allows parallel detection of highly abundant proteins, as well as lowly concentrated PTMs from a single sample with limited protein amount available.

RPPA represent an alternative approach for antibody-based investigation of a vast number of proteins. With the RPPA approach, investigation of several hundred samples in one assay is feasible ¹⁷. Yet, the RPPA procedure is more time consuming, which can be a disadvantage in the clinical setting where sample processing time often plays a critical role. Especially in a diagnostic setting or for explorative clinical studies where a moderate number of samples has to be analysed quickly, the DigiWest approach is more suitable due to its time- and cost-effective nature. Additionally, the DigiWest output gives specific information about the molecular weight of the protein of interest, which is not given in RPPA analysis. This is especially useful for complex sample material where cross-reacting antibodies may lead to incorrect interpretation of signals ¹⁹⁷⁻¹⁹⁹. The DigiWest platform holds the advantage of selecting the correct signal at the molecular weight corresponding to the protein of interest, and therefore increases quality of generated data. These features make the DigiWest a compelling alternative for protein investigation of human sample material.

6.1. Multiplexed Serum Antibody Screening by DigiWest

Serum or plasma samples are among the most important human derived sample types. Since the outbreak of the Corona pandemic, the relevance of assay systems capable of monitoring sero-prevalence in the population has been emphasized ^{200,201}. These assays are required for monitoring antibody response induced by vaccine candidates and will help to understand the immune response after vaccination in pre-clinical and clinical trials ^{201,202}.

Additionally, the role of ADE in immunity and vaccination has recently been discussed ²⁰³⁻²⁰⁵. Detection of serum antibodies against endemic coronaviruses such as OC43, NL63 and 229E will add to the understanding of immune response against SARS-CoV-2.

Therefore, numerous assays that are able to detect humoral antibody response against corona viruses from sera or plasma samples have been developed. For example, the RPPA based VaxArray detects serum antibodies against nine different human CoV spike proteins from pandemic and endemic corona viruses ²⁰⁶. Besides its high throughput capability, this system is quantitative and displays a comparably good analytical sensitivity. Another assay, the MultiCoV-AB, utilizes six different SARS-CoV-2 antigens coupled to luminex beads, including full-length spike protein, receptor-binding domain (RBD) and full-length nucleocapsid protein ¹²⁴. By applying a combined cut-off, utilizing the full-length spike protein and RBD as antigens, a sensitivity of 90% and a specificity of 100% was achieved. However, like most serum screening platforms, these assays utilize recombinant proteins as antigens.

In the DigiWest system, authentic viral particles were employed to set up an assay system for parallel detection of humoral immune response against SARS-CoV-2 and three common cold coronaviruses. Applying antigens directly isolated from pathogens is a classical method for detecting serum antibodies as a surrogate for immune response ²⁰⁷. Challenges of this assay approach can be the need for large amounts of infectious pathogens and large batch-to-batch variability, when compared to recombinantly produced antigens or peptides. However, a major advantage of using authentic proteins instead of peptides or recombinant proteins is the detection of epitopes with post-translational modifications. Recombinant proteins expressed by bacteria often lack PTMs that are present on proteins

produced by mammalian cells, as in the case of viral infection ²⁰⁸. This can lead to the loss of crucial information about reactive serum antibodies against such PTMs. Another advantage is the fast and effective generation of protein extracts from various strains of pathogens, which is notably advantageous for the identification of cross-reacting antibodies. These characteristics make this approach especially useful for unbiased investigation of the humoral immune response after infection. By combining immobilization of antigens on microspheres and the Luminex assay readout, only 10 µg of pathogen protein is sufficient for thousands of serum analyses. The robustness of the Western-blot approach and the high throughput property of the Luminex platform facilitate good assay reproducibility. Additionally, this assay system has the ability to generate direct information about the size of the recognized protein. This can be an advantage for identifying antigenic proteins and protein variants. Screening sera from convalescent patients displayed a specific signal, corresponding to SARS-CoV-2 nucleocapsid ²⁰⁹. However, reactivity against other viral proteins was rather low. This could stem from the fact that DigiWest utilizes denatured and reduced proteins. These protein forms are not present during viral infection and are therefore not recognized by most serum antibodies. Comparison of the DigiWest assay for detecting anti-SARS-CoV-2 serum antibodies with serum-assays from Roche, Siemens and Euroimmun (IgG and IgA), which are used in clinical laboratories, displayed a high concordance between all assay systems. Highest concordances were found between test systems from Siemens and Euroimmun IgG as well as DigiWest and Roche. A reason for that could be that Siemens and Euroimmun IgG both are detecting spike protein, whereas the DigiWest and Roche assay both identify the nucleocapsid protein. Concomitantly, the weakest concordance to all other assays was displayed by the Euroimmun IgA assay, which can be attributed to the fact that this is the only assay detecting IgA antibodies.

When expanding the assay system to endemic coronaviruses (229E, NL63 and OC43), no indication of cross reactivity against SARS-CoV-2 proteins was observed, as was also seen in studies with similar approaches ^{124,206}. However, by utilizing the DigiWest serum screening assay assistance in neutralization of SARS-CoV-2 through prevalence of 229E specific IgGs was implicated ²¹⁰.

With the approach described above the serological analytical potential of DigiWest was demonstrated and this highly specific assay was set up within a short period

of time. The flexible nature of the DigiWest allows for integration of antigen extracts from various sources. Mixtures of antigens can be probed in parallel, which allows for detection of a vast variety of antibody responses in one assay.

6.2. Treatment Evaluation by Protein Analysis of FFPE Fixed Samples

In biomedical research, human tissue extracts are another valuable source of information. For histopathological examination, it is important to conserve the morphological structure of the tissue. Therefore, collected samples are routinely fixed with formalin and subsequently embedded in paraffin wax. This method of fixation facilitates sample handling and enables long-term storage at room temperature.

However, molecular changes induced through formalin fixation can make multiplexed protein analysis a challenge. Especially separation of proteins based on molecular size is difficult, since protein aggregates formed upon fixation lead to comparably low amounts of molecular weight-representative proteins. Hence, several extraction protocols for subsequent protein analysis have been developed. Despite being indeed clinical routine, the fixation process is not globally standardized. Fixation time can vary from one hour up to several days and may even be different within a given sample set. Fixation time has a negative influence on extracted protein amount⁵⁶. As is known from RNA extraction, over-fixation can lead to stronger crosslinking between analytes, which in turn makes extraction more difficult²¹¹⁻²¹³. Other factors that influence quality of the extracted sample material are storage time and conditions. For instance, humidity can lead to loss of protein and reduced antigenicity²¹⁴. Additionally, long-term exposure to oxygen can lead to oxidation of antigens and consequently reduce signals in antibody-dependent detection methods^{214,215}. Therefore, results can vary independently of the used extraction and analysis method, making comparison between different methods challenging²¹⁶. According to the literature, extraction is commonly performed in buffers containing detergents as well as reducing agents under application of high heat (95-100 °C) for 20-60 minutes followed by 1-3 h of moderate heat (60-80 °C)²¹⁶. To analyse protein expression in FFPE material with multiplexed immunoassays, it is vital to identify and validate antibodies, which can

detect proteins reliably after extraction. Antibodies suitable for immunohistochemistry are not always usable in most other immunoassays, even when investigating the same material. Huge efforts have been made to validate antibodies for expression analysis by DigiWest in FFPE samples^{20,61}; however, antibodies need to be tested for each tissue type individually.

In our study, minuscule macro-dissected punch biopsies of CIN were analysed. Protein extraction was performed by applying a combination of a modified heptane-based extraction protocol⁶¹ and protein concentration through a vacuum concentrator. Here, samples were heated for 20 minutes at 100 °C followed by 2 h at 80 °C. DigiWest could identify 69 antibodies suitable for protein expression analysis in FFPE fixed cervical punch biopsies, while 132 antibodies were tested in a human CSCC cell line, 44 antibodies were matching for both applications. Despite not originating from the same material, the observed overlap of antibody suitability for FFPE and non-fixed samples is comparable to literature^{61,216,217}. This facilitated the investigation of *in vivo* NIPP treatment of CIN and the comparison with NIPP-treated CSCC cells, which has not yet been reported in this fashion so far.

NIPP treatment induces cell cycle arrest followed by apoptosis¹³¹, which was demonstrated by a transient induction of CK8 and CK18, followed by downregulation of pro-proliferative factors, like Akt, p38 MAPK, Src and RAF. It has been shown that CK8/18 can act as a regulator of apoptosis and is released during apoptosis and necrosis^{130,141}, which can be independent of caspase activity¹⁴². Therefore, the observed results indicate that a cell survival response followed by apoptosis is directly induced through NIPP treatment. Both *in vivo* and *in vitro* NIPP treatment induced a significant reduction of expression and phosphorylation of the proto-oncogene tyrosine kinase Src, which is known to be upregulated in several tumour entities²¹⁸. Src is involved in many pro-proliferative cell responses and interacts with important regulatory factors^{135,136}. Concomitantly, many of these interaction factors, such as p38 and STAT3, showed a reduced expression after NIPP treatment of CSCC cells. Yet, this could not be confirmed by *in vivo* NIPP treatment of CIN, possibly due to differences in sample preparation, which in turn result in lower protein abundance and lower absolute intensities detected in FFPE samples. However, normalization to the total protein amount loaded on microspheres should compensate this effect. These

findings suggest that changes in protein expression observed in vitro may not always be translatable to in vivo treatment. This emphasises the relevance of protein investigation in human derived material for the consecutive analysis of treatment effects, which may differ substantially from results generated in cell culture experiments.

Overall, it has been demonstrated that the DigiWest enables extensive protein analysis from minuscule FFPE primary tissue biopsies for evaluation of treatment effects. The described approach was utilized in a clinical trial, investigating the therapeutic benefit of NIPP treatment directly in CIN patients. The generated results have been featured in a joined publication ²¹⁹.

6.3. Protein Profiling of Fresh Frozen Resectates and Assessment of Immune Cell Infiltration

Despite being infrequently available, fresh frozen tissue extracts are often preferred over FFPE tissue samples for molecular research, as no chemical modifications are made to the proteins ²²⁰. However, sample storage, processing and analysis needs to be firmly regulated and standardized to avoid artefacts through protein degradation ⁶⁴. In our study, we adapted the DigiWest system for the assessment of tumour-infiltrating immune cells in fresh frozen breast cancer biopsies.

The assessment of tumour infiltrating immune cells is a novel auxiliary factor for patient stratification, risk evaluation and treatment decision ^{109,221}. In colorectal cancer it has been shown that the immune score was an even better prognostic factor for survival than the classical TNM system ²²²⁻²²⁴. Several studies showed similar observations in breast cancer ¹¹³⁻¹¹⁷. Most of these studies use genetic approaches, evaluate immune cells in general, or assess individual markers with image-based methods, which can make quantification and evaluation challenging ¹⁵⁰.

Expression of several immune cell markers in the tumour tissue was investigated in parallel by adaptation of the DigiWest. Furthermore, protein expression profiles were compared between highly (hot) and lowly (cold) infiltrated tumours in order to elucidate biological mechanisms underlying the tumour immune response.

A problem for molecular investigation of fresh frozen biopsies is the spatial heterogeneity of tumour tissue. Parts of resectates may consist of different cell types and tumour content may vary between investigated samples or within a sample itself ^{225,226}. The DigiWest approach lacks spatial information that image-based methods can provide, however holds higher throughput and sensitivity. To avoid artificial differences in protein expression that arise when healthy and cancerous tissue extracts are directly compared, a pathologist assessed the tumour content of each sample before sample processing. Pathological examination revealed that only 60% of the enrolled samples displayed a tumour content of 50% or higher. Surprisingly, 2.5% of samples were even classified as healthy tissue. By applying a comparably high threshold of at least 50% tumour content ^{61,227}, the sample set size was reduced by app. 40%. This, however, increased data quality, since the investigated sample set became more homogenous, as was confirmed by measurement of common tumour markers such as Ki67 and CK8/18 in the analysis cohort and comparing them to control samples with less than 10% tumour content.

Following extensive protein expression analysis, covering cell cycle control, apoptosis, Jak/Stat-, MAPK-, Pi3K/Akt-, Wnt- and autophagic signalling as well as general tumour and immune-cell markers, assessment of immune infiltration, via DigiWest was evaluated. CD8 α , CD11c, CD16 and CD68 displayed similar expression profiles and a high correlation to each other. Unsupervised hierarchical cluster analysis, of these four markers revealed two distinct subgroups of tumours differing in immune cell infiltration (referred to as hot and cold carcinomas). By integrating a newly developed analysis and evaluation pipeline ²⁷, analysis of DigiWest results as well as integration of additional meta-data, such as survival-data, was facilitated. Hot carcinomas had a significantly better event free survival after primary surgery without any adjuvant treatments. Even though the four immune cell markers used for stratification represent general immune cell lineages, and not special cellular subtypes, this agrees with current literature ^{118,228-230}. These results indicate that patients with lower immune cell infiltration require stricter monitoring after primary surgery. The hot carcinoma subgroup displayed increased Jak/Stat signalling activity, which is important for cytokine response and immune cell activity ^{231,232}. This suggests that higher expression of members of the Jak/Stat signalling pathway may be an indicator for immune cell

infiltration. Gene expression analysis has shown that tumours with higher apoptotic activity also display elevated infiltration with immune cells ²³³. Concomitantly, increased expression of pro-apoptotic proteins was observed in samples with higher immune cell infiltration. In addition, cold carcinoma samples showed elevated levels FOXP3, a regulatory T-cell marker that propagate immunological tolerance ²³⁴⁻²³⁶, which may be a reason for the observed retention of immune cells. Interestingly phosphorylation of PPAR γ (pS112) was also enriched in these tumour samples. It has been proposed that PPAR γ is involved in an immune escape mechanism in muscle-invasive bladder cancer ²³⁷. Hence, this observation suggests, that breast cancer may harness a similar immune evasion mechanism. This makes PPAR γ phosphorylation a possible therapeutic target or marker for patient stratification.

By adapting and optimizing the DigiWest workflow, differential protein expression analysis in breast cancer resectates was achieved and important immune cell markers were assessed. The generated results demonstrate the unique potential of protein analysis from complex human samples such as fresh frozen biopsies by DigiWest.

6.4. Conclusion

The aim of precision medicine is to advance diagnosis, choice of therapy and monitoring of treatment effects. For this purpose, the need for molecular analysis tools for human sample material is ever increasing. Genome analysis and imaged based methods are the gold standard in this field. A shortcoming of genetic analysis is the fact that the genetic information does not always translate to the proteomic level. Hence, benefit for the patient is often limited. Therefore, it is crucial to include methods that can investigate pathological mechanisms on the proteomic level as well. Among the most important challenges for protein analysis in the clinical setting are the detection of multiple protein markers in parallel and the limited amount of available sample and time. Another challenge is the multitude of different sample types that need to be analysed. Most common types of clinical samples are FFPE or fresh frozen tissue extracts and bio fluids such as

blood samples, all of which offer unique challenges for molecular investigation. The DigiWest technology, a multiplexed immunoassay, combines the robustness of western blotting with the throughput and sensitivity of miniaturized assay systems. It is able to detect hundreds of proteins and protein variants from minimal amount of sample material. It has been demonstrated that its flexible nature makes it an attractive tool for protein analysis in all kinds of human specimen. Through modification of the DigiWest a novel serum-screening platform for the parallel detection of antibodies against different pathogens was developed and validated. By utilizing authentic antigens, serum screening against different antigens became possible in a short timeframe. Further, it was confirmed that protein analysis from minuscule amounts of complex samples such as FFPE cervical punch biopsies is achievable by this approach. Results generated from in vivo treated cells revealed similar proteomic changes as cell culture experiments. However, observed differences in particular protein expression also emphasizes the need for in vivo studies of treatment effects. Finally, multiplexed assessment of different immune cells and comparative protein analysis from fresh frozen resectates was achieved. With a newly developed analysis and evaluation pipeline integrative analysis of protein expression profiles and metadata could be performed ²⁷. In combination with clinical metadata, immune cell patterns indicating beneficial patient outcome were observed, and differences in expression of proteins and protein variants was investigated. This demonstrates the unique potential of the DigiWest to analyse proteins in human specimen. The ongoing development and improvement of this technique will enhance its potential for future applications in the biomedical field.

References

- 1 Collins, F. S. & Varmus, H. A new initiative on precision medicine. *N Engl J Med* **372**, 793-795, doi:10.1056/NEJMp1500523 (2015).
- 2 Dzaou, V. J. & Ginsburg, G. S. Realizing the Full Potential of Precision Medicine in Health and Health Care. *JAMA* **316**, 1659-1660, doi:10.1001/jama.2016.14117 (2016).
- 3 Letai, A. Functional precision cancer medicine-moving beyond pure genomics. *Nat Med* **23**, 1028-1035, doi:10.1038/nm.4389 (2017).
- 4 Ashley, E. A. Towards precision medicine. *Nat Rev Genet* **17**, 507-522, doi:10.1038/nrg.2016.86 (2016).
- 5 Roden, D. M. & Tyndale, R. F. Genomic medicine, precision medicine, personalized medicine: what's in a name? *Clin Pharmacol Ther* **94**, 169-172, doi:10.1038/clpt.2013.101 (2013).
- 6 West, H. J. No Solid Evidence, Only Hollow Argument for Universal Tumor Sequencing: Show Me the Data. *JAMA Oncol* **2**, 717-718, doi:10.1001/jamaoncol.2016.0075 (2016).
- 7 Zhang, M. *et al.* Evidence for the importance of post-transcriptional regulatory changes in ovarian cancer progression and the contribution of miRNAs. *Sci Rep* **7**, 8171, doi:10.1038/s41598-017-08502-z (2017).
- 8 Jiang, L. *et al.* A Quantitative Proteome Map of the Human Body. *Cell* **183**, 269-283 e219, doi:10.1016/j.cell.2020.08.036 (2020).
- 9 Akbani, R. *et al.* A pan-cancer proteomic perspective on The Cancer Genome Atlas. *Nat Commun* **5**, 3887, doi:10.1038/ncomms4887 (2014).
- 10 Klaeger, S. *et al.* The target landscape of clinical kinase drugs. *Science* **358**, doi:10.1126/science.aan4368 (2017).
- 11 Chong, B. E., Lubman, D. M., Rosenspire, A. & Miller, F. Protein profiles and identification of high performance liquid chromatography isolated proteins of cancer cell lines using matrix-assisted laser desorption/ionization time-of-flight mass spectrometry. *Rapid Commun Mass Spectrom* **12**, 1986-1993, doi:10.1002/(SICI)1097-0231(19981230)12:24<1986::AID-RCM419>3.0.CO;2-H (1998).
- 12 Chaurand, P., Stoeckli, M. & Caprioli, R. M. Direct profiling of proteins in biological tissue sections by MALDI mass spectrometry. *Anal Chem* **71**, 5263-5270, doi:10.1021/ac990781q (1999).
- 13 Longuespee, R. *et al.* Proteomics in Pathology. *Proteomics* **18**, 1700361, doi:10.1002/pmic.201700361 (2018).
- 14 Kulasingam, V., Prassas, I. & Diamandis, E. P. Towards personalized tumor markers. *NPJ Precis Oncol* **1**, 17, doi:10.1038/s41698-017-0021-2 (2017).
- 15 Jurgensmeier, J. M., Eder, J. P. & Herbst, R. S. New strategies in personalized medicine for solid tumors: molecular markers and clinical trial

References

- designs. *Clin Cancer Res* **20**, 4425-4435, doi:10.1158/1078-0432.CCR-13-0753 (2014).
- 16 Ellington, A. A., Kullo, I. J., Bailey, K. R. & Klee, G. G. Measurement and quality control issues in multiplex protein assays: a case study. *Clin Chem* **55**, 1092-1099, doi:10.1373/clinchem.2008.120717 (2009).
- 17 Akbani, R. *et al.* Realizing the promise of reverse phase protein arrays for clinical, translational, and basic research: a workshop report: the RPPA (Reverse Phase Protein Array) society. *Mol Cell Proteomics* **13**, 1625-1643, doi:10.1074/mcp.O113.034918 (2014).
- 18 Treindl, F. *et al.* A bead-based western for high-throughput cellular signal transduction analyses. *Nat Commun* **7**, 12852, doi:10.1038/ncomms12852 (2016).
- 19 Ellington, A. A., Kullo, I. J., Bailey, K. R. & Klee, G. G. Antibody-based protein multiplex platforms: technical and operational challenges. *Clin Chem* **56**, 186-193, doi:10.1373/clinchem.2009.127514 (2010).
- 20 Treindl, F. *et al.* Array-based Western-blotting reveals spatial differences in hepatic signaling and metabolism following CAR activation. *Arch Toxicol* **94**, 1265-1278, doi:10.1007/s00204-020-02680-y (2020).
- 21 Jevtic, M. *et al.* Impact of intercellular crosstalk between epidermal keratinocytes and dermal fibroblasts on skin homeostasis. *Biochim Biophys Acta Mol Cell Res* **1867**, 118722, doi:10.1016/j.bbamcr.2020.118722 (2020).
- 22 Naskou, J. *et al.* EZH2 Loss Drives Resistance to Carboplatin and Paclitaxel in Serous Ovarian Cancers Expressing ATM. *Mol Cancer Res* **18**, 278-286, doi:10.1158/1541-7786.MCR-19-0141 (2020).
- 23 Inder, S. *et al.* Multiplex profiling identifies clinically relevant signalling proteins in an isogenic prostate cancer model of radioresistance. *Sci Rep* **9**, 17325, doi:10.1038/s41598-019-53799-7 (2019).
- 24 Ekins, R. Chapter 2.5 - Ambient Analyte Assay in *The Immunoassay Handbook*, 109-121 (Elsevier, 2013).
- 25 Halder, A., Verma, A., Biswas, D. & Srivastava, S. Recent advances in mass-spectrometry based proteomics software, tools and databases. *Drug Discov Today Technol* **39**, 69-79, doi:10.1016/j.ddtec.2021.06.007 (2021).
- 26 Baryshnikova, A. Data libraries - the missing element for modeling biological systems. *FEBS J* **287**, 4594-4601, doi:10.1111/febs.15261 (2020).
- 27 Kersten, N. A software pipeline for fast and interpretable evaluation of high-content protein profile analyses. [Unpublished manuscript]. *Intelligent Systems and Production Engineering (ISPE)*, FZI Research Center for Information Technology, Karlsruhe, Germany (2022).
- 28 Kiseleva, O., Kurbatov, I., Ilgisonis, E. & Poverennaya, E. Defining Blood Plasma and Serum Metabolome by GC-MS. *Metabolites* **12**, 15, doi:10.3390/metabo12010015 (2021).

-
- 29 Anderson, N. L. & Anderson, N. G. The human plasma proteome: history, character, and diagnostic prospects. *Mol Cell Proteomics* **1**, 845-867, doi:10.1074/mcp.r200007-mcp200 (2002).
- 30 Jelkmann, W. Blut in *Physiologie*, Vol. 4 (Thieme, 2005).
- 31 Jacobs, J. M. *et al.* Utilizing human blood plasma for proteomic biomarker discovery. *J Proteome Res* **4**, 1073-1085, doi:10.1021/pr0500657 (2005).
- 32 Adkins, J. N. *et al.* Toward a human blood serum proteome: analysis by multidimensional separation coupled with mass spectrometry. *Mol Cell Proteomics* **1**, 947-955, doi:10.1074/mcp.m200066-mcp200 (2002).
- 33 Herrick, S., Blanc-Brude, O., Gray, A. & Laurent, G. Fibrinogen. *Int J Biochem Cell Biol* **31**, 741-746, doi:10.1016/s1357-2725(99)00032-1 (1999).
- 34 Hsieh, S. Y., Chen, R. K., Pan, Y. H. & Lee, H. L. Systematical evaluation of the effects of sample collection procedures on low-molecular-weight serum/plasma proteome profiling. *Proteomics* **6**, 3189-3198, doi:10.1002/pmic.200500535 (2006).
- 35 Villanueva, J. *et al.* Correcting common errors in identifying cancer-specific serum peptide signatures. *J Proteome Res* **4**, 1060-1072, doi:10.1021/pr050034b (2005).
- 36 Lima-Oliveira, G., Monneret, D., Guerber, F. & Guidi, G. C. Sample management for clinical biochemistry assays: Are serum and plasma interchangeable specimens? *Crit Rev Clin Lab Sci* **55**, 480-500, doi:10.1080/10408363.2018.1499708 (2018).
- 37 Lum, G. & Gambino, S. R. A comparison of serum versus heparinized plasma for routine chemistry tests. *Am J Clin Pathol* **61**, 108-113, doi:10.1093/ajcp/61.1.108 (1974).
- 38 Ladenson, J. H., Tsai, L. M., Michael, J. M., Kessler, G. & Joist, J. H. Serum versus heparinized plasma for eighteen common chemistry tests: is serum the appropriate specimen? *Am J Clin Pathol* **62**, 545-552, doi:10.1093/ajcp/62.4.545 (1974).
- 39 Dumas, B. T., Hause, L. L., Simuncak, D. M. & Breitenfeld, D. Differences between values for plasma and serum in tests performed in the Ektachem 700 XR Analyzer, and evaluation of "plasma separator tubes (PST)". *Clin Chem* **35**, 151-153 (1989).
- 40 Katrukha, A., Bereznikova, A., Filatov, V. & Esakova, T. Biochemical factors influencing measurement of cardiac troponin I in serum. *Clin Chem Lab Med* **37**, 1091-1095, doi:10.1515/CCLM.1999.159 (1999).
- 41 Zhao, X. *et al.* Pre-analytical effects of blood sampling and handling in quantitative immunoassays for rheumatoid arthritis. *J Immunol Methods* **378**, 72-80, doi:10.1016/j.jim.2012.02.007 (2012).
- 42 Castro, C. & Gourley, M. Diagnostic testing and interpretation of tests for autoimmunity. *J Allergy Clin Immunol* **125**, S238-247, doi:10.1016/j.jaci.2009.09.041 (2010).

- 43 Chan, Y. *et al.* Determining seropositivity-A review of approaches to define population seroprevalence when using multiplex bead assays to assess burden of tropical diseases. *PLoS Negl Trop Dis* **15**, e0009457, doi:10.1371/journal.pntd.0009457 (2021).
- 44 Gustafsson, O. J., Arentz, G. & Hoffmann, P. Proteomic developments in the analysis of formalin-fixed tissue. *Biochim Biophys Acta* **1854**, 559-580, doi:10.1016/j.bbapap.2014.10.003 (2015).
- 45 O'Rourke, M. B. & Padula, M. P. Analysis of formalin-fixed, paraffin-embedded (FFPE) tissue via proteomic techniques and misconceptions of antigen retrieval. *Biotechniques* **60**, 229-238, doi:10.2144/000114414 (2016).
- 46 Gorzolka, K. & Walch, A. MALDI mass spectrometry imaging of formalin-fixed paraffin-embedded tissues in clinical research. *Histol Histopathol* **29**, 1365-1376, doi:10.14670/HH-29.1365 (2014).
- 47 Fowler, C. B., Cunningham, R. E., O'Leary, T. J. & Mason, J. T. 'Tissue surrogates' as a model for archival formalin-fixed paraffin-embedded tissues. *Lab Invest* **87**, 836-846, doi:10.1038/labinvest.3700596 (2007).
- 48 Donczo, B. & Guttman, A. Biomedical analysis of formalin-fixed, paraffin-embedded tissue samples: The Holy Grail for molecular diagnostics. *J Pharm Biomed Anal* **155**, 125-134, doi:10.1016/j.jpba.2018.03.065 (2018).
- 49 Nirmalan, N. J., Harnden, P., Selby, P. J. & Banks, R. E. Mining the archival formalin-fixed paraffin-embedded tissue proteome: opportunities and challenges. *Mol Biosyst* **4**, 712-720, doi:10.1039/b800098k (2008).
- 50 Zhang, Y. *et al.* Unrestricted modification search reveals lysine methylation as major modification induced by tissue formalin fixation and paraffin embedding. *Proteomics* **15**, 2568-2579, doi:10.1002/pmic.201400454 (2015).
- 51 Puchtler, H. & Meloan, S. N. On the chemistry of formaldehyde fixation and its effects on immunohistochemical reactions. *Histochemistry* **82**, 201-204, doi:10.1007/BF00501395 (1985).
- 52 Specht, K. *et al.* Quantitative gene expression analysis in microdissected archival formalin-fixed and paraffin-embedded tumor tissue. *Am J Pathol* **158**, 419-429, doi:10.1016/S0002-9440(10)63985-5 (2001).
- 53 Palmer-Toy, D. E., Krastins, B., Sarracino, D. A., Nadol, J. B., Jr. & Merchant, S. N. Efficient method for the proteomic analysis of fixed and embedded tissues. *J Proteome Res* **4**, 2404-2411, doi:10.1021/pr050208p (2005).
- 54 Holfeld, A., Valdes, A., Malmstrom, P. U., Segersten, U. & Lind, S. B. Parallel Proteomic Workflow for Mass Spectrometric Analysis of Tissue Samples Preserved by Different Methods. *Anal Chem* **90**, 5841-5849, doi:10.1021/acs.analchem.8b00379 (2018).
- 55 Mansour, A., Chatila, R., Bejjani, N., Dagher, C. & Faour, W. H. A novel xylene-free deparaffinization method for the extraction of proteins from human derived formalin-fixed paraffin embedded (FFPE) archival tissue blocks. *MethodsX* **1**, 90-95, doi:10.1016/j.mex.2014.07.006 (2014).

-
- 56 Wolff, C., Schott, C., Porschewski, P., Reischauer, B. & Becker, K. F. Successful protein extraction from over-fixed and long-term stored formalin-fixed tissues. *PLoS One* **6**, e16353, doi:10.1371/journal.pone.0016353 (2011).
- 57 Chung, J. Y. *et al.* A well-based reverse-phase protein array applicable to extracts from formalin-fixed paraffin-embedded tissue. *Proteomics Clin Appl* **2**, 1539-1547, doi:10.1002/prca.200800005 (2008).
- 58 Wimmer, I. *et al.* Systematic evaluation of RNA quality, microarray data reliability and pathway analysis in fresh, fresh frozen and formalin-fixed paraffin-embedded tissue samples. *Sci Rep* **8**, 6351, doi:10.1038/s41598-018-24781-6 (2018).
- 59 Foll, M. C. *et al.* Reproducible proteomics sample preparation for single FFPE tissue slices using acid-labile surfactant and direct trypsinization. *Clin Proteomics* **15**, 11, doi:10.1186/s12014-018-9188-y (2018).
- 60 Shi, S. R., Cote, R. J. & Taylor, C. R. Antigen retrieval immunohistochemistry: past, present, and future. *J Histochem Cytochem* **45**, 327-343, doi:10.1177/002215549704500301 (1997).
- 61 Bockmayr, T. *et al.* Multiclass cancer classification in fresh frozen and formalin-fixed paraffin-embedded tissue by DigiWest multiplex protein analysis. *Lab Invest* **100**, 1288-1299, doi:10.1038/s41374-020-0455-y (2020).
- 62 Chatterjee, S. Artefacts in histopathology. *J Oral Maxillofac Pathol* **18**, S111-116, doi:10.4103/0973-029X.141346 (2014).
- 63 Meng, H. *et al.* Tissue triage and freezing for models of skeletal muscle disease. *J Vis Exp*, e51586, doi:10.3791/51586 (2014).
- 64 Morente, M. M. *et al.* TuBaFrost 2: Standardising tissue collection and quality control procedures for a European virtual frozen tissue bank network. *Eur J Cancer* **42**, 2684-2691, doi:10.1016/j.ejca.2006.04.029 (2006).
- 65 Vrana, M., Goodling, A., Afkarian, M. & Prasad, B. An Optimized Method for Protein Extraction from OCT-Embedded Human Kidney Tissue for Protein Quantification by LC-MS/MS Proteomics. *Drug Metab Dispos* **44**, 1692-1696, doi:10.1124/dmd.116.071522 (2016).
- 66 Johnson, H. & White, F. M. Quantitative analysis of signaling networks across differentially embedded tumors highlights interpatient heterogeneity in human glioblastoma. *J Proteome Res* **13**, 4581-4593, doi:10.1021/pr500418w (2014).
- 67 Young D, B. E., Haverstick D. Specimen collection and other preanalytical variables. in *Fundamentals of clinical chemistry.*, pages 42–62 (Saunders Elsevier, 2008).
- 68 Zhao, X. *et al.* Quantitative Proteomic Analysis of Optimal Cutting Temperature (OCT) Embedded Core-Needle Biopsy of Lung Cancer. *J Am Soc Mass Spectrom* **28**, 2078-2089, doi:10.1007/s13361-017-1706-z (2017).

References

- 69 Zhang, W., Sakashita, S., Taylor, P., Tsao, M. S. & Moran, M. F. Comprehensive proteome analysis of fresh frozen and optimal cutting temperature (OCT) embedded primary non-small cell lung carcinoma by LC-MS/MS. *Methods* **81**, 50-55, doi:10.1016/j.ymeth.2015.02.008 (2015).
- 70 Dapic, I. *et al.* Proteome analysis of tissues by mass spectrometry. *Mass Spectrom Rev* **38**, 403-441, doi:10.1002/mas.21598 (2019).
- 71 Zhu, N. *et al.* A Novel Coronavirus from Patients with Pneumonia in China, 2019. *N Engl J Med* **382**, 727-733, doi:10.1056/NEJMoa2001017 (2020).
- 72 Mofijur, M. *et al.* Impact of COVID-19 on the social, economic, environmental and energy domains: Lessons learnt from a global pandemic. *Sustain Prod Consum* **26**, 343-359, doi:10.1016/j.spc.2020.10.016 (2021).
- 73 Corman, V. M., Muth, D., Niemeyer, D. & Drosten, C. Hosts and Sources of Endemic Human Coronaviruses. *Adv Virus Res* **100**, 163-188, doi:10.1016/bs.aivir.2018.01.001 (2018).
- 74 Huang, A. T. *et al.* A systematic review of antibody mediated immunity to coronaviruses: kinetics, correlates of protection, and association with severity. *Nat Commun* **11**, 4704, doi:10.1038/s41467-020-18450-4 (2020).
- 75 Su, S. *et al.* Epidemiology, Genetic Recombination, and Pathogenesis of Coronaviruses. *Trends Microbiol* **24**, 490-502, doi:10.1016/j.tim.2016.03.003 (2016).
- 76 Wu, A. *et al.* Genome Composition and Divergence of the Novel Coronavirus (2019-nCoV) Originating in China. *Cell Host Microbe* **27**, 325-328, doi:10.1016/j.chom.2020.02.001 (2020).
- 77 Li, W. *et al.* Angiotensin-converting enzyme 2 is a functional receptor for the SARS coronavirus. *Nature* **426**, 450-454, doi:10.1038/nature02145 (2003).
- 78 Hoffmann, M. *et al.* SARS-CoV-2 Cell Entry Depends on ACE2 and TMPRSS2 and Is Blocked by a Clinically Proven Protease Inhibitor. *Cell* **181**, 271-280 e278, doi:10.1016/j.cell.2020.02.052 (2020).
- 79 Bai, Z., Cao, Y., Liu, W. & Li, J. The SARS-CoV-2 Nucleocapsid Protein and Its Role in Viral Structure, Biological Functions, and a Potential Target for Drug or Vaccine Mitigation. *Viruses* **13**, 1115, doi:10.3390/v13061115 (2021).
- 80 Kumar V, A. A., Fausto N, Mitchell RN Cervical Dysplasia: Overview, Risk Factors. in *Robbins Basic Pathology* 718–721 (Saunders Elsevier, 2007).
- 81 Ferlay, J. *et al.* Cancer incidence and mortality worldwide: sources, methods and major patterns in GLOBOCAN 2012. *Int J Cancer* **136**, E359-386, doi:10.1002/ijc.29210 (2015).
- 82 Zhou, W. *et al.* Survey of cervical cancer survivors regarding quality of life and sexual function. *J Cancer Res Ther* **12**, 938-944, doi:10.4103/0973-1482.175427 (2016).
- 83 Nayar, R. & Wilbur, D. C. The Bethesda System for Reporting Cervical Cytology: A Historical Perspective. *Acta Cytol* **61**, 359-372, doi:10.1159/000477556 (2017).

- 84 Mathevet, P., Dargent, D., Roy, M. & Beau, G. A randomized prospective study comparing three techniques of conization: cold knife, laser, and LEEP. *Gynecol Oncol* **54**, 175-179, doi:10.1006/gyno.1994.1189 (1994).
- 85 Kyrgiou, M. *et al.* Obstetric outcomes after conservative treatment for cervical intraepithelial lesions and early invasive disease. *Cochrane Database Syst Rev* **11**, CD012847, doi:10.1002/14651858.CD012847 (2017).
- 86 Sadler, L. *et al.* Treatment for cervical intraepithelial neoplasia and risk of preterm delivery. *JAMA* **291**, 2100-2106, doi:10.1001/jama.291.17.2100 (2004).
- 87 Jakobsson, M., Gissler, M., Paavonen, J. & Tapper, A. M. Long-term mortality in women treated for cervical intraepithelial neoplasia. *BJOG* **116**, 838-844, doi:10.1111/j.1471-0528.2009.02115.x (2009).
- 88 McIndoe, W. A., McLean, M. R., Jones, R. W. & Mullins, P. R. The invasive potential of carcinoma in situ of the cervix. *Obstet Gynecol* **64**, 451-458 (1984).
- 89 Ostor, A. G. Natural history of cervical intraepithelial neoplasia: a critical review. *Int J Gynecol Pathol* **12**, 186-192 (1993).
- 90 Wenzel, T. *et al.* Trans-Mucosal Efficacy of Non-Thermal Plasma Treatment on Cervical Cancer Tissue and Human Cervix Uteri by a Next Generation Electrosurgical Argon Plasma Device. *Cancers (Basel)* **12**, 267, doi:10.3390/cancers12020267 (2020).
- 91 Hirst, A. M., Frame, F. M., Arya, M., Maitland, N. J. & O'Connell, D. Low temperature plasmas as emerging cancer therapeutics: the state of play and thoughts for the future. *Tumour Biol* **37**, 7021-7031, doi:10.1007/s13277-016-4911-7 (2016).
- 92 Mitra, S. *et al.* Impact of ROS Generated by Chemical, Physical, and Plasma Techniques on Cancer Attenuation. *Cancers (Basel)* **11**, 1030, doi:10.3390/cancers11071030 (2019).
- 93 Koensgen, D. *et al.* Cold Atmospheric Plasma (CAP) and CAP-Stimulated Cell Culture Media Suppress Ovarian Cancer Cell Growth - A Putative Treatment Option in Ovarian Cancer Therapy. *Anticancer Res* **37**, 6739-6744, doi:10.21873/anticancerres.12133 (2017).
- 94 Weiss, M. *et al.* Inhibition of Cell Growth of the Prostate Cancer Cell Model LNCaP by Cold Atmospheric Plasma. *In Vivo* **29**, 611-616 (2015).
- 95 Weiss, M. *et al.* Cold Atmospheric Plasma Treatment Induces Anti-Proliferative Effects in Prostate Cancer Cells by Redox and Apoptotic Signaling Pathways. *PLoS One* **10**, e0130350, doi:10.1371/journal.pone.0130350 (2015).
- 96 Brany, D., Dvorska, D., Halasova, E. & Skovierova, H. Cold Atmospheric Plasma: A Powerful Tool for Modern Medicine. *Int J Mol Sci* **21**, doi:10.3390/ijms21082932 (2020).
- 97 Sung, H. *et al.* Global Cancer Statistics 2020: GLOBOCAN Estimates of Incidence and Mortality Worldwide for 36 Cancers in 185 Countries. *CA Cancer J Clin* **71**, 209-249, doi:10.3322/caac.21660 (2021).

References

- 98 Henry-Tillman, R. S. & Klimberg, V. S. In situ breast cancer. *Curr Treat Options Oncol* **1**, 199-209, doi:10.1007/s11864-000-0031-z (2000).
- 99 Hergueta-Redondo, M., Palacios, J., Cano, A. & Moreno-Bueno, G. "New" molecular taxonomy in breast cancer. *Clin Transl Oncol* **10**, 777-785, doi:10.1007/s12094-008-0290-x (2008).
- 100 Sims, A. H., Howell, A., Howell, S. J. & Clarke, R. B. Origins of breast cancer subtypes and therapeutic implications. *Nat Clin Pract Oncol* **4**, 516-525, doi:10.1038/ncponc0908 (2007).
- 101 Zhang, M. H., Man, H. T., Zhao, X. D., Dong, N. & Ma, S. L. Estrogen receptor-positive breast cancer molecular signatures and therapeutic potentials (Review). *Biomed Rep* **2**, 41-52, doi:10.3892/br.2013.187 (2014).
- 102 Goldhirsch, A. *et al.* Personalizing the treatment of women with early breast cancer: highlights of the St Gallen International Expert Consensus on the Primary Therapy of Early Breast Cancer 2013. *Ann Oncol* **24**, 2206-2223, doi:10.1093/annonc/mdt303 (2013).
- 103 Perou, C. M. *et al.* Molecular portraits of human breast tumours. *Nature* **406**, 747-752, doi:10.1038/35021093 (2000).
- 104 Meisel, J. L., Venur, V. A., Gnant, M. & Carey, L. Evolution of Targeted Therapy in Breast Cancer: Where Precision Medicine Began. *Am Soc Clin Oncol Educ Book* **38**, 78-86, doi:10.1200/EDBK_201037 (2018).
- 105 Slamon, D. J. *et al.* Use of chemotherapy plus a monoclonal antibody against HER2 for metastatic breast cancer that overexpresses HER2. *N Engl J Med* **344**, 783-792, doi:10.1056/NEJM200103153441101 (2001).
- 106 Sparano, J. A. *et al.* Clinical and Genomic Risk to Guide the Use of Adjuvant Therapy for Breast Cancer. *N Engl J Med* **380**, 2395-2405, doi:10.1056/NEJMoa1904819 (2019).
- 107 Buyse, M. *et al.* Validation and clinical utility of a 70-gene prognostic signature for women with node-negative breast cancer. *J Natl Cancer Inst* **98**, 1183-1192, doi:10.1093/jnci/djj329 (2006).
- 108 Wallden, B. *et al.* Development and verification of the PAM50-based Prosigna breast cancer gene signature assay. *BMC Med Genomics* **8**, 54, doi:10.1186/s12920-015-0129-6 (2015).
- 109 Binnewies, M. *et al.* Understanding the tumor immune microenvironment (TIME) for effective therapy. *Nat Med* **24**, 541-550, doi:10.1038/s41591-018-0014-x (2018).
- 110 Ingold Heppner, B., Loibl, S. & Denkert, C. Tumor-Infiltrating Lymphocytes: A Promising Biomarker in Breast Cancer. *Breast Care (Basel)* **11**, 96-100, doi:10.1159/000444357 (2016).
- 111 Stanton, S. E. & Disis, M. L. Clinical significance of tumor-infiltrating lymphocytes in breast cancer. *J Immunother Cancer* **4**, 59, doi:10.1186/s40425-016-0165-6 (2016).
- 112 Mair, F. *et al.* Extricating human tumour immune alterations from tissue inflammation. *Nature*, doi:10.1038/s41586-022-04718-w (2022).

- 113 Ali, H. R., Chlon, L., Pharoah, P. D., Markowitz, F. & Caldas, C. Patterns of Immune Infiltration in Breast Cancer and Their Clinical Implications: A Gene-Expression-Based Retrospective Study. *PLoS Med* **13**, e1002194, doi:10.1371/journal.pmed.1002194 (2016).
- 114 Aran, D., Hu, Z. & Butte, A. J. xCell: digitally portraying the tissue cellular heterogeneity landscape. *Genome Biol* **18**, 220, doi:10.1186/s13059-017-1349-1 (2017).
- 115 Ali, H. R. *et al.* Association between CD8+ T-cell infiltration and breast cancer survival in 12,439 patients. *Ann Oncol* **25**, 1536-1543, doi:10.1093/annonc/mdu191 (2014).
- 116 Loi, S. *et al.* Tumor infiltrating lymphocytes are prognostic in triple negative breast cancer and predictive for trastuzumab benefit in early breast cancer: results from the FinHER trial. *Ann Oncol* **25**, 1544-1550, doi:10.1093/annonc/mdu112 (2014).
- 117 Nelson, M. A., Ngamcherdtrakul, W., Luoh, S. W. & Yantasee, W. Prognostic and therapeutic role of tumor-infiltrating lymphocyte subtypes in breast cancer. *Cancer Metastasis Rev* **40**, 519-536, doi:10.1007/s10555-021-09968-0 (2021).
- 118 Salgado, R. *et al.* The evaluation of tumor-infiltrating lymphocytes (TILs) in breast cancer: recommendations by an International TILs Working Group 2014. *Ann Oncol* **26**, 259-271, doi:10.1093/annonc/mdu450 (2015).
- 119 Darvishian, F. *et al.* Macrophage density is an adverse prognosticator for ipsilateral recurrence in ductal carcinoma in situ. *Breast* **64**, 35-40, doi:10.1016/j.breast.2022.04.004 (2022).
- 120 Arvin, A. M. *et al.* A perspective on potential antibody-dependent enhancement of SARS-CoV-2. *Nature* **584**, 353-363, doi:10.1038/s41586-020-2538-8 (2020).
- 121 Tetro, J. A. Is COVID-19 receiving ADE from other coronaviruses? *Microbes Infect* **22**, 72-73, doi:10.1016/j.micinf.2020.02.006 (2020).
- 122 Shrock, E. *et al.* Viral epitope profiling of COVID-19 patients reveals cross-reactivity and correlates of severity. *Science* **370**, eabd4250, doi:10.1126/science.abd4250 (2020).
- 123 Amanat, F. *et al.* A serological assay to detect SARS-CoV-2 seroconversion in humans. *Nat Med* **26**, 1033-1036, doi:10.1038/s41591-020-0913-5 (2020).
- 124 Becker, M. *et al.* Exploring beyond clinical routine SARS-CoV-2 serology using MultiCoV-Ab to evaluate endemic coronavirus cross-reactivity. *Nat Commun* **12**, 1152, doi:10.1038/s41467-021-20973-3 (2021).
- 125 Fink, S. *et al.* Multiplexed Serum Antibody Screening Platform Using Virus Extracts from Endemic Coronaviridae and SARS-CoV-2. *ACS Infect Dis* **7**, 1596-1606, doi:10.1021/acsinfecdis.0c00725 (2021).
- 126 Nelde, A. *et al.* SARS-CoV-2-derived peptides define heterologous and COVID-19-induced T cell recognition. *Nat Immunol* **22**, 74-85, doi:10.1038/s41590-020-00808-x (2021).

References

- 127 Tang, M. S. *et al.* Clinical Performance of Two SARS-CoV-2 Serologic Assays. *Clin Chem* **66**, 1055-1062, doi:10.1093/clinchem/hvaa120 (2020).
- 128 Tang, M. S. *et al.* Clinical Performance of the Roche SARS-CoV-2 Serologic Assay. *Clin Chem* **66**, 1107-1109, doi:10.1093/clinchem/hvaa132 (2020).
- 129 Weiss, M. *et al.* Dose-Dependent Tissue-Level Characterization of a Medical Atmospheric Pressure Argon Plasma Jet. *ACS Appl Mater Interfaces* **11**, 19841-19853, doi:10.1021/acsami.9b04803 (2019).
- 130 Dubuc, A. *et al.* Use of cold-atmospheric plasma in oncology: a concise systematic review. *Ther Adv Med Oncol* **10**, 1758835918786475, doi:10.1177/1758835918786475 (2018).
- 131 Weiss, M. & Stope, M. B. Physical plasma: a new treatment option in gynecological oncology. *Arch Gynecol Obstet* **298**, 853-855, doi:10.1007/s00404-018-4889-z (2018).
- 132 Ruoff, F. *et al.* Targeted Protein Profiling of In Vivo NIPP-Treated Tissues Using DigiWest Technology. *Applied Sciences* **11**, 11238, doi:10.3390/app112311238 (2021).
- 133 Kyriakis, J. M. *et al.* Raf-1 activates MAP kinase-kinase. *Nature* **358**, 417-421, doi:10.1038/358417a0 (1992).
- 134 Shaul, Y. D. & Seger, R. The MEK/ERK cascade: from signaling specificity to diverse functions. *Biochim Biophys Acta* **1773**, 1213-1226, doi:10.1016/j.bbamcr.2006.10.005 (2007).
- 135 Abeyrathna, P. & Su, Y. The critical role of Akt in cardiovascular function. *Vascul Pharmacol* **74**, 38-48, doi:10.1016/j.vph.2015.05.008 (2015).
- 136 Ram, P. T. & Iyengar, R. G protein coupled receptor signaling through the Src and Stat3 pathway: role in proliferation and transformation. *Oncogene* **20**, 1601-1606, doi:10.1038/sj.onc.1204186 (2001).
- 137 Yuan, Z. L. *et al.* Central role of the threonine residue within the p+1 loop of receptor tyrosine kinase in STAT3 constitutive phosphorylation in metastatic cancer cells. *Mol Cell Biol* **24**, 9390-9400, doi:10.1128/MCB.24.21.9390-9400.2004 (2004).
- 138 Abbas, T. & Dutta, A. p21 in cancer: intricate networks and multiple activities. *Nat Rev Cancer* **9**, 400-414, doi:10.1038/nrc2657 (2009).
- 139 Harper, J. W., Adami, G. R., Wei, N., Keyomarsi, K. & Elledge, S. J. The p21 Cdk-interacting protein Cip1 is a potent inhibitor of G1 cyclin-dependent kinases. *Cell* **75**, 805-816, doi:10.1016/0092-8674(93)90499-g (1993).
- 140 Weng, Y. R., Cui, Y. & Fang, J. Y. Biological functions of cytokeratin 18 in cancer. *Mol Cancer Res* **10**, 485-493, doi:10.1158/1541-7786.MCR-11-0222 (2012).
- 141 Sirnio, P. *et al.* Systemic inflammation is associated with circulating cell death released keratin 18 fragments in colorectal cancer. *Oncoimmunology* **9**, 1783046, doi:10.1080/2162402X.2020.1783046 (2020).

- 142 Abraham, M. C. & Shaham, S. Death without caspases, caspases without death. *Trends Cell Biol* **14**, 184-193, doi:10.1016/j.tcb.2004.03.002 (2004).
- 143 Li, Y., Dowbenko, D. & Lasky, L. A. AKT/PKB phosphorylation of p21Cip/WAF1 enhances protein stability of p21Cip/WAF1 and promotes cell survival. *J Biol Chem* **277**, 11352-11361, doi:10.1074/jbc.M109062200 (2002).
- 144 Nicholson, K. M. & Anderson, N. G. The protein kinase B/Akt signalling pathway in human malignancy. *Cell Signal* **14**, 381-395, doi:10.1016/s0898-6568(01)00271-6 (2002).
- 145 Smolarz, B., Nowak, A. Z. & Romanowicz, H. Breast Cancer-Epidemiology, Classification, Pathogenesis and Treatment (Review of Literature). *Cancers (Basel)* **14**, doi:10.3390/cancers14102569 (2022).
- 146 Hewitt, K. *et al.* The Evolution of Our Understanding of the Biology of Cancer Is the Key to Avoiding Overdiagnosis and Overtreatment. *Cancer Epidemiol Biomarkers Prev* **29**, 2463-2474, doi:10.1158/1055-9965.EPI-20-0110 (2020).
- 147 Topalian, S. L., Drake, C. G. & Pardoll, D. M. Immune checkpoint blockade: a common denominator approach to cancer therapy. *Cancer Cell* **27**, 450-461, doi:10.1016/j.ccell.2015.03.001 (2015).
- 148 Szeitz, B. *et al.* Investigating the Prognostic Relevance of Tumor Immune Microenvironment and Immune Gene Assembly in Breast Carcinoma Subtypes. *Cancers (Basel)* **14**, doi:10.3390/cancers14081942 (2022).
- 149 Adams, S. *et al.* Prognostic value of tumor-infiltrating lymphocytes in triple-negative breast cancers from two phase III randomized adjuvant breast cancer trials: ECOG 2197 and ECOG 1199. *J Clin Oncol* **32**, 2959-2966, doi:10.1200/JCO.2013.55.0491 (2014).
- 150 Locy, H. *et al.* Assessing Tumor-Infiltrating Lymphocytes in Breast Cancer: A Proposal for Combining Immunohistochemistry and Gene Expression Analysis to Refine Scoring. *Front Immunol* **13**, 794175, doi:10.3389/fimmu.2022.794175 (2022).
- 151 Jaiswal, A. *et al.* An activation to memory differentiation trajectory of tumor-infiltrating lymphocytes informs metastatic melanoma outcomes. *Cancer Cell* **40**, 524-544 e525, doi:10.1016/j.ccell.2022.04.005 (2022).
- 152 Ruoff, F. *et al.* Protein Profiling of Breast Carcinomas Reveals Expression of Immune-Suppressive Factors and Signatures Relevant for Patient Outcome. *Cancers* **14**, 4542, doi:10.3390/cancers14184542 (2022).
- 153 Komohara, Y., Jinushi, M. & Takeya, M. Clinical significance of macrophage heterogeneity in human malignant tumors. *Cancer Sci* **105**, 1-8, doi:10.1111/cas.12314 (2014).
- 154 Robertson, M. J. & Ritz, J. Biology and clinical relevance of human natural killer cells. *Blood* **76**, 2421-2438 (1990).
- 155 Fehervari, Z., Yamaguchi, T. & Sakaguchi, S. The dichotomous role of IL-2: tolerance versus immunity. *Trends Immunol* **27**, 109-111, doi:10.1016/j.it.2006.01.005 (2006).

References

- 156 Ochs, H. D., Gambineri, E. & Torgerson, T. R. IPEX, FOXP3 and regulatory T-cells: a model for autoimmunity. *Immunol Res* **38**, 112-121, doi:10.1007/s12026-007-0022-2 (2007).
- 157 Mercer, F. & Unutmaz, D. The biology of FoxP3: a key player in immune suppression during infections, autoimmune diseases and cancer. *Adv Exp Med Biol* **665**, 47-59, doi:10.1007/978-1-4419-1599-3_4 (2009).
- 158 Thierfelder, W. E. *et al.* Requirement for Stat4 in interleukin-12-mediated responses of natural killer and T cells. *Nature* **382**, 171-174, doi:10.1038/382171a0 (1996).
- 159 Ihle, J. N. *et al.* Signaling by the cytokine receptor superfamily: JAKs and STATs. *Trends Biochem Sci* **19**, 222-227, doi:10.1016/0968-0004(94)90026-4 (1994).
- 160 Leonard, W. J. & O'Shea, J. J. Jaks and STATs: biological implications. *Annu Rev Immunol* **16**, 293-322, doi:10.1146/annurev.immunol.16.1.293 (1998).
- 161 Nishimura, H., Nose, M., Hiai, H., Minato, N. & Honjo, T. Development of lupus-like autoimmune diseases by disruption of the PD-1 gene encoding an ITIM motif-carrying immunoreceptor. *Immunity* **11**, 141-151, doi:10.1016/s1074-7613(00)80089-8 (1999).
- 162 Thomas, S. M. & Brugge, J. S. Cellular functions regulated by Src family kinases. *Annu Rev Cell Dev Biol* **13**, 513-609, doi:10.1146/annurev.cellbio.13.1.513 (1997).
- 163 Madan, E. *et al.* Flower isoforms promote competitive growth in cancer. *Nature* **572**, 260-264, doi:10.1038/s41586-019-1429-3 (2019).
- 164 Eder, J. P., Vande Woude, G. F., Boerner, S. A. & LoRusso, P. M. Novel therapeutic inhibitors of the c-Met signaling pathway in cancer. *Clin Cancer Res* **15**, 2207-2214, doi:10.1158/1078-0432.CCR-08-1306 (2009).
- 165 Benayoun, B. A., Caburet, S. & Veitia, R. A. Forkhead transcription factors: key players in health and disease. *Trends Genet* **27**, 224-232, doi:10.1016/j.tig.2011.03.003 (2011).
- 166 Brock, T. *et al.* The Influence of VE-Cadherin on Adhesion and Incorporation of Breast Cancer Cells into Vascular Endothelium. *Int J Mol Sci* **22**, doi:10.3390/ijms22116049 (2021).
- 167 Wang, Z. *et al.* Cyclin B1/Cdk1 coordinates mitochondrial respiration for cell-cycle G2/M progression. *Dev Cell* **29**, 217-232, doi:10.1016/j.devcel.2014.03.012 (2014).
- 168 Hans, F. & Dimitrov, S. Histone H3 phosphorylation and cell division. *Oncogene* **20**, 3021-3027, doi:10.1038/sj.onc.1204326 (2001).
- 169 Hsu, J. & Sage, J. Novel functions for the transcription factor E2F4 in development and disease. *Cell Cycle* **15**, 3183-3190, doi:10.1080/15384101.2016.1234551 (2016).
- 170 Hirao, A. *et al.* DNA damage-induced activation of p53 by the checkpoint kinase Chk2. *Science* **287**, 1824-1827, doi:10.1126/science.287.5459.1824 (2000).

- 171 Zhao, S. *et al.* Glioma-derived mutations in IDH1 dominantly inhibit IDH1 catalytic activity and induce HIF-1 α . *Science* **324**, 261-265, doi:10.1126/science.1170944 (2009).
- 172 Zeng, Q. & Hong, W. The emerging role of the hippo pathway in cell contact inhibition, organ size control, and cancer development in mammals. *Cancer Cell* **13**, 188-192, doi:10.1016/j.ccr.2008.02.011 (2008).
- 173 Zou, H., Li, Y., Liu, X. & Wang, X. An APAF-1-cytochrome c multimeric complex is a functional apoptosome that activates procaspase-9. *J Biol Chem* **274**, 11549-11556, doi:10.1074/jbc.274.17.11549 (1999).
- 174 Slee, E. A. *et al.* Ordering the cytochrome c-initiated caspase cascade: hierarchical activation of caspases-2, -3, -6, -7, -8, and -10 in a caspase-9-dependent manner. *J Cell Biol* **144**, 281-292, doi:10.1083/jcb.144.2.281 (1999).
- 175 Wei, M. C. *et al.* Proapoptotic BAX and BAK: a requisite gateway to mitochondrial dysfunction and death. *Science* **292**, 727-730, doi:10.1126/science.1059108 (2001).
- 176 Walter, K. R., Balko, J. M. & Hagan, C. R. Progesterone receptor promotes degradation of STAT2 to inhibit the interferon response in breast cancer. *Oncoimmunology* **9**, 1758547, doi:10.1080/2162402X.2020.1758547 (2020).
- 177 Anurag, M. *et al.* Immune Checkpoint Profiles in Luminal B Breast Cancer (Alliance). *J Natl Cancer Inst* **112**, 737-746, doi:10.1093/jnci/djz213 (2020).
- 178 Sweis, R. F. *et al.* Molecular Drivers of the Non-T-cell-Inflamed Tumor Microenvironment in Urothelial Bladder Cancer. *Cancer Immunol Res* **4**, 563-568, doi:10.1158/2326-6066.CIR-15-0274 (2016).
- 179 Kardos, J. *et al.* Claudin-low bladder tumors are immune infiltrated and actively immune suppressed. *JCI Insight* **1**, e85902, doi:10.1172/jci.insight.85902 (2016).
- 180 Glass, C. K. & Saijo, K. Nuclear receptor transrepression pathways that regulate inflammation in macrophages and T cells. *Nat Rev Immunol* **10**, 365-376, doi:10.1038/nri2748 (2010).
- 181 Chan, I. S. & Ginsburg, G. S. Personalized medicine: progress and promise. *Annu Rev Genomics Hum Genet* **12**, 217-244, doi:10.1146/annurev-genom-082410-101446 (2011).
- 182 Ginsburg, G. S. & Phillips, K. A. Precision Medicine: From Science To Value. *Health Aff (Millwood)* **37**, 694-701, doi:10.1377/hlthaff.2017.1624 (2018).
- 183 Terry, S. F. Obama's Precision Medicine Initiative. *Genet Test Mol Biomarkers* **19**, 113-114, doi:10.1089/gtmb.2015.1563 (2015).
- 184 Eastel, J. M. *et al.* Application of NanoString technologies in companion diagnostic development. *Expert Rev Mol Diagn* **19**, 591-598, doi:10.1080/14737159.2019.1623672 (2019).

References

- 185 Orgogozo, V., Morizot, B. & Martin, A. The differential view of genotype-phenotype relationships. *Front Genet* **6**, 179, doi:10.3389/fgene.2015.00179 (2015).
- 186 Klose, J. Genotypes and phenotypes. *Electrophoresis* **20**, 643-652, doi:10.1002/(SICI)1522-2683(19990101)20:4/5<643::AID-ELPS643>3.0.CO;2-M (1999).
- 187 Fincham, R. E. A., Bashiri, H., Lau, M. C. & Yeong, J. Editorial: Multiplex Immunohistochemistry/Immunofluorescence Technique: The Potential and Promise for Clinical Application. *Frontiers in Molecular Biosciences* **9**, 831383, doi:10.3389/fmolb.2022.831383 (2022).
- 188 Barua, S. *et al.* A Functional Spatial Analysis Platform for Discovery of Immunological Interactions Predictive of Low-Grade to High-Grade Transition of Pancreatic Intraductal Papillary Mucinous Neoplasms. *Cancer Inform* **17**, 1-8, doi:10.1177/1176935118782880 (2018).
- 189 Tan, W. C. C. *et al.* Overview of multiplex immunohistochemistry/immunofluorescence techniques in the era of cancer immunotherapy. *Cancer Commun (Lond)* **40**, 135-153, doi:10.1002/cac2.12023 (2020).
- 190 Pusch, W., Flocco, M. T., Leung, S. M., Thiele, H. & Kostrzewa, M. Mass spectrometry-based clinical proteomics. *Pharmacogenomics* **4**, 463-476, doi:10.1517/phgs.4.4.463.22753 (2003).
- 191 Meyer, J. G. & Schilling, B. Clinical applications of quantitative proteomics using targeted and untargeted data-independent acquisition techniques. *Expert Rev Proteomics* **14**, 419-429, doi:10.1080/14789450.2017.1322904 (2017).
- 192 Baker, E. S. *et al.* Mass spectrometry for translational proteomics: progress and clinical implications. *Genome Med* **4**, 63, doi:10.1186/gm364 (2012).
- 193 Trobbiani, S., Stockham, P. & Scott, T. Increasing the linear dynamic range in LC-MS: is it valid to use a less abundant isotopologue? *Drug Test Anal* **9**, 1630-1636, doi:10.1002/dta.2175 (2017).
- 194 Hartmann, M. *et al.* Expanding assay dynamics: a combined competitive and direct assay system for the quantification of proteins in multiplexed immunoassays. *Clin Chem* **54**, 956-963, doi:10.1373/clinchem.2007.099812 (2008).
- 195 Jewer, M., Findlay, S. D. & Postovit, L. M. Post-transcriptional regulation in cancer progression : Microenvironmental control of alternative splicing and translation. *J Cell Commun Signal* **6**, 233-248, doi:10.1007/s12079-012-0179-x (2012).
- 196 Truitt, M. L. & Ruggero, D. New frontiers in translational control of the cancer genome. *Nat Rev Cancer* **16**, 288-304, doi:10.1038/nrc.2016.27 (2016).
- 197 Michel, M. C., Wieland, T. & Tsujimoto, G. How reliable are G-protein-coupled receptor antibodies? *Naunyn Schmiedebergs Arch Pharmacol* **379**, 385-388, doi:10.1007/s00210-009-0395-y (2009).

- 198 Begley, C. G. & Ellis, L. M. Drug development: Raise standards for preclinical cancer research. *Nature* **483**, 531-533, doi:10.1038/483531a (2012).
- 199 Egelhofer, T. A. *et al.* An assessment of histone-modification antibody quality. *Nat Struct Mol Biol* **18**, 91-93, doi:10.1038/nsmb.1972 (2011).
- 200 Bryant, J. E. *et al.* Serology for SARS-CoV-2: Apprehensions, opportunities, and the path forward. *Sci Immunol* **5**, eabc6347, doi:10.1126/sciimmunol.abc6347 (2020).
- 201 Theel, E. S. *et al.* The Role of Antibody Testing for SARS-CoV-2: Is There One? *J Clin Microbiol* **58**, doi:10.1128/JCM.00797-20 (2020).
- 202 Lipsitch, M., Kahn, R. & Mina, M. J. Antibody testing will enhance the power and accuracy of COVID-19-prevention trials. *Nat Med* **26**, 818-819, doi:10.1038/s41591-020-0887-3 (2020).
- 203 Negro, F. Is antibody-dependent enhancement playing a role in COVID-19 pathogenesis? *Swiss Med Wkly* **150**, w20249, doi:10.4414/smw.2020.20249 (2020).
- 204 Iwasaki, A. & Yang, Y. The potential danger of suboptimal antibody responses in COVID-19. *Nat Rev Immunol* **20**, 339-341, doi:10.1038/s41577-020-0321-6 (2020).
- 205 Peeples, L. News Feature: Avoiding pitfalls in the pursuit of a COVID-19 vaccine. *Proc Natl Acad Sci U S A* **117**, 8218-8221, doi:10.1073/pnas.2005456117 (2020).
- 206 Dawson, E. D. *et al.* Multiplexed, microscale, microarray-based serological assay for antibodies against all human-relevant coronaviruses. *J Virol Methods* **291**, 114111, doi:10.1016/j.jviromet.2021.114111 (2021).
- 207 Leung, D. T. *et al.* Antibody response of patients with severe acute respiratory syndrome (SARS) targets the viral nucleocapsid. *J Infect Dis* **190**, 379-386, doi:10.1086/422040 (2004).
- 208 Maksimenko, O. G., Deykin, A. V., Khodarovich, Y. M. & Georgiev, P. G. Use of transgenic animals in biotechnology: prospects and problems. *Acta Naturae* **5**, 33-46 (2013).
- 209 Lu, S. *et al.* The SARS-CoV-2 nucleocapsid phosphoprotein forms mutually exclusive condensates with RNA and the membrane-associated M protein. *Nat Commun* **12**, 502, doi:10.1038/s41467-020-20768-y (2021).
- 210 Ruetalo, N. *et al.* Antibody Response against SARS-CoV-2 and Seasonal Coronaviruses in Nonhospitalized COVID-19 Patients. *mSphere* **6**, e01145-01120, doi:10.1128/mSphere.01145-20 (2021).
- 211 Bhudevi, B. & Weinstock, D. Detection of bovine viral diarrhea virus in formalin fixed paraffin embedded tissue sections by real time RT-PCR (Taqman). *J Virol Methods* **109**, 25-30, doi:10.1016/s0166-0934(03)00040-5 (2003).
- 212 Bresters, D., Schipper, M. E., Reesink, H. W., Boeser-Nunnink, B. D. & Cuypers, H. T. The duration of fixation influences the yield of HCV cDNA-

References

- PCR products from formalin-fixed, paraffin-embedded liver tissue. *J Virol Methods* **48**, 267-272, doi:10.1016/0166-0934(94)90125-2 (1994).
- 213 Macabeo-Ong, M. *et al.* Effect of duration of fixation on quantitative reverse transcription polymerase chain reaction analyses. *Mod Pathol* **15**, 979-987, doi:10.1097/01.MP.0000026054.62220.FC (2002).
- 214 Xie, R. *et al.* Factors influencing the degradation of archival formalin-fixed paraffin-embedded tissue sections. *J Histochem Cytochem* **59**, 356-365, doi:10.1369/0022155411398488 (2011).
- 215 Blind, C. *et al.* Antigenicity testing by immunohistochemistry after tissue oxidation. *J Clin Pathol* **61**, 79-83, doi:10.1136/jcp.2007.047340 (2008).
- 216 Bayer, M., Angenendt, L., Schliemann, C., Hartmann, W. & Konig, S. Are formalin-fixed and paraffin-embedded tissues fit for proteomic analysis? *J Mass Spectrom* **55**, e4347, doi:10.1002/jms.4347 (2020).
- 217 Addis, M. F. *et al.* Generation of high-quality protein extracts from formalin-fixed, paraffin-embedded tissues. *Proteomics* **9**, 3815-3823, doi:10.1002/pmic.200800971 (2009).
- 218 Dehm, S. M. & Bonham, K. SRC gene expression in human cancer: the role of transcriptional activation. *Biochem Cell Biol* **82**, 263-274, doi:10.1139/o03-077 (2004).
- 219 Marzi, J. *et al.* Noninvasive Physical Plasma as Innovative and Tissue-Preserving Therapy for Women Positive for Cervical Intraepithelial Neoplasia. *Cancers (Basel)* **14**, 1933, doi:10.3390/cancers14081933 (2022).
- 220 Shabihkhani, M. *et al.* The procurement, storage, and quality assurance of frozen blood and tissue biospecimens in pathology, biorepository, and biobank settings. *Clin Biochem* **47**, 258-266, doi:10.1016/j.clinbiochem.2014.01.002 (2014).
- 221 Galon, J., Angell, H. K., Bedognetti, D. & Marincola, F. M. The continuum of cancer immunosurveillance: prognostic, predictive, and mechanistic signatures. *Immunity* **39**, 11-26, doi:10.1016/j.immuni.2013.07.008 (2013).
- 222 Mlecnik, B. *et al.* Histopathologic-based prognostic factors of colorectal cancers are associated with the state of the local immune reaction. *J Clin Oncol* **29**, 610-618, doi:10.1200/JCO.2010.30.5425 (2011).
- 223 Galon, J. *et al.* Type, density, and location of immune cells within human colorectal tumors predict clinical outcome. *Science* **313**, 1960-1964, doi:10.1126/science.1129139 (2006).
- 224 Angell, H. & Galon, J. From the immune contexture to the Immunoscore: the role of prognostic and predictive immune markers in cancer. *Curr Opin Immunol* **25**, 261-267, doi:10.1016/j.coi.2013.03.004 (2013).
- 225 Geyer, F. C. *et al.* Molecular analysis reveals a genetic basis for the phenotypic diversity of metaplastic breast carcinomas. *J Pathol* **220**, 562-573, doi:10.1002/path.2675 (2010).

-
- 226 Patani, N. *et al.* Direct evidence for concurrent morphological and genetic heterogeneity in an invasive ductal carcinoma of triple-negative phenotype. *J Clin Pathol* **64**, 822-828, doi:10.1136/jclinpath-2011-200135 (2011).
- 227 Schroth, W. *et al.* Gene Expression Signatures of BRCAness and Tumor Inflammation Define Subgroups of Early-Stage Hormone Receptor-Positive Breast Cancer Patients. *Clin Cancer Res* **26**, 6523-6534, doi:10.1158/1078-0432.CCR-20-1923 (2020).
- 228 Liu, S. *et al.* Prognostic significance of FOXP3+ tumor-infiltrating lymphocytes in breast cancer depends on estrogen receptor and human epidermal growth factor receptor-2 expression status and concurrent cytotoxic T-cell infiltration. *Breast Cancer Res* **16**, 432, doi:10.1186/s13058-014-0432-8 (2014).
- 229 Mahmoud, S. M. *et al.* Tumor-infiltrating CD8+ lymphocytes predict clinical outcome in breast cancer. *J Clin Oncol* **29**, 1949-1955, doi:10.1200/JCO.2010.30.5037 (2011).
- 230 Palano, M. T. *et al.* Neutrophil and Natural Killer Cell Interactions in Cancers: Dangerous Liaisons Instructing Immunosuppression and Angiogenesis. *Vaccines (Basel)* **9**, 1488, doi:10.3390/vaccines9121488 (2021).
- 231 Liongue, C., O'Sullivan, L. A., Trengove, M. C. & Ward, A. C. Evolution of JAK-STAT pathway components: mechanisms and role in immune system development. *PLoS One* **7**, e32777, doi:10.1371/journal.pone.0032777 (2012).
- 232 Seif, F. *et al.* The role of JAK-STAT signaling pathway and its regulators in the fate of T helper cells. *Cell Commun Signal* **15**, 23, doi:10.1186/s12964-017-0177-y (2017).
- 233 Murthy, V., Oshi, M., Tokumaru, Y., Endo, I. & Takabe, K. Increased apoptosis is associated with robust immune cell infiltration and cytolytic activity in breast cancer. *Am J Cancer Res* **11**, 3674-3687 (2021).
- 234 Fontenot, J. D., Gavin, M. A. & Rudensky, A. Y. Foxp3 programs the development and function of CD4+CD25+ regulatory T cells. *Nat Immunol* **4**, 330-336, doi:10.1038/ni904 (2003).
- 235 Brunkow, M. E. *et al.* Disruption of a new forkhead/winged-helix protein, scurfin, results in the fatal lymphoproliferative disorder of the scurfy mouse. *Nat Genet* **27**, 68-73, doi:10.1038/83784 (2001).
- 236 Khattri, R., Cox, T., Yasayko, S. A. & Ramsdell, F. An essential role for Scurfin in CD4+CD25+ T regulatory cells. *Nat Immunol* **4**, 337-342, doi:10.1038/ni909 (2003).
- 237 Korpala, M. *et al.* Evasion of immunosurveillance by genomic alterations of PPARgamma/RXRalpha in bladder cancer. *Nat Commun* **8**, 103, doi:10.1038/s41467-017-00147-w (2017).

Acknowledgements

Ein besonderer Dank gilt meiner Doktormutter Prof. Katja Schenke-Leyland, die mir mit fachlichem Rat und Expertise stets zur Seite stand. Des Weiteren möchte ich mich bei meinem zweiten Prüfer Prof. Stoll für seine stets willkommenen Einschätzungen und wissenschaftlichen Diskussionen bedanken.

Ein außerordentlicher Dank gilt meinem Betreuer Dr. Markus Templin, der mich auf diesem Weg geführt hat und mich stets bei meinem Vorhaben mit wissenschaftlichen Ideen und hilfreichen Gesprächen begleitet hat.

Ebenso bedanken möchte ich mich bei Dr. Thomas Joos der stets ein offenes Ohr für mich hatte.

Ein großer Dank gilt allen Mitarbeitern der Arbeitsgruppe Assay Entwicklung, meinen Freunden und Kollegen, Robin Kretz, Marius Gramlich, Simon Fink und Aaron Stahl die zu einem beispiellos angenehmen Arbeitsklima beigetragen haben und diese Zeit einfach unvergesslich gemacht haben.

Allen Personen, die am wissenschaftlichen Inhalt dieser Arbeit mitgewirkt haben, insbesondere Nicolas Kersten und Prof. Dr. Martin Weiss, gilt mein herzliches Dankeschön. Die exzellente wissenschaftliche Zusammenarbeit und offene Kommunikation haben mich bei meinem Vorhaben außerordentlich unterstützt.

Ganz besonders möchte ich mich bei meinen Eltern, Karl-Reiner und Brigitte Ruoff, meiner Schwester Franziska Ruoff, meiner Ehefrau Nadine Schäfer und meiner ganzen Familie bedanken, die mir durch schwere Zeiten geholfen haben und immer an mich geglaubt haben selbst dann, wenn ich es nicht konnte.

Declaration

Ich erkläre hiermit, dass ich die zur Promotion eingereichte Arbeit mit dem Titel “Protein Profiling of Primary Human Samples for Pathway Analysis and Patient Stratification” selbstständig verfasst, nur die angegebenen Quellen und Hilfsmittel benutzt und wörtlich oder inhaltlich übernommene Zitate als solche gekennzeichnet habe. Ich erkläre, dass die Richtlinien zur Sicherung guter wissenschaftlicher Praxis der Universität Tübingen beachtet wurden. Ich versichere an Eides statt, dass diese Angaben wahr sind und dass ich nichts verschwiegen habe. Mir ist bekannt, dass die falsche Angabe einer Versicherung an Eides statt mit Freiheitsstrafe bis zu drei Jahren oder mit Geldstrafe bestraft wird.

Felix Schäfer-Ruoff

Appendix

Appendix 1:

Simon Fink*, **Felix Ruoff***, Aaron Stahl, Matthias Becker, Philipp Kaiser, Bjoern Traenkle, Daniel Junker, Frank Weise, Natalia Ruetalo, Sebastian Hörber, Andreas Peter, Annika Nelde, Juliane Walz, Gérard Krause, Armin Baillot, Katja Schenke-Layland, Thomas O. Joos, Ulrich Rothbauer, Nicole Schneiderhan-Marra, Michael Schindler, and Markus F. Templin. Multiplexed Serum Antibody Screening Platform Using Virus Extracts from Endemic Coronaviridae and SARS-CoV-2. *ACS Infectious Diseases*; 7, (6), 1596-1606 (2021).

<https://doi.org/10.1021/acsinfecdis.0c00725>

*authors contributed equally

Reprinted with permission from *ACS Infect. Dis.* 2021, 7, 6, 1596–1606. Copyright © 2021 American Chemical Society. <https://doi.org/10.1021/acsinfecdis.0c00725>.

Multiplexed Serum Antibody Screening Platform Using Virus Extracts from Endemic *Coronaviridae* and SARS-CoV-2

Simon Fink,[△] Felix Ruoff,[△] Aaron Stahl, Matthias Becker, Philipp Kaiser, Bjoern Traenkle, Daniel Junker, Frank Weise, Natalia Ruetalo, Sebastian Hörber, Andreas Peter, Annika Nelde, Juliane Walz, Gérard Krause, Armin Baillot, Katja Schenke-Layland, Thomas O. Joos, Ulrich Rothbauer, Nicole Schneiderhan-Marra, Michael Schindler, and Markus F. Templin*

Cite This: *ACS Infect. Dis.* 2021, 7, 1596–1606

Read Online

ACCESS |

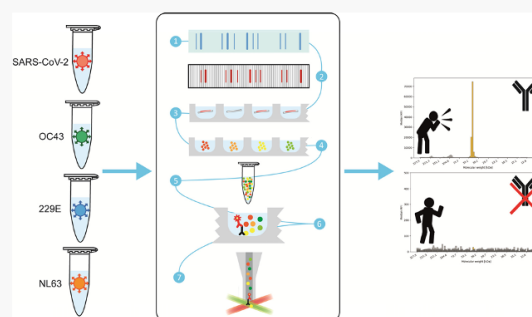
Metrics & More

Article Recommendations

Supporting Information

ABSTRACT: The presence of antibodies against endemic coronaviruses has been linked to disease severity after SARS-CoV-2 infection. Assays capable of concomitantly detecting antibodies against endemic coronaviridae such as OC43, 229E, NL63, and SARS-CoV-2 may help to elucidate this question. We developed a serum screening platform using a bead-based Western blot system called DigiWest, capable of running hundreds of assays using microgram amounts of protein prepared directly from different viruses. Characterization of the immunoassay for detection of SARS-CoV-2 specific antibodies revealed a sensitivity of 90.3% and a diagnostic specificity of 98.1%. Concordance analysis with the SARS-CoV-2 immunoassays available by Roche, Siemens, and Euroimmun indicates comparable assay performances (Cohen's κ ranging from 0.8874 to 0.9508). Analogous assays for OC43, 229E, and NL63 were established and combined into one multiplex with the SARS-CoV-2 assay. Seroreactivity for different coronaviruses was detected with high incidence, and the multiplex assay was adapted for serum screening.

KEYWORDS: SARS-CoV-2, COVID-19, endemic coronavirus, serology, Luminex, Western blot



Severe acute respiratory syndrome coronavirus 2 (SARS-CoV-2) is a newly identified beta coronavirus that crossed the species barrier and found its way into the human population in 2019. It causes the coronavirus disease 2019 (COVID-19), and the ongoing pandemic has a devastating effect on wide parts of the human population.¹ The virus is highly contagious causing the disease to spread very rapidly, yet symptoms of infected individuals vary widely. A fraction of COVID-19 patients develop a fatal course of the disease, while mild COVID-19 cases are frequently observed.² Different comorbidity factors were recently identified, whereas the prediction of the course of the disease is not yet possible.³ Protective antibodies formed after infection are associated with viral clearance, but the occurrence of high antibody titers has also been linked to more serious forms of the disease.⁴ A role of pre-existing and cross-reacting antibodies, from endemic coronaviruses, that recognize proteins from SARS-CoV-2 is discussed,^{5,6} and a phenomenon termed antibody-dependent enhancement (ADE), which is linked to existing antibodies, might be one of the reasons for life-threatening symptoms occurring during later stages of COVID-19.^{7–9} In contrast, a pre-existing cross-reactive T cell memory for SARS-CoV-2 does exist in a significant proportion of the population,^{10,11} and

it is likely to be caused by previous infections with endemic coronaviruses. This observation might explain some of the heterogeneity observed in COVID-19, yet the role of the antibody response against these viruses remains elusive. Assays capable of detecting antibodies against endemic coronaviridae, such as OC43, 229E, and NL63, will help us to understand a possible role of existing antibodies against these human coronaviruses during COVID-19. Available systems are using recombinant antigens to detect viral protein-directed antibodies in serum or plasma samples. This approach is not only economical but also makes the generation of large reagent batches feasible, allowing for the generation of vast numbers of assays required for systematic sample screening.^{12,13} Here, we employ a novel way of building a serologic assay system to detect and characterize anti-SARS-CoV-2 antibodies. The

Received: October 16, 2020

Published: March 16, 2021



utilized approach is based on the classical Western blot procedure, which has been modified to be run as a high-throughput assay system. The use of antigens reflecting the complete pathogen proteome for antibody detection has been employed since the late 1970s¹⁴ and was subsequently proven to be useful for identifying proteins recognized during the humoral immune response. In lysates prepared from infectious virus particles, not only are all possible viral proteins present and can be probed in one assay, but also the use of native-like antigens should enable the detection of antibodies recognizing relevant protein modifications present in the naturally occurring pathogen.

The DigiWest procedure, which is employed here, is a variant of the classical Western blot. It addresses the most obvious disadvantages of Western blotting, namely, its low throughput, high antigen consumption, and poor reproducibility.¹⁵ In the DigiWest, the assay signal is generated on microspheres rather than on a membrane, thus allowing the use of fast and standardized assay protocols on the Luminex platform. Due to the possibility of multiplexing, multiple antigens from different viruses can be probed at the same time, enabling the setup of semiquantitative seroreactivity screens.

RESULTS

DigiWest for Detecting Serum Antibodies against SARS-CoV-2. Here, we used the DigiWest for size dependent separation of virus proteins representing the entire viral proteome and for their subsequent immobilization on microspheres in order to adapt this technology to serum analysis (Figure 1). As a first step for detecting serum antibodies recognizing viral proteins, lysates from infectious SARS-CoV-2 virus particles were prepared in SDS-PAGE loading buffer. DigiWest was performed as described using 0.5 μ g of virus protein, and Luminex microspheres sufficient to run hundreds of assays were generated. Detection of total protein on the loaded DigiWest beads (Figure 2a) showed characteristic protein bands for the lysate. Using an antibody generated against the SARS-CoV-2 nucleocapsid, a prominent peak at 47.2 kDa (Figure 2b) was detected, which is consistent with the expected size of the protein. Another antibody generated against the SARS-CoV-2 spike protein detects a prominent peak at 141 kDa, the expected molecular weight (Figure 2c). In the next step, human sera were diluted 1:200 in an optimized and modified serum assay buffer and incubated with the DigiWest microspheres. High signals were detected from COVID-19 convalescent sera. Most sera showed their main peak of reactivity at 47 kDa, i.e., the size corresponding to the SARS-CoV-2 nucleocapsid protein (Figure 2e). For SARS-CoV-2 negative samples, no or very low signals were obtained (Figure 2d). Assay background was found to be variable, but since the determined signal intensities only consist of the peak area, reliable values were calculated using the DigiWest evaluation tool.¹⁵ Since reactivity against the nucleocapsid protein was consistently found in COVID-19 convalescent sera, these values were used for describing SARS-CoV-2 seroreactivity.

Multiplexed DigiWest for Detecting Serum Antibodies Recognizing Different Human *Coronaviridae*. In order to expand the assay to cover human endemic coronaviruses, virus lysates from the two alpha coronaviruses 229E and NL63 and from the beta coronavirus OC43 were processed as described, and equivalent DigiWest assays were established and combined into one assay system. When using

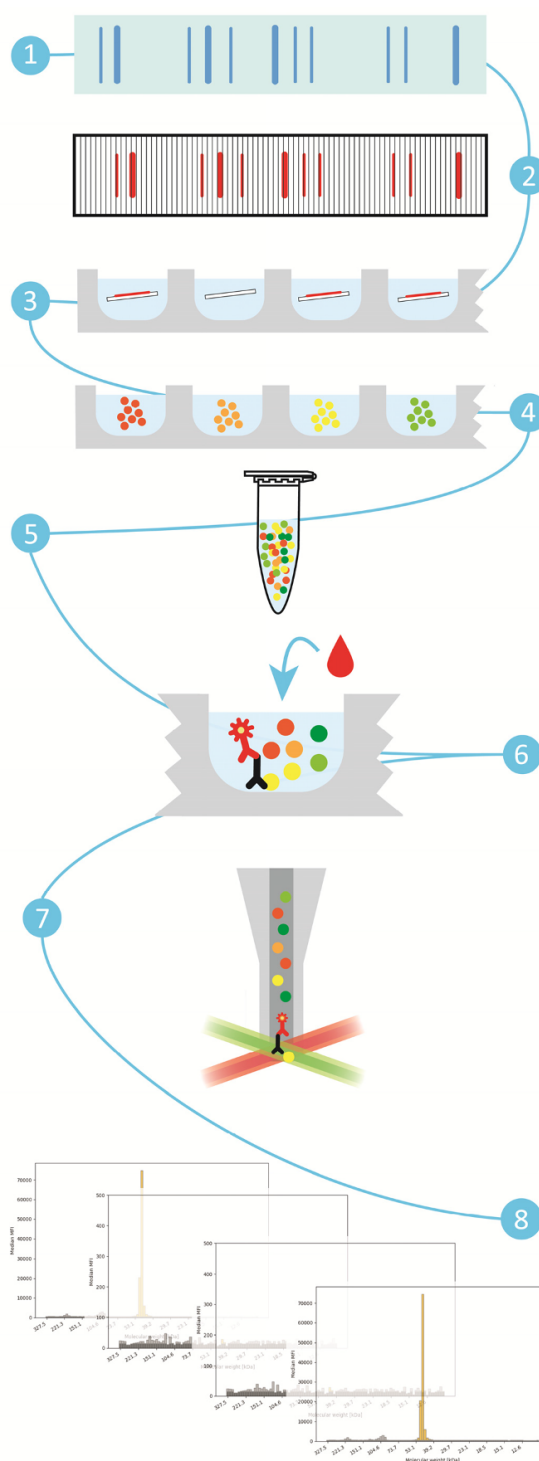


Figure 1. Schematic overview of the DigiWest workflow (modified from Treindl et al.¹⁵ CC BY 4.0): (1) Protein separation by sodium dodecyl sulfate polyacrylamide gel electrophoresis (SDS-PAGE). (2) Blotting of proteins to membrane and biotinylation of immobilized proteins directly on the membrane. Cutting of sample lanes into 96

Figure 1. continued

stripes to generate 96 molecular weight fractions immobilized on the membrane. (3) Elution of the proteins in 96-well plates. (4) Loading of biotinylated proteins onto 96 distinct Neutravidin-coated magnetic Luminex bead populations. (5) Pooling into bead pools and reconstitution of the initial sample lane. (6) Immunoassay: aliquots of the generated bead pool (<0.5%) are incubated with specimen before PE-labeled secondary antibodies are added for signal generation. (7) Readout using a Luminex instrument, (8) reconstitution of the initial lane and data analysis.

sera from SARS-CoV-2 negative individuals, seroreactivity against endemic viral proteins was found for a large fraction of tested samples. As for the SARS-CoV-2 DigiWest assay, the main serological activity for the different viruses was detected at a molecular weight corresponding to nucleocapsid proteins. To prove that the detected proteins are indeed the nucleocapsids of the different coronaviruses, we produced recombinant versions of the nucleocapsid proteins of all tested viruses. We used the purified proteins in a different DigiWest experiment and compared the obtained signals with the signals obtained from the whole virus lysate DigiWest (Figure 3a). In the whole virus lysate, the observed molecular weight of SARS-CoV-2 nucleocapsid protein was 47.2 kDa with a calculated molecular weight of 45.6 kDa. For OC43 nucleocapsid protein, 229E nucleocapsid protein, and NL63 nucleocapsid protein, the values were 53.1 kDa (calculated 49.3 kDa), 45.4 kDa (calculated 43.5 kDa), and 42.1 kDa (calculated 42.3 kDa),

respectively. Thus, in all cases obtained, molecular weights are in good agreement with the expected values. The molecular weights were confirmed via DigiWest using recombinant proteins (Figure 3b). A small set of 12 sera was used to detect seroreactivity on virus lysates and on the recombinant nucleocapsid proteins. The correlating signal was detected, and this confirmed that the detected reactivity is directed against the nucleocapsid proteins.

Evaluation of the Characteristics of the SARS-CoV-2 Serological Assay. To characterize the performance of the DigiWest, we used the final multiplexed assay now comprising virus lysates of SARS-CoV-2, 229E, OC43 and NL63 to screen a set of characterized samples.¹¹ Among the analyzed sera, there were 195 SARS-CoV-2 PCR positive specimens, 49 prepandemic samples and 19 self-reported negative samples. The complete data set is available online in [Supplementary Data 1](#). To define the assay cutoff for SARS-CoV-2 seropositivity, 49 prepandemic and noninfected control samples were employed. The highest signal value detected in this group was 1295 average fluorescence intensity (AFI). In a second step, the lowest value of all SARS-CoV-2 PCR-positive specimens still above this intensity (1968 AFI) was defined as a seropositive for SARS-CoV-2. The mean of these two measurements was calculated and defined to be the cutoff for seroconversion (1632 AFI). After the definition of the cutoff, a test set of 53 negative and 31 positive samples was used to determine specificity and sensitivity. The complete data set is available in [Supplementary Data 3](#). Using the defined cutoff, an assay specificity of 98.1% (CI 94.5–100%)

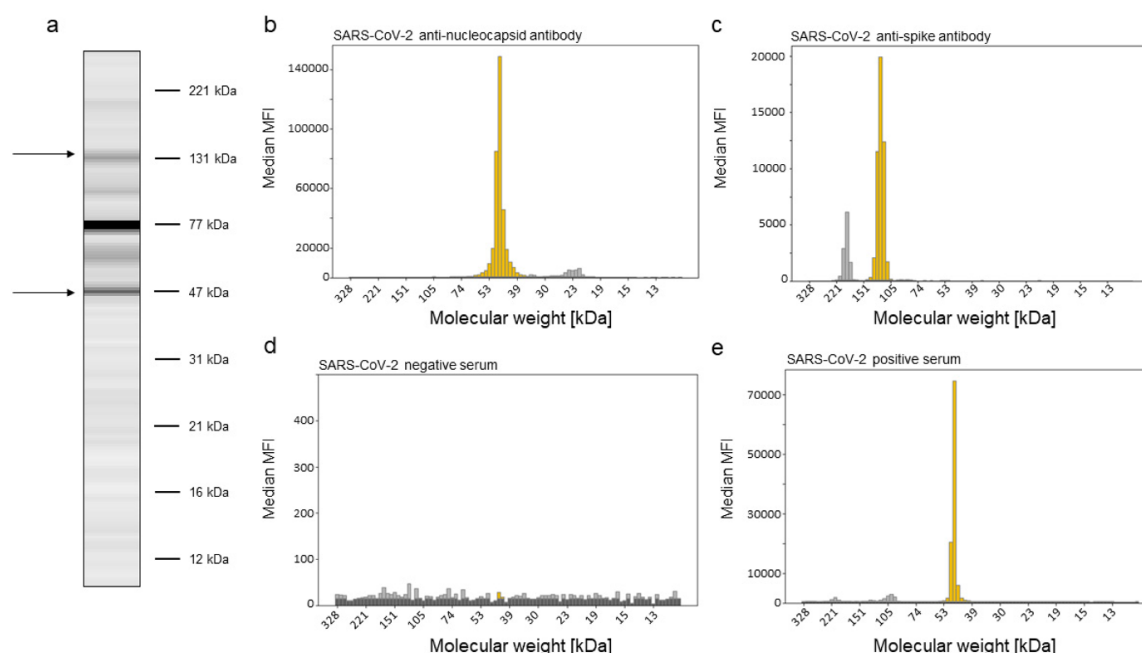


Figure 2. Protein detection on SARS-CoV-2 virus lysate loaded DigiWest beads. Virus proteins were size separated by the DigiWest procedure and transferred to microspheres. In (a), a total protein stain of the separated proteins is shown; data are represented as a Western blot mimic,¹⁵ thereby resembling a SDS-PAGE lane. The marked protein bands corresponds to the viral spike and nucleocapsid protein. An anti-SARS-CoV-2 nucleocapsid antibody detects this protein at the expected molecular weight (47.2 kDa) (b). A different antibody detects the spike protein at the expected molecular weight (141 kDa) (c). Serum from a SARS-CoV-2 PCR positive patient reacts with the nucleocapsid protein (47.2 kDa), giving high fluorescent intensity (e), whereas in a negative serum no peaks are detected (d).

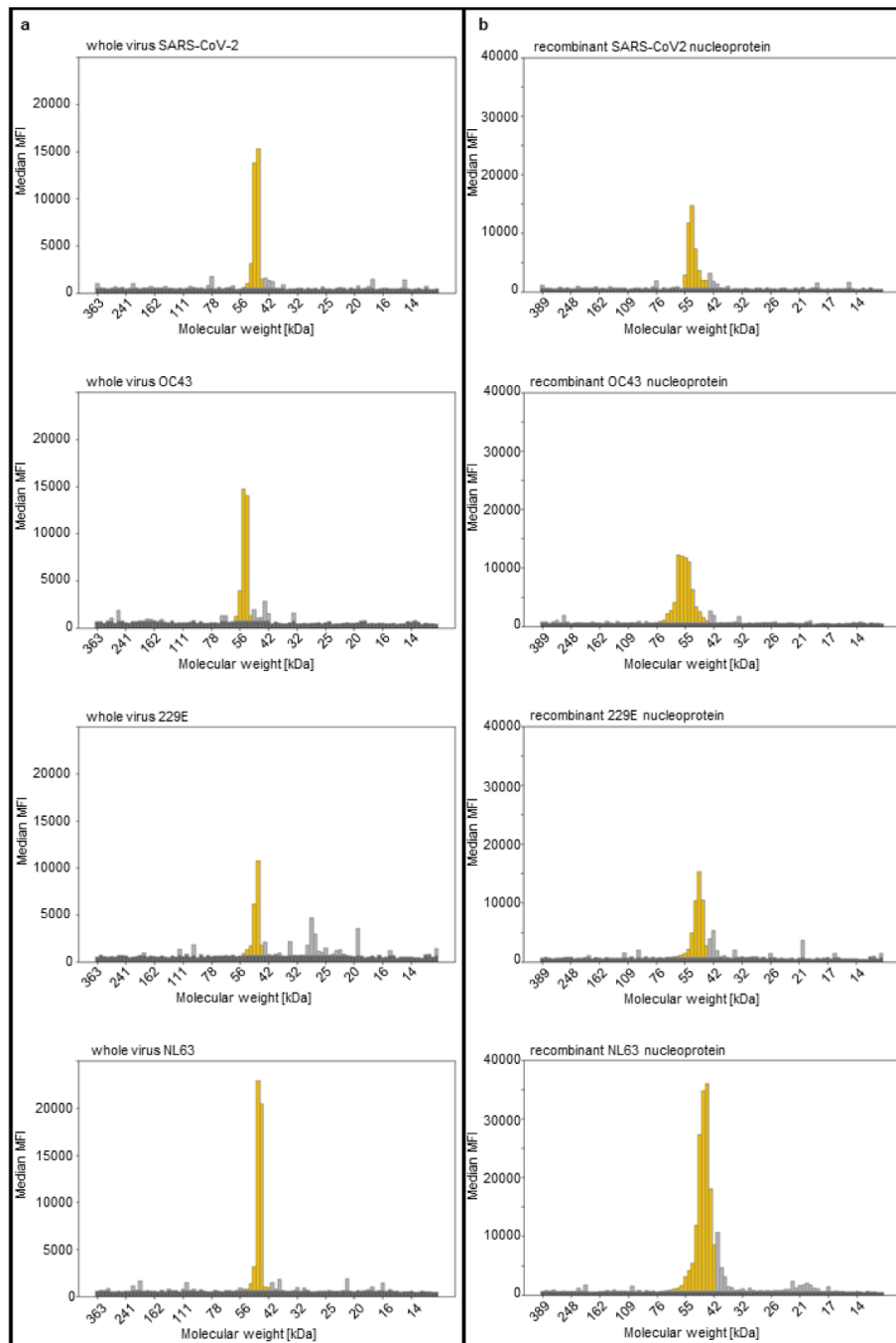


Figure 3. Multiplexed detection of nucleocapsid protein from SARS-CoV-2, OC43, 229E, and NL63. Reactivity of a patient serum was tested on whole virus lysates of the different coronavirus types (a) and on recombinant nucleocapsid proteins of the different viruses (b) using multiplexed DigiWest assays. The used SARS-CoV-2 positive serum shows antibody reactivity on whole virus lysates for (i) SARS-CoV-2, (ii) OC43, (iii) 229E, and (iv) NL63 (a). In (b), the same serum is incubated with a DigiWest bead set loaded with recombinant nucleocapsid from (i) SARS-CoV-2, (ii) OC43, (iii) 229E, and (iv) NL63. As for the whole virus lysates, antibody reactivity is observed; for SARS-CoV-2, a peak at 47.2 is kDa detected; for the endemic *Coronaviridae* OC43, 229E, and NL63, peaks at the molecular weights at the respective sizes of 53.1, 45.4, and 42.1 kDa, respectively, are found.

was found. Furthermore, 3/28 (10.7%) samples from SARS-CoV-2 PCR positive specimens showed no seroconversion, yielding a sensitivity of 90.3% (CI 79.9–100%). The positive predictive value is 0.966 (CI 0.899–1.0), and the negative predictive value is 0.945 (CI 0.855–1.0). These fundamental characteristics of the newly established assay system are comparable to published values for different commercially available SARS-CoV-2 immunoassays.^{16,17}

To demonstrate the dynamic range of the serologic DigiWest assay, three SARS-CoV-2 positive sera with different AFI were serially diluted with a negative serum (Figure 4). Good signal linearity was seen in the dilution curve and seropositivity was detected for higher AFI down to a serum dilution of 1:5000.

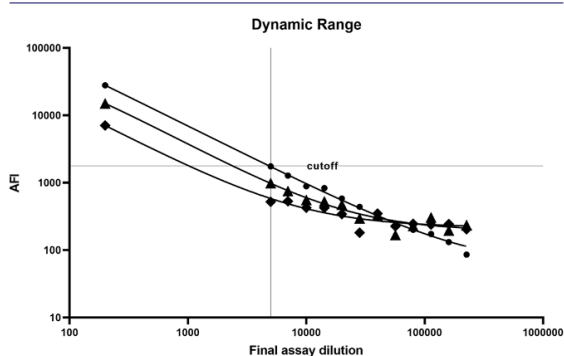


Figure 4. Dynamic range of the DigiWest serological assay. Sera of three SARS-CoV-2 positive patients were diluted in serum of a SARS-CoV-2 negative donor (serial dilution, 13 steps ranging from 1:25 to 1:1131). The mixtures were further diluted 1:200 in serum assay buffer, and the immunoassay was performed. Shown are the final dilutions of positive sera (X-axis) and the resulting average fluorescence intensities (AFI). Logistic regression was performed using a sigmoidal fit and 4-parameter logistics: (●) positive sample 1 (bottom, 54.50; top, 1052419; IC_{50} , 3.317; Hill slope, -0.8797 ; $\log IC_{50}$, 0.5208); (▲) positive sample 2 (bottom, 192.5; top, 106 711; IC_{50} , 29.65; Hill slope, -0.9556 ; $\log IC_{50}$, 1.472); (◆) positive sample 3 (bottom, 217.7; top, 938327; IC_{50} , 0.9145; Hill slope, -0.9118 ; $\log IC_{50}$, -0.03881)

For closer evaluation of the assay performance, we reanalyzed the complete sample set using the (i) Elecsys anti-SARS-CoV-2 assay (Roche Diagnostics), (ii) ADVIA Centaur SARS-CoV-2 (Siemens Healthcare Diagnostics),¹⁸ (iii) EUROIMMUN SARS-CoV-2 IgG ELISA, and (iv) EUROIMMUN SARS-CoV-2 IgA ELISA test systems. Further information on the assay procedures is provided in the **Methods** section. Concordance (Cohen's κ) and correlation (Spearman's r) analyses were performed, and the different assay characteristics were compared and visualized (Figure 5). Concordance of DigiWest vs Roche was found to be 0.9508 (95% CI; 0.91–0.99 Figure 5a), and for DigiWest vs Siemens Cohen's κ was 0.9100 (95% CI; 0.86–0.96 Figure 5b). Concordance of DigiWest vs Euroimmun IgG was calculated in two ways: if the borderline results were considered positive, Cohen's κ was found to be 0.9180 (95% CI; 0.87–0.97), and if considered negative the concordance was 0.8874 (95% CI; 0.83–0.94 Figure 5c). When comparing the DigiWest based IgG detection to the Euroimmun based IgA test and borderline results were considered positive, a value of 0.7493 (95% CI;

0.67–0.83) was found. If the borderline results were considered negative, Cohen's κ was found to be 0.7512 (95% CI; 0.67–0.83).

Correlation analysis utilizing Spearman's r revealed a positive correlation of all investigated assays (Figure 5d). The highest correlation for DigiWest was found with the Roche system (Spearman's $r = 0.91$; 95% CI; 0.89–0.93). Spearman's r for DigiWest and Siemens was found to be 0.87 (95% CI; 0.83–0.90). Spearman's r for DigiWest and Euroimmun IgG and IgA was calculated at 0.87 (95% CI; 0.84–0.90) and 0.78 (95% CI; 0.72–0.82), respectively. The highest overall correlation was found between Siemens and Euroimmun IgG (Spearman's $r = 0.94$; 95% CI; 0.93–0.96), and the lowest overall correlation was found between Euroimmun IgA and Roche (Spearman's $r = 0.73$; 95% CI; 0.66–0.78).

Multiplexed Detection of Antibodies against SARS-CoV-2, OC43, 229E, and NL63. By integrating DigiWest assays for 229E, OC43, and NL63 into the detection system for SARS-CoV-2, concomitant detection of the presence of antibodies binding to antigens derived from the different *Coronaviridae* becomes possible. In the analyzed sample set, reactive antibodies against all endemic coronaviruses were detected with high frequency (Supplementary Data 1). To estimate the reactivity against the other human endemic coronaviruses, a provisional cutoff for OC43, 229E, and NL63 was defined at the same value as was determined for SARS-CoV-2 (1632 AFI). For SARS-CoV-2 negative sera, 82.4% showed reactivity against OC43 nucleocapsid, 95.6% against 229E, and 100% against NL63. For SARS-CoV-2 positive samples, the numbers were 79.5% against OC43, 99% against 229E, and 98.5% against NL63. The overall reactivity was 80.2% against OC43, 98.1% against 229E, and 98.9% against NL63. Despite the high frequency of antibodies directed against the endemic coronaviruses OC43, 229E, and NL63 in SARS-CoV-2 negative sera, no recognition of SARS-CoV-2 proteins was observed in these samples. This directly translates into the high specificity of the SARS-CoV-2 assay system and reveals only minor or no cross-reactivity of existing antibodies with the existing SARS-CoV-2 nucleocapsid protein. The correlation analysis between all coronaviruses (including SARS-CoV-2) showed values ranging from 0.03 to 0.75 (Figure 6). The highest correlation was observed for antibodies recognizing the nucleocapsid protein of 229E and NL63 with a Spearman's r of 0.75 indicating a possible cross-reactivity.

DISCUSSION

The use of proteins from clinically relevant pathogens as antigens for antibody detection is a classical method for identifying an individual immune response.¹⁹ While this classical approach has distinct drawbacks, e.g., the need for isolation of large amounts of pathogen and poor assay reproducibility when using different protein batches, it also provides substantial advantages. With this assay, using denatured and reduced virus lysates, linear epitopes with and without post-translational modifications could be detected. Modifications only found in the authentic proteins are present in antigen preparations, and therefore, the identification of reactive antibodies against these possible pathogen-derived antigens should be feasible. In addition, the generation of protein extract from pathogens of different strains is often technically uncomplicated and fast. This may turn out to be especially useful when a comparative analysis of antigen

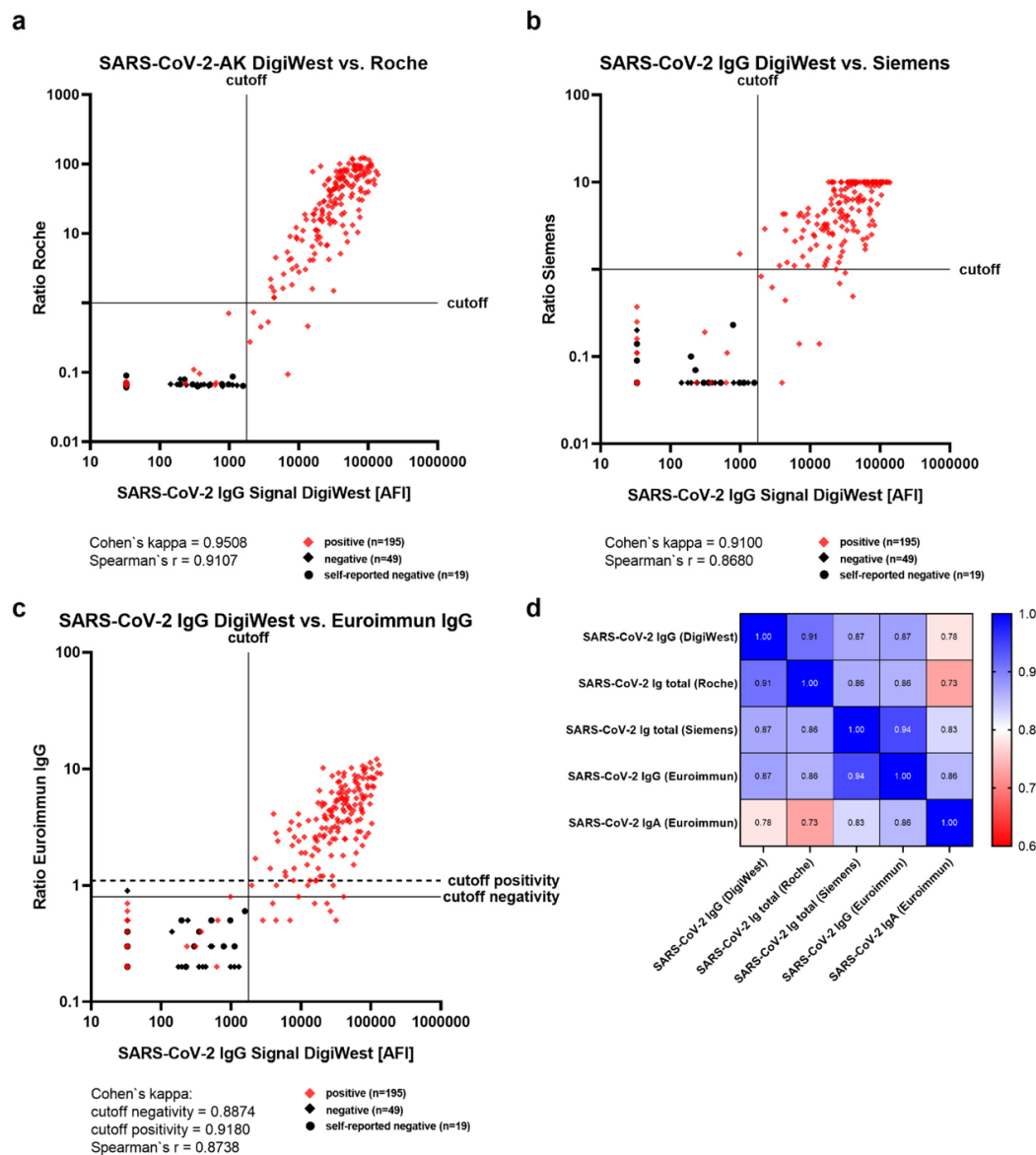


Figure 5. Comparison of the DigiWest seroconversion assay with commercially available SARS-CoV-2 assays. Concordance (Cohen's κ) and correlation coefficients (Spearman's r) of DigiWest data and the commercially assays from Roche (a), Siemens (b), and Euroimmun IgG (c) were calculated and are shown below the plotted data; cutoff values are depicted as a black line in the scatter plot. For the Euroimmun IgG, two different κ values were calculated; when borderline results (as defined by the manufacturer) were considered positive, κ was 0.9180. If the borderline results were considered negative, the concordance for Euroimmun IgG was 0.8874. In (d), the correlation coefficients (Spearman's r) between all used assays are shown in a heat map. The highest value (Spearman's r = 0.91) for DigiWest was found for the Roche system, and the lowest value (Spearman's r = 0.78) for DigiWest vs Euroimmun IgA is shown of Spearman's r values.

preparations from closely related pathogenic agents is of interest. Such an analysis may facilitate the identification of relevant cross-reacting antibodies directly on a wide variety of antigenic structures. These advantages may help set up systems that take an unbiased approach to characterize the humoral immune response.

Here we describe the setup of such an assay system using protein extracts prepared directly from infectious SARS-CoV-2 virus particles. The employed DigiWest procedure is an

immunoblot system that closely resembles the classical Western blot procedure. After SDS-PAGE based protein size separation, proteins are immobilized on polystyrene microspheres and assay readout is performed on the Luminex assay platform. An amount of 10 μg of protein is sufficient to generate batches of assay material sufficient for thousands of serum analyses; this directly translates into good assay reproducibility. In addition, the use of the Luminex platform for readout enables a high assay throughput without the need

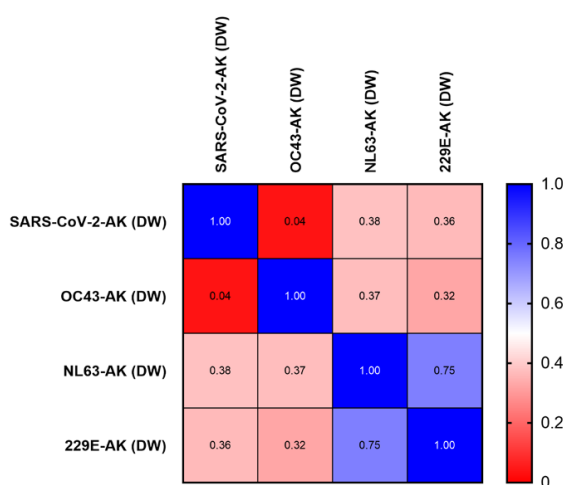


Figure 6. Spearman's rank correlation of SARS-CoV2 and endemic coronavirus types in the serological DigiWest (DW) assay. Data generated for SARS-CoV-2, OC43, 229E, and NL63 were used for correlation analysis, and Spearman's rank coefficients were calculated for assay pairing. Results are displayed as heat map of Spearman's r values. A high correlation (Spearman's r 0.75) was found between NL63 and 229E indicating cross-reactivity.

for producing recombinant proteins. As in Western blotting, the assay gives direct information on the size of the recognized proteins, and antigenic proteins can often be directly identified. When using COVID-19 convalescent sera, a specific antibody response to a protein of 47 kDa corresponding to the nucleocapsid protein of SARS-CoV-2 was recurrently seen. Reactivity against other viral proteins was present in individual serum samples, yet the nucleocapsid protein was identified as the major antigen in this assay. The observed low seroreactivity against the spike protein could be due to the fact that reduced and denatured proteins are present in the DigiWest and that these are not recognized by most of the anti-spike antibodies in the serum. This indicates that a strong antibody response can be detected on denatured N protein, while other viral proteins are not detected.

For detailed evaluation of the performance of the newly developed assay for detecting anti-SARS-CoV-2 antibodies, a set of more than 250 well-characterized sera was employed, in which sera were mainly taken from a clinical study on T-cell response after SARS-CoV-2 infection.¹¹ By using four different serological assays that are in use in clinical routine laboratories, we showed high concordance (Cohen's κ 0.86–0.94) between all systems. This demonstrates high standards for all tested assays. Interestingly, the highest concordance (0.94) was found between the Siemens assay system and the Euroimmun IgG assay, with both assays mainly detecting the spike protein. Nearly the same κ value (0.91) was calculated for the Roche and the DigiWest system, both of which use the nucleocapsid protein as the detected antigen. The Euroimmun IgA showed slightly different assay characteristics, which is most likely due to the fact that it is the only assay that exclusively detects IgA immunoglobulins. Yet, no principal differences in assay characteristics were observed and all assays showed reliable detection of seroprevalence after SARS-CoV-2 infection.

Antibodies against endemic coronaviruses are frequently found in human individuals.²⁰ These viruses cause mild

diseases and are associated with approximately 20% of the common colds.^{21,22} However, when comparing the sequences of the virus genome, the degree of similarity between the SARS-CoV-2 and these viruses is astonishingly high.²³ This similarity has led to speculations that antibodies against these endemic viruses may also possess protective properties against SARS-CoV-2.²⁴ The presence of these antibodies might explain the vastly diverse courses of disease. Therefore, the DigiWest assay system was expanded by using lysates from alpha coronaviruses 229E and NL63 as well as from the beta coronaviruses OC43, thus enabling the detection of serum antibodies recognizing antigens from four coronaviruses in one assay. The implementation of these assays directly succeeded the method used for SARS-CoV-2 and seroreactivity toward the nucleocapsid protein was frequently found for these coronaviruses.

As expected, a very high rate of infection for all of the coronaviruses was found, yet no obvious indication of cross-reactivity to the SARS-CoV-2 proteins was seen in negative SARS-CoV-2 samples. This is in contrast to the described T-cell response that can be triggered by peptides derived from the SARS-CoV-2 nucleocapsid.^{11,25} In a first, smaller scale screening approach the described assay system was used in combination with an antibody neutralization assay that detects the presence of serum antibodies capable of neutralizing SARS-CoV-2.²⁶ In this work, we show evidence that antibodies against the endemic coronavirus 229E contribute to SARS-CoV-2 neutralization. This result proves the advantage of a multiplexed system for detecting serum antibodies directed against different closely related viral pathogens, and this may help to understand the highly variable immune responses observed in different individuals.

As a serological assay system, the DigiWest is not only a novelty, but it allows the setup of a highly specific assay within a very short time frame. Its flexibility enables the integration of antigen extracts from all kinds of sources, and it is capable of detecting a wide variety of serum antibodies since complex mixtures of different pathogen-derived proteins can be probed in one reaction. Yet, the setup of the system is complex and requires (i) propagation and handling of the pathogens and (ii) generation of the antigen loaded microspheres, (iii) before the actual serum assay is performed. Only specialized research laboratories do have the capability to perform all of these steps. The fact that the three steps of the DigiWest procedure can easily be separated changes the situation. It opens the possibility to bring the technology to the large number of clinical and research laboratories that use the widely distributed Luminex platform for serum analysis. Large batches of antigen loaded beads, sufficient to run tens of thousands of assays can be produced by specialized laboratories using the established DigiWest workflow. These bead sets are stable, and the actual serum screening is easily performed in such clinical laboratories.

While this will broaden the applicability of the approach substantially, the setup of such an assay is mainly interesting when approaching specific questions that cannot be answered easily when using standard serological assay systems. Here we show that the fast setup of an assay for detecting antibodies against novel pathogens is possible by using crude protein extracts. Other questions may include the identification of antigenic structures in complex protein mixtures from bacteria and viruses. Running multiplexed serological assays that combine antigens from similar pathogens to identify the

binding characteristics of existing antibodies may even be important to identify changes in immunogenicity during the development of new pathogenic strains.

METHODS

Experimental Design. Assays capable of detecting antibodies against endemic *Coronaviridae* such as OC43, 229E, and NL63 will provide a better understanding of pre-existing antibodies against these closely related *Coronaviridae* during COVID-19. The use of antigens prepared directly from isolated virus particles and their use in the bead-based Western blot system DigiWest provide a fast and simple way of generating a multiplexed assay capable of detecting seroreactivity against these viruses. Starting with clinically characterized serum samples with a documented presence of anti SARS-CoV-2 antibodies and protein lysates prepared from SARS-CoV-2, a specific assay is built and the characteristics of the system are determined. In a second step, protein extracts from OC43, 229E, and NL63 are used to setup analogous assays and are later integrated into one multiplexed assay system.

Patients and Blood Samples. A total of 263 pre-existing and deidentified serum samples were used for assay development. Ethical approval was granted from the Ethics Committee of University Hospital Tübingen; samples from 193 SARS-CoV-2 polymerase chain reaction (PCR) positive individuals (179/2020/BO2) and of 18 self-reported negative samples were collected (179/2020/BO2). A self-reported healthy serum sample ($n = 1$) and self-reported convalescent serum after SARS-CoV-2 infection ($n = 2$) were obtained at the NMI under the guidelines of the local ethics committees (495/2018/BO2). Sample collection for each donor was performed approximately 3–8 weeks after the end of symptoms and/or negative virus smear. In addition, samples from healthy donors obtained from Central BioHub before 8/2019 were used as negative controls ($n = 49$). All available information can be found in [Supplementary Data 1 and 2](#). For the determination of sensitivity and specificity, a test set of 31 SARS-CoV-2 PCR positive individuals and 53 self-reported negative individuals was used (9122/BO/K/2020). All information on these samples can be found in [Supplementary Data 3](#).

SARS-CoV-2 Virus Lysate. To prepare SARS-CoV-2 virus lysate, the supernatant of infected human Caco-2 cells was purified. Briefly, Caco-2 cells were infected 1:10–1:500 with clinical isolate 200325_Tü1. At 48 h postinfection, the supernatant was collected, centrifuged, and frozen. A volume of 900 μL of supernatant was added to 200 μL of 20% sucrose and centrifuged for 90 min at 4 °C and 14 000 rpm. The supernatant was discarded, and a PBS washing step was done, followed by another centrifugation step. The supernatant was discarded, and the viral pellet was resuspended in 25 μL of lithium dodecyl sulfate (LDS) sample buffer (Life Technologies) and heated for 5 min at 95 °C.

Multiplex Serum Reactivity Test via DigiWest. Whole viral protein lysates from 229E, OC43, and NL63 (ZeptoMatrix Corp) and SARS-CoV-2 were used for DigiWest as described. First, viral protein lysates were subjected to gel electrophoresis and Western blotting using the NuPAGE system. Membranes were washed with PBST (0.1% Tween-20, PBS), and membrane-bound proteins were biotinylated by adding 50 μM NHS-PEG12-Biotin (Thermo Fisher Scientific) in PBST for 1 h. After washing in PBST, membranes were dried overnight. Subsequently, the Western blot lanes were cut

into 96 strips of 0.5 mm width and were transferred to a 96-well plate (Greiner Bio-One). For protein elution, 10 μL of elution buffer was added to each well (8 M urea, 1% Triton-X100 in 100 mM Tris-HCl pH 9.5). The protein eluates were diluted with 90 μL of dilution buffer (5% BSA in PBST, 0.02% sodium azide). Neutravidin-coated MagPlex beads (Luminex) of a distinct color ID were added to the protein eluates, and binding was allowed overnight; 500 μM PEG12-biotin in PBST was added to block remaining Neutravidin binding sites. The bead containing fractions were pooled, and thereby the original Western blot lanes were reconstituted. Beads were washed in PBST and resuspended in storage buffer (1% BSA, 0.05% azide, PBS). The generated bead set represents the proteomes of the four coronaviruses (SARS-CoV-2, OC43, 229E, NL63), and reactivity against all proteins can be tested in one assay.

For serum incubation, 5 μL of the bead mix was equilibrated in 50 μL of serum assay buffer (Blocking Reagent for ELISA (Roche) supplemented with 0.2% milk powder, 0.05% Tween-20 and 0.02% sodium azide, 25% Low Cross buffer (Candor Bioscience), 25% IgM-reducing agent buffer (ImmunoChemistry)). Serum assay buffer was discarded, and 30 μL of diluted patient serum (1:200 in serum assay buffer) was added and incubated for 2 h at room temperature on a shaker. After washing in PBST, 30 μL of phycoerythrin labeled anti-human IgG secondary antibody (diluted 1:200 in serum assay buffer; Dianova) was added and the plate was incubated for 45 min at 23 °C. The beads were washed twice with PBST, and readout was performed on a Luminex FlexMAP 3D platform.

The DigiWest analysis tool was used to assess serum reactivity against the viral proteins.¹⁵ Virus protein-specific peaks were identified, and average fluorescence intensity (AFI) values were calculated by integration of peak areas. To detect the nucleocapsid and the spike protein of SARS-CoV-2, commercially available antibodies were used (Sino Biologicals; nucleocapsid 40143-R019; spike protein 40591-MM42). Incubation was performed as described previously.²⁷

Generation of Expression Constructs for Production of Viral Antigens. The cDNAs encoding the nucleocapsid proteins of SARS-CoV-2, OC43, NL63, and 229E (GenBank accession numbers QHD43423.2; YP_009555245.1; YP_003771.1; NP_073556.1) were produced by gene synthesis (Thermo Fisher Scientific) and cloned including N-terminal hexahistidine (His6)-tag by standard techniques into NdeI/HindIII sites of the bacterial expression vector pRSET2b (Thermo Fisher Scientific).

Protein Expression and Purification. For production of the viral nucleocapsid proteins, the respective expression constructs were used to transform *E. coli* BL21(DE3) cells. Protein expression was induced in 1 L of TB medium at an optical density (OD600) of 2.5–3 by addition of 0.2 mM isopropyl- β -D-thiogalactopyranoside (IPTG) for 16 h at 20 °C. Cells were harvested by centrifugation (10 min 6000g), and the pellets were suspended in binding buffer (1 \times PBS, 0.5 M NaCl, 50 mM imidazole, 2 mM phenylmethylsulfonyl fluoride (PMSF), 2 mM MgCl₂, 150 $\mu\text{g}/\text{mL}$ lysozyme (Merck), and 625 $\mu\text{g}/\text{mL}$ DNaseI (Applichem)). The cell suspensions were sonified for 15 min (Bandelin Sonopuls HD70, power MS72/D, cycle 50%) on ice, incubated for 1 h at 4 °C in a rotary shaker, and sonified again. After centrifugation (30 min at 20 000g), urea was added to a final concentration of 6 M to the soluble protein extract. The extract was filtered through a 0.45 μm filter and loaded on a pre-equilibrated 1 mL

HisTrapFF column (GE Healthcare). The bound His-tagged nucleocapsid proteins were eluted by a linear gradient (30 mL) ranging from 50 to 500 mM imidazole in elution buffer (1× PBS, pH 7.4, 0.5 M NaCl, 6 M urea). Elution fractions (0.5 mL) containing the His-tagged purified proteins were analyzed via standard SDS-PAGE followed by staining with InstantBlue Coomassie stain (Expedeon). Immunoblotting using an anti-His antibody (Penta-His antibody, #34660, Qiagen) in combination with a donkey anti-mouse antibody labeled with AlexaFluor647 (Invitrogen) on a Typhoon Trio analyzer (GE-Healthcare, excitation 633 nm, emission filter settings 670 nm BP 30) was performed to confirm protein integrity.

Commercial Serological Assays. SARS-CoV-2 IgG and IgA ELISA (EUROIMMUN AG). The 96-well SARS-CoV-2 IgG ELISA and the 96-well SARS-CoV-2 IgA ELISA assay (EUROIMMUN) were performed on an automated BEP 2000 Advance system (Siemens Healthcare Diagnostics GmbH) according to the manufacturer's instructions. The ELISA assay detects anti-SARS-CoV-2 IgG and IgA, directed against the S1 domain of the viral spike protein, and relies on an assay-specific calibrator to report a ratio of specimen absorbance to calibrator absorbance. The final interpretation of positivity is determined by a ratio above a threshold value given by the manufacturer: positive (ratio ≥ 1.1), borderline (ratio = 0.8–1.0), or negative (ratio < 0.8). Quality control was performed following the manufacturer's instructions on each day of testing.

Elecsys Anti-SARS-CoV-2 Immunoassay (Roche Diagnostics GmbH). The Elecsys anti-SARS-CoV-2 assay is an ECLIA (electrogenenerated chemoluminescence immunoassay) assay designed by Roche Diagnostics GmbH and was used according to the manufacturer's instructions. It is intended for the detection of high affinity antibodies (including IgG) directed against the nucleocapsid protein of SARS-CoV-2 in human serum. Readout was performed on the Cobas ae411 analyzer. Negative results were defined by a cutoff index (COI) of < 1.0 . Quality control was performed following the manufacturer's instructions on each day of testing.

SARS-CoV-2 Total (COV2T) Immunoassay (Siemens Healthcare Diagnostics Inc.). The ADVIA Centaur SARS-CoV-2 Total (COV2T) assay is a chemiluminescent immunoassay intended for qualitative detection of total antibodies (including IgG and IgM) against SARS-CoV-2 in human serum and was used according to the manufacturer's instructions. The system reports ADVIA Centaur COV2T assay results in index values and as nonreactive < 1.0 or reactive ≥ 1.0 . Nonreactive samples are considered negative for SARS-CoV-2 antibodies; reactive samples are considered positive for SARS-CoV-2 antibodies.

Statistical Analysis. Sensitivity and specificity for each assay were calculated using the results of the PCR-testing as the gold standard. Concordance was calculated using Cohen's κ with 95% confidence intervals (CI).²⁸ Correlation was calculated using Spearman's r with 95% CI. For determining the dynamic range, a sigmoidal, 4-parameter logistic regression was used to fit the data and interpolate the dilution factor at the cutoff signal. All statistical analyses were performed using GraphPad Prism 8 or R studio (ver. 1.3.959).

Data Availability. The data sets generated during and/or analyzed during the current study are available from the corresponding author on reasonable request.

■ ASSOCIATED CONTENT

Supporting Information

The Supporting Information is available free of charge at <https://pubs.acs.org/doi/10.1021/acsinfecdis.0c00725>.

Raw data and graphical representation of DigiWest results of serum samples; calculation of Cohen's κ and AFI vs dT; calculation of sensitivity and specificity (ZIP)

■ AUTHOR INFORMATION

Corresponding Author

Markus F. Templin – NMI Natural and Medical Sciences Institute at the University of Tübingen, 72770 Reutlingen, Germany; orcid.org/0000-0002-6569-6489; Email: templin@nmi.de

Authors

Simon Fink – NMI Natural and Medical Sciences Institute at the University of Tübingen, 72770 Reutlingen, Germany

Felix Ruoff – NMI Natural and Medical Sciences Institute at the University of Tübingen, 72770 Reutlingen, Germany

Aaron Stahl – NMI Natural and Medical Sciences Institute at the University of Tübingen, 72770 Reutlingen, Germany

Matthias Becker – NMI Natural and Medical Sciences Institute at the University of Tübingen, 72770 Reutlingen, Germany

Philipp Kaiser – NMI Natural and Medical Sciences Institute at the University of Tübingen, 72770 Reutlingen, Germany

Bjoern Traenkle – Pharmaceutical Biotechnology, Eberhard-Karls-University, 72076 Tübingen, Germany

Daniel Junker – NMI Natural and Medical Sciences Institute at the University of Tübingen, 72770 Reutlingen, Germany

Frank Weise – NMI Natural and Medical Sciences Institute at the University of Tübingen, 72770 Reutlingen, Germany

Natalia Ruetalo – Institute for Medical Virology and Epidemiology of Viral Diseases, University Hospital Tübingen, 72076 Tübingen, Germany

Sebastian Hörber – Central Laboratory, Institute for Clinical Chemistry and Pathobiochemistry, University Hospital Tübingen, Tübingen 72076, Germany; Institute for Diabetes Research and Metabolic Diseases of the Helmholtz Center Munich at the University of Tübingen, 72076 Tübingen, Germany; German Center for Diabetes Research (DZD), München-Neuherberg 85764, Germany

Andreas Peter – Central Laboratory, Institute for Clinical Chemistry and Pathobiochemistry, University Hospital Tübingen, Tübingen 72076, Germany; Institute for Diabetes Research and Metabolic Diseases of the Helmholtz Center Munich at the University of Tübingen, 72076 Tübingen, Germany; German Center for Diabetes Research (DZD), München-Neuherberg 85764, Germany

Annika Nelde – Clinical Collaboration Unit Translational Immunology, German Cancer Consortium (DKTK), Department of Internal Medicine, University Hospital Tübingen, 72076 Tübingen, Germany; Department of Immunology, Institute for Cell Biology and Cluster of Excellence iFIT (EXC2180) "Image-Guided and Functionally Instructed Tumor Therapies", University of Tübingen, 72076 Tübingen, Germany

Juliane Walz – Clinical Collaboration Unit Translational Immunology, German Cancer Consortium (DKTK), Department of Internal Medicine and Department of Hematology, Oncology, Clinical Immunology and

- (11) Nelde, A., Bilich, T., Heitmann, J. S., Maringer, Y., Salih, H. R., Roerden, M., Lubke, M., Bauer, J., Rieth, J., Wacker, M., Peter, A., Horber, S., Traenkle, B., Kaiser, P. D., Rothbauer, U., Becker, M., Junker, D., Krause, G., Strengert, M., Schneiderhan-Marra, N., Templin, M. F., Joos, T. O., Kowalewski, D. J., Stos-Zweifel, V., Fehr, M., Rabsteyn, A., Mirakaj, V., Karbach, J., Jager, E., Graf, M., Gruber, L.-C., Rachfalski, D., Preuß, B., Hagelstein, I., Marklin, M., Bakchoul, T., Gouttefangeas, C., Kohlbacher, O., Klein, R., Stevanovic, S., Rammensee, H.-G., and Walz, J. S. (2021) SARS-CoV-2 T-Cell Epitopes Define Heterologous and COVID-19-Induced T-Cell Recognition. *Nat. Immunol.* *22*, 74–85.
- (12) Amanat, F., Stadlbauer, D., Strohmaier, S., Nguyen, T. H. O., Chromikova, V., McMahon, M., Jiang, K., Arunkumar, G. A., Jurczynszak, D., Polanco, J., Bermudez-Gonzalez, M., Kleiner, G., Aydilto, T., Miorin, L., Fierer, D. S., Lugo, L. A., Kojic, E. M., Stoeber, J., Liu, S. T. H., Cunningham-Rundles, C., Felgner, P. L., Moran, T., Garcia-Sastre, A., Caplivski, D., Cheng, A. C., Kedzierska, K., Vapalahti, O., Hepojoki, J. M., Simon, V., and Krammer, F. (2020) A Serological Assay to Detect SARS-CoV-2 Seroconversion in Humans. *Nat. Med.* *26* (7), 1033–1036.
- (13) Becker, M., Strengert, M., Junker, D., Kerrinnes, T., Kaiser, P. D., Traenkle, B., Dinter, H., Haering, J., Zeck, A., Weise, F., Peter, A., Hoerber, S., Fink, S., Ruoff, F., Bakchoul, T., Baillet, A., Lohse, S., Cornberg, M., Illig, T., Gottlieb, J., Smola, S., Karch, A., Berger, K., Rammensee, H.-G., Schenke-Layland, K., Nelde, A., Maerklin, M., Heitmann, J. S., Walz, J. S., Templin, M. F., Joos, T. O., Rothbauer, U., Krause, G. G., and Schneiderhan-Marra, N. (2021) Exploring beyond clinical routine SARS-CoV-2 serology using MultiCoV-Ab to evaluate endemic coronavirus cross-reactivity. *Nat. Commun.* *12*, 1152.
- (14) Burnette, W. N. (1981) Western Blotting[®]: Electrophoretic Transfer of Proteins from Sodium Dodecyl Sulfate-Polyacrylamide Gels to Unmodified Nitrocellulose and Radiographic Detection with Antibody and Radioiodinated Protein A. *Anal. Biochem.* *112* (2), 195–203.
- (15) Treindl, F., Ruprecht, B., Beiter, Y., Schultz, S., Döttinger, A., Staebler, A., Joos, T. O., Kling, S., Poetz, O., Fehm, T., Neubauer, H., Kuster, B., and Templin, M. F. (2016) A Bead-Based Western for High-Throughput Cellular Signal Transduction Analyses. *Nat. Commun.* *7* (1), 12852.
- (16) Tang, M. S., Hock, K. G., Logsdon, N. M., Hayes, J. E., Gronowski, A. M., Anderson, N. W., and Farnsworth, C. W. (2020) Clinical Performance of Two SARS-CoV-2 Serologic Assays. *Clin. Chem.* *66*, 1055.
- (17) Tang, M. S., Hock, K. G., Logsdon, N. M., Hayes, J. E., Gronowski, A. M., Anderson, N. W., and Farnsworth, C. W. (2020) Clinical Performance of the Roche SARS-CoV-2 Serologic Assay. *Clin. Chem.* *66*, 1107.
- (18) Hörber, S., Soldo, J., Relker, L., Jürgens, S., Guther, J., Peter, S., Lehmann, R., and Peter, A. (2020) Evaluation of Three Fully-Automated SARS-CoV-2 Antibody Assays. *Clin. Chem. Lab. Med.* *58*, 2113.
- (19) Leung, D. T. M., Tam, F. C. H., Ma, C. H., Chan, P. K. S., Cheung, J. L. K., Niu, H., Tam, J. S. L., and Lim, P. L. (2004) Antibody Response of Patients with Severe Acute Respiratory Syndrome (SARS) Targets the Viral Nucleocapsid. *J. Infect. Dis.* *190* (2), 379–386.
- (20) Sariol, A., and Perlman, S. (2020) Lessons for COVID-19 Immunity from Other Coronavirus Infections. *Immunity* *53*, 248.
- (21) Masse, S., Capai, L., Villechenaud, N., Blanchon, T., Charrel, R., and Falchi, A. (2020) Epidemiology and Clinical Symptoms Related to Seasonal Coronavirus Identified in Patients With. *Viruses* *12* (6), 630.
- (22) Gorse, G. J., Patel, G. B., Vitale, J. N., and O'Connor, T. Z. (2010) Prevalence of Antibodies to Four Human Coronaviruses Is Lower in Nasal Secretions than in Serum. *Clin. Vaccine Immunol.* *17* (12), 1875–1880.
- (23) Wu, A., Peng, Y., Huang, B., Ding, X., Wang, X., Niu, P., Meng, J., Zhu, Z., Zhang, Z., Wang, J., Sheng, J., Quan, L., Xia, Z., Tan, W., Cheng, G., and Jiang, T. (2020) Genome Composition and Divergence of the Novel Coronavirus (2019-nCoV) Originating in China. *Cell Host Microbe* *27* (3), 325–328.
- (24) Nickbakhsh, S., Ho, A., Marques, D. F. P., McMenamin, J., Gunson, R. N., and Murcia, P. R. (2020) Epidemiology of Seasonal Coronaviruses: Establishing the Context for the Emergence of Coronavirus Disease 2019. *J. Infect. Dis.* *222* (1), 17–25.
- (25) Grifoni, A., Weiskopf, D., Ramirez, S. I., Mateus, J., Dan, J. M., Moderbacher, C. R., Rawlings, S. A., Sutherland, A., Premkumar, L., Jodi, R. S., Marrama, D., de Silva, A. M., Frazier, A., Carlin, A. F., Greenbaum, J. A., Peters, B., Krammer, F., Smith, D. M., Crotty, S., and Sette, A. (2020) Targets of T Cell Responses to SARS-CoV-2 Coronavirus in Humans with COVID-19 Disease and Unexposed Individuals. *Cell* *181* (7), 1489–1501.
- (26) Ruetalo, N., Businger, R., Althaus, K., Fink, S., Ruoff, F., Hamprecht, K., Flehmig, B., Bakchoul, T., Templin, M. F., and Schindler, M. Neutralizing Antibody Response in Non-Hospitalized SARS-CoV-2 Patients. *medRxiv*, September 22, 2020, ver. 1. DOI: 10.1101/2020.08.07.20169961.
- (27) Treindl, F., Zabinsky, E., Kling, S., Schwarz, M., Braeuning, A., and Templin, M. F. (2020) Array-Based Western-Blotting Reveals Spatial Differences in Hepatic Signaling and Metabolism Following CAR Activation. *Arch. Toxicol.* *94* (4), 1265–1278.
- (28) McHugh, M. L. (2012) Lessons in Biostatistics Interrater Reliability: The Kappa Statistic. *Biochem. Medica* *22* (3), 276–282.

Supporting Information

The Supporting Information is available at ACS Infectious Diseases (<https://pubs.acs.org/doi/10.1021/acsinfecdis.0c00725>).

Supporting Information includes raw data and complete graphical representation of the data set, calculation of Cohen's κ , as well as calculation of sensitivity and specificity.

Appendix 2:

Felix Ruoff, Melanie Henes, Markus F. Templin, Markus Enderle, Hans Bösmüller, Diethelm Wallwiener, Sara Y. Brucker, Katja Schenke-Layland, and Martin Weiss. *Targeted Protein Profiling of In Vivo NIPP-Treated Tissues Using DigiWest Technology*. *Applied Sciences*; 11, (23), 11238 (2021).

<https://doi.org/10.3390/app112311238>

Article

Targeted Protein Profiling of In Vivo NIPP-Treated Tissues Using DigiWest Technology

Felix Ruoff ¹, Melanie Henes ², Markus Templin ¹, Markus Enderle ³, Hans Bösmüller ⁴, Diethelm Wallwiener ², Sara Y. Brucker ², Katja Schenke-Layland ^{1,5,6,7} and Martin Weiss ^{1,2,*}

¹ NMI Natural and Medical Sciences Institute, University of Tübingen, 72770 Reutlingen, Germany;

Felix.Ruoff@nmi.de (F.R.); markus.templin@nmi.de (M.T.); kschenkelayland@me.com (K.S.-L.)

² Department of Women's Health, University of Tübingen, 72076 Tübingen, Germany;

melanie.henes@med.uni-tuebingen.de (M.H.); Diethelm.Wallwiener@med.uni-tuebingen.de (D.W.);

sara.brucker@med.uni-tuebingen.de (S.Y.B.)

³ Erbe Elektromedizin GmbH, 72072 Tübingen, Germany; Markus.Enderle@erbe-med.com

⁴ Department of Pathology and Neuropathology, Eberhard Karls University, 72076 Tübingen, Germany;

hans.boesmueller@med.uni-tuebingen.de

⁵ Department of Biomedical Engineering, Eberhard Karls University, 72076 Tübingen, Germany

⁶ Cluster of Excellence iFIT (EXC 2180) "Image-Guided and Functionally Instructed Tumor Therapies",

Eberhard Karls University, 72074 Tübingen, Germany

⁷ Department of Medicine/Cardiology, University of California, Los Angeles, CA 90095, USA

* Correspondence: martin.weiss@med.uni-tuebingen.de; Tel.: +49-7071-29-82211



Citation: Ruoff, F.; Henes, M.; Templin, M.; Enderle, M.; Bösmüller, H.; Wallwiener, D.; Brucker, S.Y.; Schenke-Layland, K.; Weiss, M. Targeted Protein Profiling of In Vivo NIPP-Treated Tissues Using DigiWest Technology. *Appl. Sci.* **2021**, *11*, 11238. <https://doi.org/10.3390/app112311238>

Academic Editor: Eun Ha Choi

Received: 20 September 2021

Accepted: 15 November 2021

Published: 26 November 2021

Publisher's Note: MDPI stays neutral with regard to jurisdictional claims in published maps and institutional affiliations.



Copyright: © 2021 by the authors. Licensee MDPI, Basel, Switzerland. This article is an open access article distributed under the terms and conditions of the Creative Commons Attribution (CC BY) license (<https://creativecommons.org/licenses/by/4.0/>).

Abstract: Non-invasive physical plasma (NIPP) is a novel therapeutic tool, currently being evaluated for the treatment of cancer and precancerous lesions in gynecology and other disciplines. Additionally, patients with cervical intraepithelial neoplasia (CIN) may benefit from NIPP treatment due to its non-invasive, side-effect-free, and tissue-sparing character. However, the molecular impact of in vivo NIPP treatment needs to be further investigated. For this purpose, usually only very small tissue biopsies are available after NIPP treatment. Here, we adapted DigiWest technology, a high-throughput bead-based Western blot, for the analysis of formalin-fixed paraffin-embedded (FFPE) cervical punch biopsies with a minimal sample amount. We investigated the molecular effects of NIPP treatment directly after (0 h) and 24 h after in vivo application. Results were compared to in vitro NIPP-treated human malignant cervical cells. NIPP effects were primarily based on an inhibitory impact on the cell cycle and cell growth factors. DigiWest technology was suitable for detailed protein profiling of small, primary FFPE biopsies.

Keywords: FFPE protein extraction; non-invasive physical plasma; DigiWest; CIN; in vivo treatment

1. Introduction

Physical plasma is defined as a highly energized gas, forming reactive oxygen and nitrogen species (ROS and RNS) by interacting with the atmosphere, fluids, and organic surfaces. Consequently, ROS and RNS cause distinct cellular responses, including anti-proliferative and apoptotic cell mechanisms [1,2]. This enables the induction of protherapeutic biomedical effects regarding precancerous and cancerous tissue. In recent studies, non-invasive physical plasma (NIPP) treatment offered promising anti-neoplastic effects on a wide range of tumors in the field of gynecology and other medical subspecialties [3–9].

Cervical intraepithelial neoplasia (CIN) are very frequent precancerous lesions in young women, which may lead to cervical cancer. Thus, cervical cancer is still the fourth most common cancer for women worldwide, with about 270,000 cancer-related deaths per year [10,11]. Despite the fact that only few CIN lesions become invasive in the end, current guidelines recommend local excision procedures, which are associated with invasiveness, the need for local or general anesthesia, and serious short- and long-term side effects and risks, especially during pregnancy [12,13]. Therefore, overtreatment is a problem

for affected women and health economy. Recently, we deeply characterized NIPP as an innovative, non-invasive treatment procedure for CIN treatment [14].

To date, most of the knowledge about NIPP-related effects on human cells originates from *in vitro* experiments. To improve our understanding about the mode of action and about the conceivable medical applications of this innovative treatment approach it is important to investigate the molecular NIPP effects within a patient and to gain the maximum amount of possible information from *in vivo* NIPP-treated and formalin-fixed paraffin-embedded (FFPE) small tissue samples. Since the 1980s and the 1990s, it has been possible to extract and subsequently analyze DNA and RNA from FFPE tissue. This technique is even used in clinical routine nowadays [15]. Yet, to further enhance functional precision medicine it is essential to move beyond pure genetic and transcriptional analysis. Post-transcriptional regulatory mechanisms can have a tremendous impact on the molecular function of cells, and malfunctions induced through changes in protein level can be missed by pure genomic approaches [16]. To make it worse, cervical punch biopsies are characterized by a very small sample size (Figure 1).

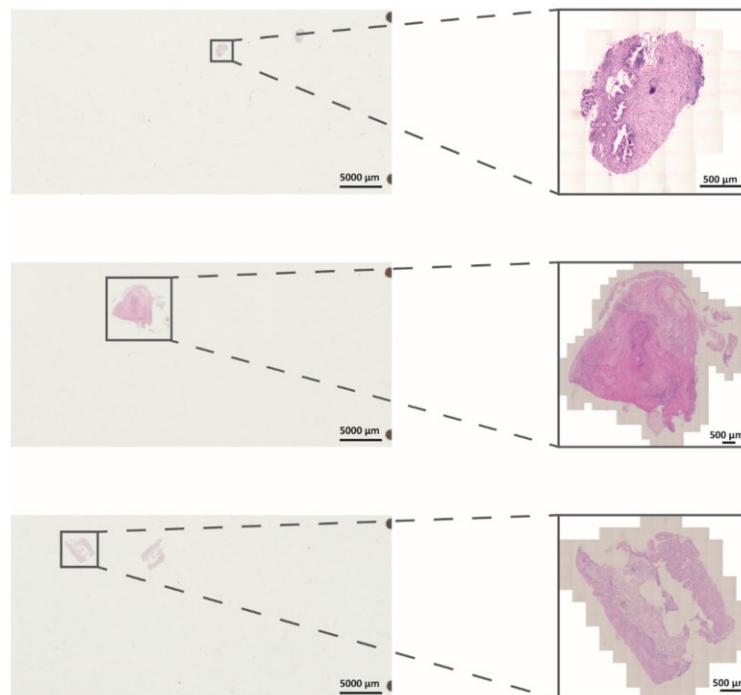


Figure 1. Representative light microscopic H&E staining of FFPE samples on slides. Shown are overview pictures of slides and magnified tissue areas (black boxes). Pictures were taken utilizing an Axio Scan Z.1 (Zeiss).

Hence, we established a workflow for targeted protein analysis from FFPE tissue samples from cervical punch biopsies by adapting a commercially available lysis protocol and utilizing DigiWest technology to obtain valuable molecular insights regarding *in vivo* NIPP treatment of CIN [17].

2. Materials and Methods

2.1. *In Vitro* and *In Vivo* NIPP Treatment

For NIPP treatment the electrosurgical device VIO® 3, APC 3 (Erbe Elektromedizin, Tübingen, Germany) was used (argon gas flow: 1.6 L/min; preciseAPC, effect 1). Cells were

dynamically treated in a suspension on a 6-well cell culture plate in 700 μ L of DMEM at a distance of 7 mm. The NIPP treatment of single cells was performed in a suspension for the following reasons: (i) to avoid mechanical detachment and associated cell damage, as well as drying effects due to the NIPP gas flow, and (ii) to enable NIPP treatment on a sterile, grounded metal mold with an identical electrical current and resistance. It was recently shown that the activation of media by plasma (plasma-activated media; PAM) reveals very similar anti-proliferative cell effects compared to direct plasma treatment [3]. Moreover, the unphysiological suspension state was limited to the treatment period before enabling the immediate reattachment of the cells. According to NIPP treatment, the controls were treated with argon gas alone (flow: 1.6 L/min) to exclude any alterations in cells and tissues due to the treatment procedure.

NIPP treatment of patients. Before NIPP treatment a clinical examination by colposcopy, 4% acetic acid, and Lugol's iodine staining was performed followed by NIPP treatment under a colposcopic view of visualized HSIL. The lesions were treated with NIPP for 30 s/cm² using a VIO3/APC3 and 3.2 mm APC probes (settings: preciseAPC, effect 1; ERBE Elektromedizin). The treatment was carried out on an outpatient basis and without local or general anesthesia on a conventional gynecological examination chair. A commercially available, reusable silicone electrode mat was placed under the patient as a negative electrode. The NIPP probe was passed over the tissue in defined "brush strokes" in order to avoid localized heating of the tissue. Treatment was performed within an ongoing prospective, single-armed phase IIb clinical trial (NCT03218436) at the Department for Women's Health, Tübingen, Germany. NIPP treatment and tissue analysis was approved by the Ethical Committee of the Medical Faculty of the Eberhardt Karls University of Tübingen (237-2017BO1).

2.2. Propagation of Cells

Cervical squamous cell carcinoma-derived (CSCC) cells were purchased from ATCC (ATCC[®] TCP-1022[™], American Type Culture Collection). In detail, these were CaSki (ATCC CRL-1550), DoTc2-4510 (ATCC CRL-7920), and SiHa (ATCC HTB-35). CaSki and SiHa cells are positive for human papillomavirus (HPV) and are derived from squamous cell carcinomas of the cervix uteri, whereas DoTc2 4510 cells are derived from adenocarcinomas. CSCC cells were cultured in Dulbecco's Modified Eagle's Medium (DMEM F12, Fischer Scientific, Hampton, NH, USA), supplemented with 10% fetal bovine serum (Life Technologies, Carlsbad, CA, USA), 1 mM of sodium pyruvate (Life Technologies), and 1% penicillin/streptomycin (Invitrogen, Carlsbad, CA, USA) at 37 °C and 5% CO₂ in a humidified atmosphere. Every 2–3 days, a medium exchange was performed, and cells were passaged after reaching 70%–80% confluence. The adherent cells were detached by trypsin/EDTA (0.05%, 10 mM at 37 °C; Life Technologies) treatment.

2.3. Protein Extraction from FFPE Tissue

Macrodissection of FFPE tissue (10–400 mm²) mounted on 4–6 slides was performed utilizing a Qproteom FFPE Tissue kit (Quiagen, Hilden, Germany). Tissue picks (Covaris, Woburn, MA, USA) were moistened with 2 μ L of ExB+ (Quiagen, Hilden, Germany) and used to scrape off desired tissue areas. An H&E-stained master slide, marked by a pathologist, was used as a template. Samples were collected in 1.5 mL LoBind reaction tubes (Eppendorf, Hamburg, Germany). For protein extraction, the heptane-based protocol was used. The volume of ExB+ was adjusted to 20 μ L; all other steps were performed according to the manufacturer's recommendations. The volume of protein lysates was reduced using a vacuum concentrator for 1.5 h. The resulting protein lysates were diluted in loading buffer containing 212 mM of Tris, 282 mM of Tris base, 1.01 mM of EDTA, and 50 mM of DTT (Invitrogen, Carlsbad, CA, USA), supplemented with 10% glycerol, 0.22 mM of Coomassie brilliant blue, and 0.175 mM of phenol red (Figure S1a).

2.4. Lysis of Cell Culture Pellets

Dry cell pellets were lysed by adding 30 μ L of a lysis buffer, containing 4% SDS, 50 mM of DTT, cOMplete protease inhibitor, and PhosSTOP phosphatase inhibitor (Roche, Basel, Switzerland) on ice, and by subsequently being incubated for 10 min at 95 °C in a block heater. The samples were brought to room temperature, and the whole volume was transferred to a QuiaShredder spin column (Quiagen, Hilden, Germany) and then centrifuged at 16,000 \times *g* for 5 min to remove DNA. Samples were transferred to and stored in 1.5 mL LoBind reaction tubes (Eppendorf, Hamburg, Germany).

2.5. Multiplex Protein Profiling via DigiWest

DigiWest was performed as described previously [18]. Briefly, the NuPAGE system (Life Technologies, Carlsbad, CA, USA) with a 4–12% Bis-Tris gel was used for gel electrophoresis and Western blotting onto PVDF membranes. After washing with PBST, proteins were biotinylated by adding 50 μ M of NHS-PEG12-Biotin in PBST for 1 h to the membrane. After washing in PBST, membranes were dried overnight. Each Western blot lane was cut into 96 strips of 0.5 mm each. Strips of one Western blot lane were sorted into a 96-well plate (Greiner Bio-One, Frickenhausen, Germany) according to their molecular weight. Protein elution was performed using 10 μ L of elution buffer (8 M urea, 1% Triton-X100 in 100 mM of Tris-HCl with a pH of 9.5). Neutravidin-coated MagPlex beads (Luminex, Austin, TX, USA) of a distinct color ID were added to the proteins of a distinct molecular weight fraction, and coupling was performed overnight. Leftover binding sites were blocked by adding 500 μ M of deactivated NHS-PEG12-Biotin for 1 h. To reconstruct the original Western blot lane, the beads were pooled, at which point the color IDs represent the molecular weight fraction of the proteins.

For antibody incubation, 5 μ L aliquots of the DigiWest bead mixes were added to 50 μ L of an assay buffer (blocking reagent for ELISA (Roche, Rotkreuz, Switzerland) supplemented with 0.2% milk powder, 0.05% Tween-20, and 0.02% sodium azide) or PVXC buffer (0.1% casein, 0.5% PVA, 0.8% PVP, and 0.05% Tween-20 in PBS) in a 96-well plate. The buffer was discarded and 30 μ L of primary antibody diluted in assay buffer or PVXC buffer was added per well. Primary antibodies were incubated overnight at 15 °C on a shaker. Subsequently, primary antibodies were discarded and beads were washed twice with PBST. After washing, 30 μ L of species-specific secondary antibody diluted in an assay buffer or PVXC buffer labeled with phycoerythrin was added and incubation took place for 1 h at 23 °C. Before the readout on a Luminex FlexMAP 3D, beads were washed twice with PBST. Protein bands were depicted as peaks by plotting the molecular weight to the corresponding median signal intensity. An Excel macro-based algorithm was used to identify peaks at the provided molecular weight of each antibody. After subtracting the local background integrals of the area of a peak was calculated. The resulting signals were normalized to the total amount of protein that was loaded onto the beads (Figure S1b).

2.6. Statistical Analysis

Statistical comparison was carried out with a Wilcoxon rank-sum test or a Kruskal–Wallis test, (GraphPad Prism version 6.0, GraphPad Software; MultiExperiment Viewer (MeV) version 4.0.9 [19]), as specified in the figure legends. The data are expressed as mean \pm standard deviation. *p* values of <0.05 were considered statistically significant.

3. Results

3.1. Establishment and Evaluation of DigiWest from FFPE Samples after In Vivo NIPP Treatment

Due to the very small sample size of cervical punch biopsies, multiplex protein profiling from FFPE tissue obtains valuable molecular insights into NIPP treatment. To analyze protein expression levels after in vivo NIPP treatment we established DigiWest technology to FFPE tissue slides before (*n* = 5 patients), directly after (0 h; *n* = 3 patients), and 24 h after in vivo NIPP treatment (*n* = 4 patients). The tissue specimens used were

mounted on slides for histopathological assessment, and the tissue area ranged from 10 mm² to 400 mm² (Figure 1).

Using DigiWest, 69 analytes covering apoptosis machinery, DNA damage response (DDR), and cell cycle control were analyzed. Resulting median fluorescence intensity (MFI) values were compared between samples before, 0 h after treatment, and a control, as well as 24 h after treatment and a control. Twenty-nine antibodies delivered a detectable signal in all samples. After median centration and log₂ transformation, hierarchical clustering (complete linkage, Euclidean distance) revealed a similar protein expression pattern of all preNIPP samples (Figure 2). Yellow indicates a high signal level, whereas blue indicates a low signal level when compared to the median of all samples. Samples are clustered horizontally and analytes are clustered vertically. Most of the samples 0 h and 24 h postNIPP have a similar protein expression profile. This indicates a good sample quality and protein yield.

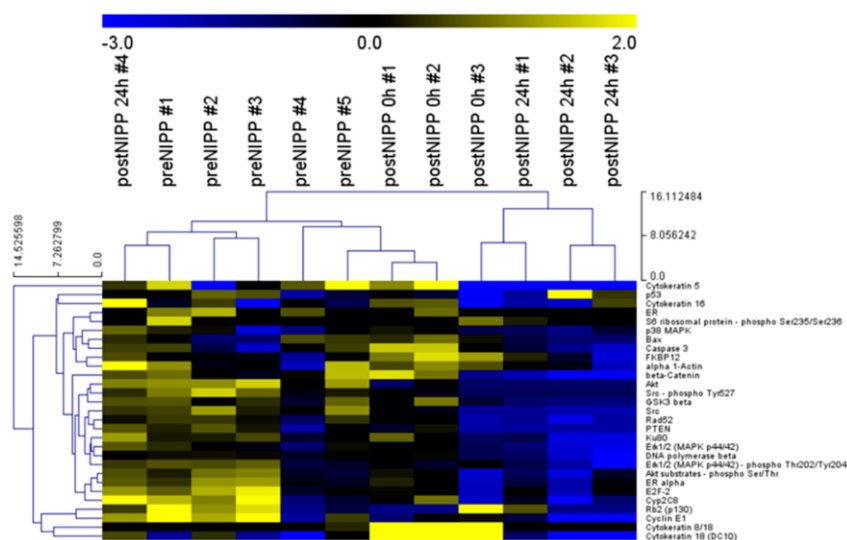


Figure 2. DigiWest protein profiles of a control (untreated) as well as 0 h and 24 h after treatment patient samples. Heat map of log₂ transformed DigiWest data. Data were median-centered, and hierarchical clustering was performed using complete linkage and Euclidean distance, utilizing the MultiExperiment Viewer (MeV version 4.9.0, ref. [19]) software. Yellow indicates high signal level and blue indicates a low signal level (compared to the median).

3.2. Protein Profiles of Patients and Cell Culture following In Vivo and In Vitro NIPP Treatment

NIPP treatment induces various biological effects, including antineoplastic efficacy [8]. Therefore, NIPP is a promising tool for the treatment of precancer and cancer. Here, we examined the overall antineoplastic properties by performing both in vitro NIPP treatment of the human malignant cervical cell line, CSCC, as well as in vivo NIPP treatment of patients with histologically confirmed lesions of CIN.

First, we analyzed cell pellets from an NIPP-treated CSCC cell culture ($n = 6$) compared to argon-treated controls ($n = 6$) harvested after 24 h. We analyzed a total of 132 proteins, covering apoptosis, DDR, and cell cycle control, forty-four of which were matching analytes with the FFPE analysis (Figures 3a and 4a). Generally, the differences in signal intensity in the cell culture sample set was rather low, due to only one analyte showing a mean log₂ foldchange greater than 1 or -1 after in vitro NIPP treatment (Figure 3b).

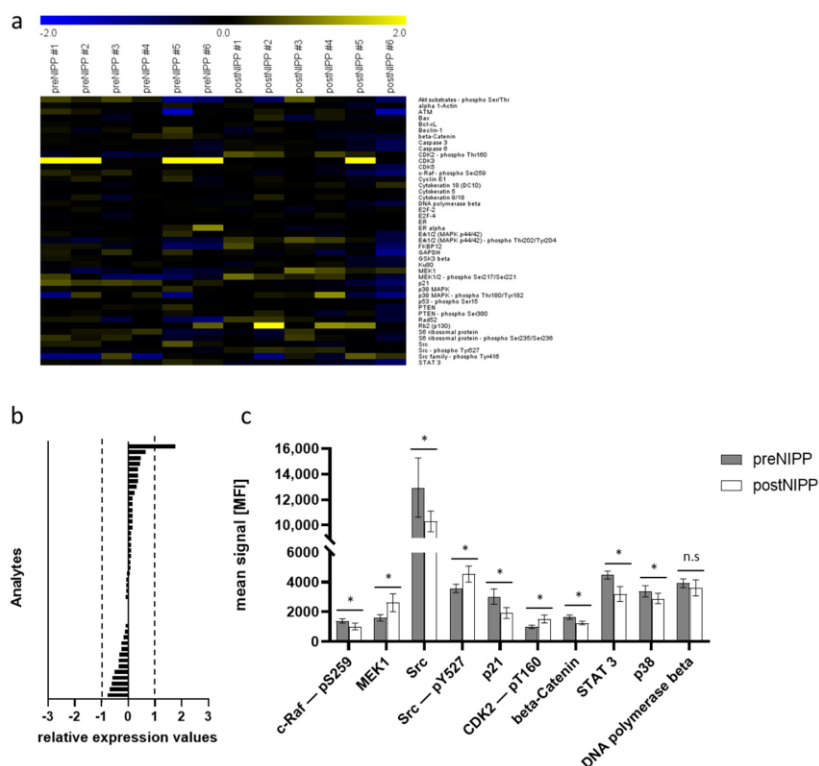


Figure 3. Protein expression after in vitro non-invasive physical plasma (NIPP) treatment of the human malignant cervical squamous cell carcinoma cell line (CSCC). (a) Heat map of \log_2 -transformed DigiWest data. Yellow indicates a high signal level and blue indicates a low signal level (compared to the median). (b) Bar graphs of \log_2 -transformed ratios calculated from the mean expression of NIPP treatment and controls, sorted from the highest positive change to the highest negative change. (c) Bar graphs of signals generated from cell culture samples. Shown are the means and standard derivation of NIPP treatment and controls. * indicates a significant difference in expression, n.s. indicates no significant difference in expression (Wilcoxon rank sum test, $p < 0.05$).

NIPP-treated CSCC cells showed significantly reduced expression levels of various pro-proliferative factors (Figure 3c). We found that the mitogen-activated protein kinase (MAPK) pathway was targeted by NIPP treatment. This was shown by a significant downregulation of p38 mitogen-activated protein kinases (p38), the RAF proto-oncogene serine/threonine-protein kinase (c-Raf) acting as a kinase cascade initiator [20], as well as the dual specificity mitogen-activated protein kinase kinase 1 (MEK1), being a dual threonine and tyrosine recognition kinase responsible for MAPK phosphorylation and activation [21]. These factors are critically involved in cell growth and apoptosis regulation and can act as oncogenes. Furthermore, the proto-oncogene tyrosine-protein kinase Src was significantly decreased, whereas it showed a slight but statistically significant increase in phosphorylation (pTyr527). As a central proto-oncogene, Src plays an important role in cell survival, proliferation, and invasion, and has been shown to interact with several signaling pathways, including MAPK/MEK1/RAF, Akt, and signal transducer and activator of transcription 3 (STAT3) [22,23].

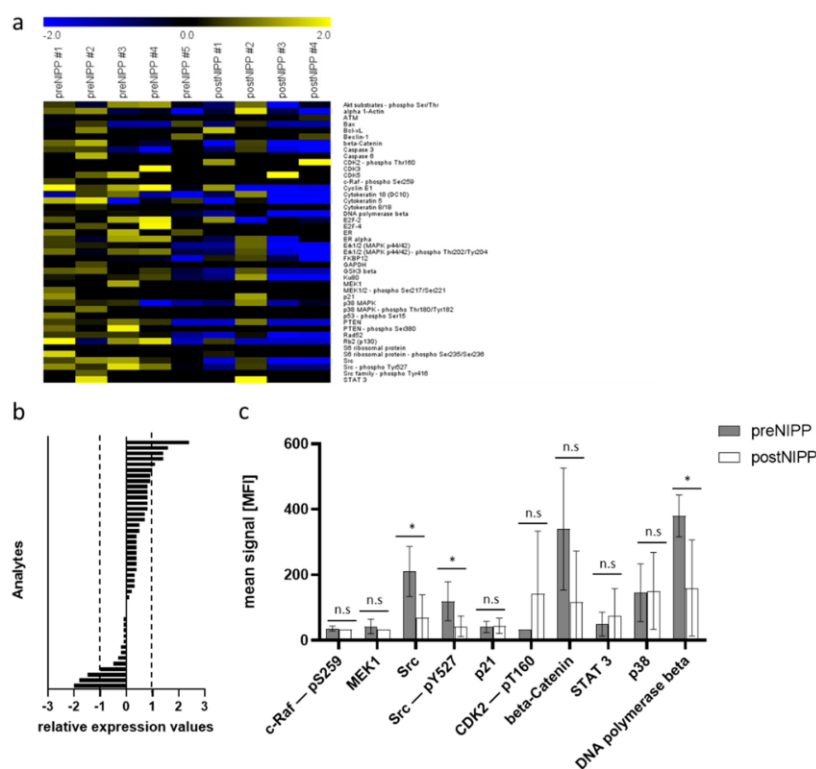


Figure 4. Protein expression after in vivo non-invasive physical plasma (NIPP) treatment of patients with cervical intraepithelial neoplasia (CIN). (a) Heat map of log₂-transformed DigiWest data. Yellow indicates a high signal level and blue indicates a low signal level (compared to the median). (b) Bar graphs of log₂-transformed ratios calculated from the mean expression of NIPP treatment and controls sorted from the highest positive change to the highest negative change. (c) Bar graphs of signals generated from patient samples. Shown are the means and standard deviation of NIPP treatment and controls. * indicates a significant difference in expression, n.s. indicates no significant difference in expression (Wilcoxon rank sum test, $p < 0.05$).

Interestingly, NIPP treatment of CSCC cells caused a significant decrease in the transcription factor STAT3, which plays an important role in many cellular processes, such as cell growth and apoptosis [24]. Furthermore, we found a downregulation of cyclin-dependent kinase inhibitor 1 (p21) being primarily associated with inhibition of cyclin-dependent kinase 2 (CDK2) [25,26]. Thus, the phosphorylation of CDK2 (CDK2-pT160) was also significantly increased, having an impact on cell growth and cell cycle regulation.

Tissue samples from in vivo NIPP-treated patients revealed comparable results. As shown in Figure 2, we were able to analyze 69 analytes using DigiWest technology. Forty-four of which were matching proteins of the previous analysis related to apoptosis machinery, DDR, and cell cycle control (Figures 3a and 4a). Overall, we detected higher differences in protein expression between when comparing FFPE tissue and cell lysates shown by more intensive signals in the heat map analysis of log₂-transformed DigiWest data. Thereby, eight analytes in the FFPE sample set showed a considerable change in expression after in vivo NIPP treatment (mean log₂ foldchange greater than 1 or -1) (Figure 4b).

Again, NIPP treatment of patients with CIN was accompanied by a significant decrease in proto-oncogene tyrosine-protein kinase Src expression and phosphorylation. Other proliferative factors shown to be up- or downregulated (such as p38, c-Raf, MEK1, STAT3, and p21) were not significantly altered. Comparable to NIPP-treated CSCC cells, CDK2 showed a valuable increase; however, this was not statistically significant.

Additionally, protein profiling immediately after *in vivo* NIPP treatment (0 h) demonstrated a transient significant increase in cytokeratin 8 (CK8) and 18 (CK18) (Figure S2). After 24 h this effect was reversed. CK18 and the co-expressed complementary partner, CK8, maintain the physiological cell function against external stress and play an important role in apoptosis and the cell cycle [27]. Furthermore, we found a significant decrease in protein kinase B (Akt) expression 0 h and 24 h following *in vivo* NIPP treatment. The Akt signal transduction pathway promotes cell survival and cell growth in response to extracellular signals by regulating apoptosis and cell cycle [28,29]. Among other functions, Akt regulates the CDK inhibitor p21 and the proto-oncogene Src, promoting cell cycle progression.

4. Discussion

To date, only a few individual case reports exist, describing *in vivo* NIPP treatment of cancer patients [6,8,14]; none have been conducted yet on NIPP treatment of precancerous diseases. Recently, we established the electrosurgical argon plasma device VIO3/APC3 (Erbe Elektromedizin, Tübingen, Germany) for the *in vivo* treatment of patients [9,30]. Currently, we are performing a prospective, single-armed phase IIb clinical trial (NCT03218436) at the Department for Women's Health, Tübingen, Germany. For this purpose, the molecular examination of tiny cervical punch biopsies obtained from *in vivo* NIPP-treated patients is becoming more and more crucial. However, although fresh, frozen tissue would be ideal for research purposes, this is not practical for a clinical setting. For histopathological assessment, the morphological structure of tissues must be conserved. Therefore, clinical samples are immediately fixed with formalin and embedded in paraffin wax. Formalin cross-links form a protein grid that preserves the tissue structure and prevents protein degradation [31]. Subsequent paraffin embedding facilitates the handling of samples and sectioning of the tissue into thin slices for staining and microscopical assessment. Furthermore, formalin fixation enables long-term storage at room temperature. As efficient as formalin fixation is for the prevention of tissue degradation, the occurring protein crosslinks disturb most bioanalytical methods. In particular, the separation of molecules based on their molecular size is usually disabled, since the crosslinks cause irreversible protein aggregation, resulting in low amounts of specific proteins. However, DigiWest technology enables Western-blot-like incubation of up to app. 200 antibodies from minimal sample amounts by transferring proteins onto microspheres and miniaturization of the assay system [18].

In the present study, we established the targeted protein analysis from small-sized FFPE tissue sections obtained from cervical punch biopsies utilizing DigiWest technology. This enabled the analysis of molecular tissue effects following *in vivo* NIPP treatment of CIN. Moreover, we compared the results with the *in vitro* NIPP-treated human malignant cervical cell line, C5637. Non-thermally operated NIPP devices lead to the formation of ROS, as shown by previous studies [6,14,32].

ROS and RNS are the responsible drivers of NIPP-related anti-neoplastic efficacy in human cervical cancer cells due to cell cycle arrest and apoptosis [9]. Additionally, in this study, NIPP treatment affected central factors in the regulation of apoptosis and cell growth pathways. In particular, NIPP treatment resulted in the transient induction of cell survival factors (CK8/18), accompanied and followed by the downregulation of pro-proliferative factors (here: Akt, p38 MAPK, Src, and RAF) and the upregulation of cell-growth-attenuating pathways. The *in vitro* cell panel used in this study includes cells from squamous epithelial tumors and adenocarcinomas. SiHa and CaSki cells harbor HPV infections; DoTc2 4510 cells originate from a metastatic CC lesion. Moreover, several well-known mutations of gynecological cancers, such as p53, BRCA2, or PIK3CA, are represented by these cell lines. In general, we found no evidence for a distinct factor resulting in increased NIPP resistance. This indicates a multifactorial intracellular process initiated by NIPP treatment.

Besides its structural function in the cytoskeleton, CK8/18 regulates apoptosis and is released during apoptosis and necrosis [33,34]. CK18 release can even occur independently of caspase activation [35]. Hence, our findings suggest that NIPP treatment may directly induce a cell survival response, followed by apoptosis.

It is likely that NIPP impairs the Akt-driven progression of the G1-S cell cycle phase by inactivating glycogen synthase kinase 3 (GSK-3) and preventing cyclin D1 degradation [36]. CDK2 is a subunit of the cyclin-dependent kinase complex, mainly involved and restricted to the regulation of the G1-S phase of the cell cycle [37]. The fully active CDK2 (in a complex with cyclins) is phosphorylated at threonine 160 (T160) [38], a regulative response which could also be shown after *in vitro* and *in vivo* NIPP treatment. Moreover, a downregulation of the CDK2 inhibitor p21 [25,26] was demonstrated in NIPP-treated CSCC cells. However, CDK2 does not seem to be essential for proceeding or arresting the transition during the G1-S phase [39].

Noticeable, *in vitro* and *in vivo* NIPP treatment caused a significantly reduced expression and phosphorylation of the proto-oncogene tyrosine-protein kinase Src, which was shown to be upregulated in about half of the tumors from the colon, liver, lung, breast, and pancreas [40]. Thereby, Src has a central impact on cell survival, proliferation, and invasion. Src has been shown to be involved in further pro-proliferative cell responses and to interact with important regulative factors including MAPK/MEK1/RAF, Akt, and STAT3 [22,23]. Interestingly, all of these interacting factors have been shown to be reduced after *in vitro* NIPP treatment of CSCC cells; however, it could be not confirmed after *in vivo* NIPP treatment of CIN. The results suggest that changes in protein expression observed in cell culture experiments may not be transferable to *in vivo* treatment.

This underlines the importance of performing studies on *in vivo* NIPP applications and consecutive analysis of the biological effects, some of which differ considerably from *in vitro* results. Overall, the analysis of cell culture samples is much easier; additionally, here, it resulted in more statistically significant changed analytes than the analysis of FFPE patient samples. However, the changes in expression after treatment were more distinct in the patient samples. This may be because FFPE samples delivered lower absolute intensities of signals compared to cell culture samples, which may be rooted in the differences in sample preparation. However, normalization to the total protein loaded on beads relativizes such effects. Additionally, the smaller samples size in this study may limit the statistical power of the used tests.

In conclusion, we demonstrated the molecular efficacy of NIPP treatment within human malignant cervical cell lines and CIN. NIPP effects were primarily based on the inhibitory impact on the cell cycle and cell growth factors. NIPP treatment effects need to be studied more frequently *in vivo*, or at least in patient-derived cell culture models such as organoids or patient-derived microtumors (PDMs) that mimic the *in vivo* situation much better [41]. DigiWest technology enables comprehensive protein profiling from very small and FFPE primary tissue biopsies.

Supplementary Materials: The following are available online at <https://www.mdpi.com/article/10.3390/app112311238/s1>, Figure S1: Overview of FFPE extraction and DigiWest workflow; Figure S2: Selected DigiWest results of a control (untreated) as well as 0 h and 24 h after treatment FFPE samples; Table S1: Raw and normalized data used for analysis; Table S2: List of used antibodies.

Author Contributions: Conceptualization, F.R., M.T. and M.W.; methodology, F.R., M.T. and M.W.; formal analysis, F.R. and M.W.; investigation, F.R. and M.W.; data curation, F.R. and M.W.; writing—original draft preparation, F.R. and M.W.; writing—review and editing, M.T., M.H., M.E., H.B., D.W., S.Y.B. and K.S.-L.; supervision, M.T., D.W., S.Y.B. and K.S.-L.; project administration, M.W. All authors have read and agreed to the published version of the manuscript.

Funding: This study was financially supported by the Faculty of Medicine of the Eberhard Karls University of Tübingen (grant No. 2432-1-0, 417-0-0 to M.W., and IZKF 2018-1-06 to M.W.), Graduate School 2543/1 “Intraoperative Multi-Sensory Tissue-Differentiation in Oncology” (project(s) A3 and C2) funded by the German Research Foundation (GRK 2543/1 to S.Y.B., K.S.-L., and M.W.; 04/2020).

We acknowledge support from the Open Access Publishing Fund of the University of Tübingen. This work received financial support from the State Ministry of Baden-Wuerttemberg for Economic Affairs, Labour and Tourism.

Institutional Review Board Statement: The study was conducted according to the guidelines of the Declaration of Helsinki, and approved by the Institutional Ethics Committee of the Medical Faculty of the Eberhard-Karls University of Tübingen (protocol code 237-2017BO1).

Informed Consent Statement: Informed consent was obtained from all subjects involved in the study.

Data Availability Statement: The data presented in this study are available in Table S1. Information about antibodies used in this study are available in Table S2.

Acknowledgments: This work was supported by Erbe Elektromedizin GmbH, Tübingen (loaner of NIPP device and equipment).

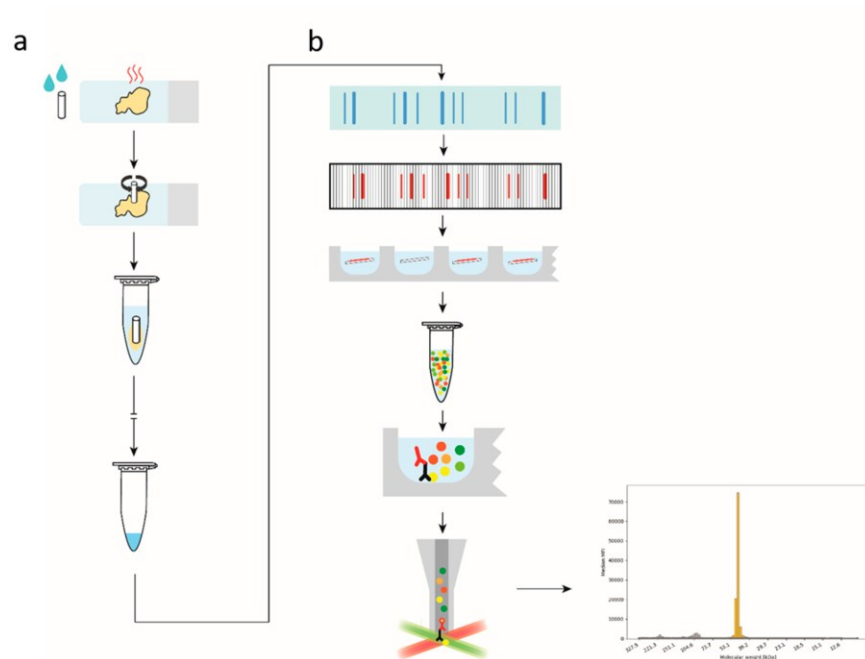
Conflicts of Interest: M.E. is an employee of Erbe Elektromedizin GmbH.

References

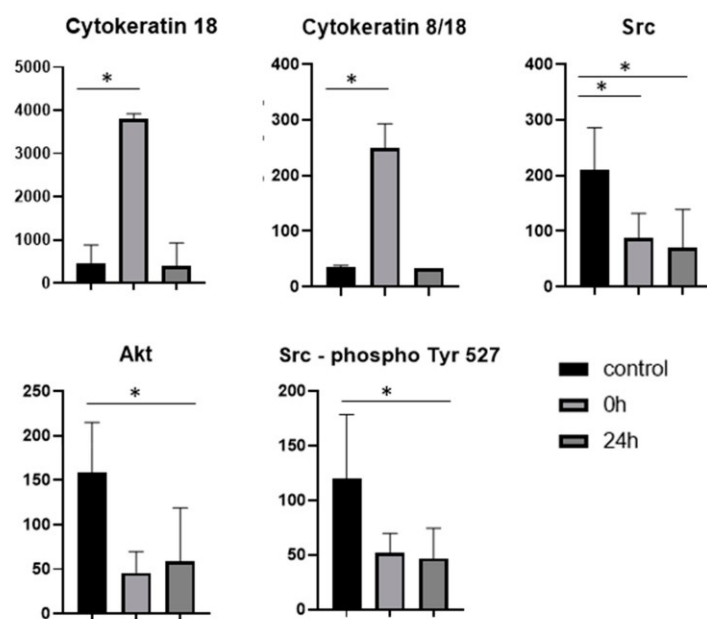
1. Hirst, A.M.; Frame, F.M.; Arya, M.; Maitland, N.J.; O'Connell, D. Low temperature plasmas as emerging cancer therapeutics: The state of play and thoughts for the future. *Tumour Biol.* **2016**, *37*, 7021–7031. [[CrossRef](#)]
2. Mitra, S.; Nguyen, L.N.; Akter, M.; Park, G.; Choi, E.H.; Kaushik, N.K. Impact of ros generated by chemical, physical, and plasma techniques on cancer attenuation. *Cancers* **2019**, *11*, 1030. [[CrossRef](#)] [[PubMed](#)]
3. Koensgen, D.; Besic, I.; Gumbel, D.; Kaul, A.; Weiss, M.; Diesing, K.; Kramer, A.; Bekeschus, S.; Mustea, A.; Stope, M.B. Cold atmospheric plasma (cap) and cap-stimulated cell culture media suppress ovarian cancer cell growth—A putative treatment option in ovarian cancer therapy. *Anticancer Res.* **2017**, *37*, 6739–6744. [[CrossRef](#)] [[PubMed](#)]
4. Weiss, M.; Gumbel, D.; Gelbrich, N.; Brandenburg, L.O.; Mandelkow, R.; Zimmermann, U.; Ziegler, P.; Burchardt, M.; Stope, M.B. Inhibition of cell growth of the prostate cancer cell model Incap by cold atmospheric plasma. *Vivo* **2015**, *29*, 611–616.
5. Weiss, M.; Gumbel, D.; Hanschmann, E.M.; Mandelkow, R.; Gelbrich, N.; Zimmermann, U.; Walther, R.; Ekkernkamp, A.; Sckell, A.; Kramer, A.; et al. Cold atmospheric plasma treatment induces anti-proliferative effects in prostate cancer cells by redox and apoptotic signaling pathways. *PLoS ONE* **2015**, *10*, e0130350. [[CrossRef](#)] [[PubMed](#)]
6. Wenzel, T.; Carvajal Berrio, D.A.; Daum, R.; Reisenauer, C.; Weltmann, K.D.; Wallwiener, D.; Brucker, S.Y.; Schenke-Layland, K.; Brauchle, E.M.; Weiss, M. Molecular effects and tissue penetration depth of physical plasma in human mucosa analyzed by contact- and marker-independent raman microspectroscopy. *ACS Appl. Mater. Interfaces* **2019**, *11*, 42885–42895. [[CrossRef](#)]
7. Weiss, M.; Barz, J.; Ackermann, M.; Utz, R.; Ghoul, A.; Weltmann, K.D.; Stope, M.B.; Wallwiener, D.; Schenke-Layland, K.; Oehr, C.; et al. Dose-dependent tissue-level characterization of a medical atmospheric pressure argon plasma jet. *ACS Appl. Mater. Interfaces* **2019**, *11*, 19841–19853. [[CrossRef](#)]
8. Braný, D.; Dvorská, D.; Halašová, E.Š.H. Cold atmospheric plasma: A powerful tool for modern medicine. *Int. J. Mol. Sci.* **2020**, *21*, 2932. [[CrossRef](#)]
9. Weiss, M.; Utz, R.; Ackermann, M.; Taran, F.; Krämer, B.; Hahn, M.; Wallwiener, D.; Brucker, S.; Haupt, M.; Barz, J.; et al. Characterization of a non-thermally operated electrosurgical argon plasma source by electron spin resonance spectroscopy. *Plasma Process. Polym.* **2019**, *16*, 1800150. [[CrossRef](#)]
10. Ferlay, J.; Soerjomataram, I.; Dikshit, R.; Eser, S.; Mathers, C.; Rebelo, M.; Parkin, D.M.; Forman, D.; Bray, F. Cancer incidence and mortality worldwide: Sources, methods and major patterns in globocan 2012. *Int. J. Cancer* **2015**, *136*, E359–E386. [[CrossRef](#)]
11. Peto, J.; Gilham, C.; Deacon, J.; Taylor, C.; Evans, C.; Binns, W.; Haywood, M.; Elanko, N.; Coleman, D.; Yule, R.; et al. Cervical hpv infection and neoplasia in a large population-based prospective study: The manchester cohort. *Br. J. Cancer* **2004**, *91*, 942–953. [[CrossRef](#)]
12. Kyrgiou, M.; Athanasiou, A.; Kalliala, I.E.J.; Paraskevaidis, M.; Mitra, A.; Martin-Hirsch, P.P.; Arbyn, M.; Bennett, P.; Paraskevaidis, E. Obstetric outcomes after conservative treatment for cervical intraepithelial lesions and early invasive disease. *Cochrane Database Syst Rev.* **2017**, *11*, CD012847. [[CrossRef](#)]
13. Sadler, L.; Saftlas, A.; Wang, W.; Exeter, M.; Whittaker, J.; McCowan, L. Treatment for cervical intraepithelial neoplasia and risk of preterm delivery. *JAMA* **2004**, *291*, 2100–2106. [[CrossRef](#)]
14. Wenzel, T.; Carvajal Berrio, D.A.; Reisenauer, C.; Layland, S.; Koch, A.; Wallwiener, D.; Brucker, S.Y.; Schenke-Layland, K.; Brauchle, E.M.; Weiss, M. Trans-mucosal efficacy of non-thermal plasma treatment on cervical cancer tissue and human cervix uteri by a next generation electrosurgical argon plasma device. *Cancers* **2020**, *12*, 267. [[CrossRef](#)] [[PubMed](#)]
15. Specht, K.; Richter, T.; Muller, U.; Walch, A.; Werner, M.; Hofler, H. Quantitative gene expression analysis in microdissected archival formalin-fixed and paraffin-embedded tumor tissue. *Am. J. Pathol.* **2001**, *158*, 419–429. [[CrossRef](#)]
16. Zhang, M.; Matyunina, L.V.; Walker, L.D.; Chen, W.; Xiao, H.; Benigno, B.B.; Wu, R.; McDonald, J.F. Evidence for the importance of post-transcriptional regulatory changes in ovarian cancer progression and the contribution of mirnas. *Sci. Rep.* **2017**, *7*, 8171. [[CrossRef](#)] [[PubMed](#)]

17. Bockmayr, T.; Erdmann, G.; Treue, D.; Jurmeister, P.; Schneider, J.; Arndt, A.; Heim, D.; Bockmayr, M.; Sachse, C.; Klauschen, F. Multiclass cancer classification in fresh frozen and formalin-fixed paraffin-embedded tissue by digiwest multiplex protein analysis. *Lab. Investig.* **2020**, *100*, 1288–1299. [[CrossRef](#)] [[PubMed](#)]
18. Treindl, F.; Ruprecht, B.; Beiter, Y.; Schultz, S.; Dottinger, A.; Staebler, A.; Joos, T.O.; Kling, S.; Poetz, O.; Fehm, T.; et al. A bead-based western for high-throughput cellular signal transduction analyses. *Nat. Commun.* **2016**, *7*, 12852. [[CrossRef](#)]
19. Saeed, A.I.; Bhagabati, N.K.; Braisted, J.C.; Liang, W.; Sharov, V.; Howe, E.A.; Li, J.; Thiagarajan, M.; White, J.A.; Quackenbush, J. Tm4 microarray software suite. *Methods Enzym.* **2006**, *411*, 134–193. [[CrossRef](#)]
20. Kyriakis, J.M.; App, H.; Zhang, X.F.; Banerjee, P.; Brautigan, D.L.; Rapp, U.R.; Avruch, J. Raf-1 activates map kinase-kinase. *Nature* **1992**, *358*, 417–421. [[CrossRef](#)]
21. Shaul, Y.D.; Seger, R. The mek/erk cascade: From signaling specificity to diverse functions. *Biochim. Biophys. Acta* **2007**, *1773*, 1213–1226. [[CrossRef](#)] [[PubMed](#)]
22. Abeyrathna, P.; Su, Y. The critical role of akt in cardiovascular function. *Vasc. Pharm.* **2015**, *74*, 38–48. [[CrossRef](#)]
23. Ram, P.T.; Iyengar, R. G protein coupled receptor signaling through the src and stat3 pathway: Role in proliferation and transformation. *Oncogene* **2001**, *20*, 1601–1606. [[CrossRef](#)]
24. Yuan, Z.L.; Guan, Y.J.; Wang, L.; Wei, W.; Kane, A.B.; Chin, Y.E. Central role of the threonine residue within the p+1 loop of receptor tyrosine kinase in stat3 constitutive phosphorylation in metastatic cancer cells. *Mol. Cell Biol.* **2004**, *24*, 9390–9400. [[CrossRef](#)]
25. Abbas, T.; Dutta, A. P21 in cancer: Intricate networks and multiple activities. *Nat. Rev. Cancer* **2009**, *9*, 400–414. [[CrossRef](#)] [[PubMed](#)]
26. Harper, J.W.; Adami, G.R.; Wei, N.; Keyomarsi, K.; Elledge, S.J. The p21 cdk-interacting protein cip1 is a potent inhibitor of g1 cyclin-dependent kinases. *Cell* **1993**, *75*, 805–816. [[CrossRef](#)]
27. Weng, Y.R.; Cui, Y.; Fang, J.Y. Biological functions of cytokeratin 18 in cancer. *Mol. Cancer Res.* **2012**, *10*, 485–493. [[CrossRef](#)] [[PubMed](#)]
28. Li, Y.; Dowbenko, D.; Lasky, L.A. Akt/pkb phosphorylation of p21cip/waf1 enhances protein stability of p21cip/waf1 and promotes cell survival. *J. Biol. Chem.* **2002**, *277*, 11352–11361. [[CrossRef](#)]
29. Nicholson, K.M.; Anderson, N.G. The protein kinase b/akt signalling pathway in human malignancy. *Cell Signal.* **2002**, *14*, 381–395. [[CrossRef](#)]
30. Feil, L.; Koch, A.; Utz, R.; Ackermann, M.; Barz, J.; Stope, M.; Kramer, B.; Wallwiener, D.; Brucker, S.Y.; Weiss, M. Cancer-selective treatment of cancerous and non-cancerous human cervical cell models by a non-thermally operated electro-surgical argon plasma device. *Cancers* **2020**, *12*, 1037. [[CrossRef](#)]
31. Bayer, M.; Angenendt, L.; Schliemann, C.; Hartmann, W.; Konig, S. Are formalin-fixed and paraffin-embedded tissues fit for proteomic analysis? *J. Mass Spectrom.* **2020**, *55*, e4347. [[CrossRef](#)]
32. Dubuc, A.; Monsarrat, P.; Virard, F.; Merbahi, N.; Sarrette, J.P.; Laurencin-Dalieux, S.; Cousty, S. Use of cold-atmospheric plasma in oncology: A concise systematic review. *Adv. Med. Oncol.* **2018**, *10*, 1758835918786475. [[CrossRef](#)]
33. Cheng, Y.; Qin, K.; Huang, N.; Zhou, Z.; Xiong, H.; Zhao, J.; Zhang, Y.; Yu, S. Cytokeratin 18 regulates the transcription and alternative splicing of apoptotic-related genes and pathways in hela cells. *Oncol. Rep.* **2019**, *42*, 301–312. [[CrossRef](#)]
34. Sirnio, P.; Vayrynen, J.P.; Mutt, S.J.; Herzig, K.H.; Walkowiak, J.; Klintrup, K.; Makela, J.; Karttunen, T.J.; Makinen, M.J.; Tuomisto, A. Systemic inflammation is associated with circulating cell death released keratin 18 fragments in colorectal cancer. *Oncoimmunology* **2020**, *9*, 1783046. [[CrossRef](#)]
35. Abraham, M.C.; Shaham, S. Death without caspases, caspases without death. *Trends Cell Biol.* **2004**, *14*, 184–193. [[CrossRef](#)] [[PubMed](#)]
36. Yang, K.; Guo, Y.; Stacey, W.C.; Harwalkar, J.; Fretthold, J.; Hitomi, M.; Stacey, D.W. Glycogen synthase kinase 3 has a limited role in cell cycle regulation of cyclin d1 levels. *BMC Cell Biol.* **2006**, *7*, 33. [[CrossRef](#)]
37. Echaliier, A.; Endicott, J.A.; Noble, M.E. Recent developments in cyclin-dependent kinase biochemical and structural studies. *Biochim. Biophys. Acta* **2010**, *1804*, 511–519. [[CrossRef](#)]
38. Bartova, I.; Otyepka, M.; Kriz, Z.; Koca, J. Activation and inhibition of cyclin-dependent kinase-2 by phosphorylation; a molecular dynamics study reveals the functional importance of the glycine-rich loop. *Protein. Sci.* **2004**, *13*, 1449–1457. [[CrossRef](#)] [[PubMed](#)]
39. Berthet, C.; Aleem, E.; Coppola, V.; Tessarollo, L.; Kaldis, P. Cdk2 knockout mice are viable. *Curr. Biol.* **2003**, *13*, 1775–1785. [[CrossRef](#)]
40. Dehm, S.M.; Bonham, K. Src gene expression in human cancer: The role of transcriptional activation. *Biochem. Cell. Biol.* **2004**, *82*, 263–274. [[CrossRef](#)] [[PubMed](#)]
41. Przystal, J.M.; Becker, H.; Canjuga, D.; Tsiami, F.; Anderle, N.; Keller, A.L.; Pohl, A.; Ries, C.H.; Schmittnaegel, M.; Korinetska, N.; et al. Targeting csf1r alone or in combination with pd1 in experimental glioma. *Cancers* **2021**, *13*, 2400. [[CrossRef](#)] [[PubMed](#)]

Supplementary Figures



Supplementary Figure S1. Overview of FFPE extraction and DigiWest workflow. (a) Tissue picks are pre-wetted with extraction buffer and used to macro direct pre-heated FFPE slides. Samples are collected and transferred into a reaction tube. Protein extraction is performed according to the Qproteom FFPE tissue kit. (b) Proteins are separated through SDS-PAGE and transferred onto a membrane. Protein lanes are cut into 96 strips and sorted according to the molecular weight into a 96 well plate. Proteins are eluted and coupled onto magPlex beads of a distinct color ID and pooled together. An aliquot is used for primary and secondary antibody incubation and read-out is performed on a Luminex FlexMAP 3D. An excel macro-based algorithm is used to depict protein bands as peaks and for calculating the area of the peak.










Supplementary Figure S2. Selected DigiWest results of control (untreated), 0 h and 24 h after treatment FFPE samples. Bar graphs for mean signals from selected proteins in control, 0 h and 24 h samples. Error bars indicate the standard deviation. (***) = $p < 0.05$; Wilcoxon rank sum test).

Appendix 3:

Felix Ruoff, Nicolas Kersten, Nicole Anderle, Sandra Jerbi, Aaron Stahl, André Koch, Annette Staebler, Andreas Hartkopf, Sara Y. Brucker, Markus Hahn, Katja Schenke-Layland, Christian Schmees, and Markus F. Templin. *Protein Profiling of Breast Carcinomas Reveals Expression of Immune-Suppressive Factors and Signatures Relevant for Patient Outcome*. *Cancers*; 14, (8), 4542 (2022).
<https://doi.org/10.3390/cancers14184542>.

Article

Protein Profiling of Breast Carcinomas Reveals Expression of Immune-Suppressive Factors and Signatures Relevant for Patient Outcome

Felix Ruoff ¹ , Nicolas Kersten ^{2,3} , Nicole Anderle ¹ , Sandra Jerbi ¹, Aaron Stahl ¹, André Koch ⁴ , Annette Staebler ⁵, Andreas Hartkopf ^{4,6}, Sara Y. Brucker ^{4,7} , Markus Hahn ⁴, Katja Schenke-Layland ^{1,7,8}, Christian Schmees ¹  and Markus F. Templin ^{1,*} 

¹ NMI Natural and Medical Sciences Institute at the University of Tuebingen, 72770 Reutlingen, Germany

² FZI Research Center for Information Technology, Intelligent Systems and Production Engineering (ISPE), 76131 Karlsruhe, Germany

³ Interfaculty Institute for Biomedical Informatics (IBMI), University of Tuebingen, 72076 Tuebingen, Germany

⁴ Department of Women's Health, University of Tuebingen, 72076 Tuebingen, Germany

⁵ Institute of Pathology and Neuropathology, University of Tuebingen, 72076 Tuebingen, Germany

⁶ Department of Women's Health, University of Ulm, 89081 Ulm, Germany

⁷ Cluster of Excellence iFIT (EXC2180) "Image-Guided and Functionally Instructed Tumor Therapies", University of Tuebingen, 72076 Tuebingen, Germany

⁸ Institute of Biomedical Engineering, Department for Medical Technologies and Regenerative Medicine, University of Tuebingen, 72076 Tuebingen, Germany

* Correspondence: markus.templin@nmi.de; Tel.: +49-7121-51530-828



Citation: Ruoff, F.; Kersten, N.; Anderle, N.; Jerbi, S.; Stahl, A.; Koch, A.; Staebler, A.; Hartkopf, A.; Brucker, S.Y.; Hahn, M.; et al. Protein Profiling of Breast Carcinomas Reveals Expression of Immune-Suppressive Factors and Signatures Relevant for Patient Outcome. *Cancers* **2022**, *14*, 4542. <https://doi.org/10.3390/cancers14184542>

Academic Editors: David Wong and Ann Richmond

Received: 30 August 2022

Accepted: 14 September 2022

Published: 19 September 2022

Publisher's Note: MDPI stays neutral with regard to jurisdictional claims in published maps and institutional affiliations.



Copyright: © 2022 by the authors. Licensee MDPI, Basel, Switzerland. This article is an open access article distributed under the terms and conditions of the Creative Commons Attribution (CC BY) license (<https://creativecommons.org/licenses/by/4.0/>).

Simple Summary: Breast cancer treatment has improved substantially over the last decade. Still, the failure of treatment and therapy resistance are urgent problems. Here, we assessed cellular signaling within primary cancer tissue to evaluate the possibility of developing strategies that lead to better patient stratification and the development of personalized treatment options. By employing DigiWest technology, the expression and activation of the regulators of key signaling pathways in breast cancer tissue were monitored. A positive correlation between immune cell infiltration and event-free survival was detected. PPAR γ activation showed a negative correlation with immune cell infiltration, suggesting a novel immune evasion mechanism.

Abstract: In cancer, the complex interplay between tumor cells and the tumor microenvironment results in the modulation of signaling processes. By assessing the expression of a multitude of proteins and protein variants in cancer tissue, wide-ranging information on signaling pathway activation and the status of the immunological landscape is obtainable and may provide viable information on the treatment response. Archived breast cancer tissues from a cohort of 84 patients (no adjuvant therapy) were analyzed by high-throughput Western blotting, and the expression of 150 proteins covering central cancer pathways and immune cell markers was examined. By assessing CD8 α , CD11c, CD16 and CD68 expression, immune cell infiltration was determined and revealed a strong correlation between event-free patient survival and the infiltration of immune cells. The presence of tumor-infiltrating lymphocytes was linked to the pronounced activation of the Jak/Stat signaling pathway and apoptotic processes. The elevated phosphorylation of PPAR γ (pS112) in non-immune-infiltrated tumors suggests a novel immune evasion mechanism in breast cancer characterized by increased PPAR γ phosphorylation. Multiplexed immune cell marker assessment and the protein profiling of tumor tissue provide functional signaling data facilitating breast cancer patient stratification.

Keywords: DigiWest; breast cancer; cellular signaling; PPAR γ ; immune cell infiltration; patient stratification

1. Introduction

Breast cancer is the fifth most common cause of cancer-related deaths worldwide, with 2.2 million new cases and around 685,000 deaths in 2020 [1]. A variety of therapeutic options, including surgery, chemo-, hormone, and biological therapies, are available, and survival rates have increased substantially over the years [2]. Nevertheless, current cancer therapies lack a more personalized approach, and long-term therapy resistance has become a focus of current research [3,4]. Novel insights into the establishment, interaction and control of the tumor immune microenvironment (TIME) have drawn a more comprehensive picture of factors that might account for treatment failure or severe side effects [3,5]. The detection of tumor-infiltrating lymphocytes (TIL) is seen as a major prognostic factor in different carcinomas and has been suggested as a routine pathological evaluation [6,7]. In general, infiltrating immune cells can be categorized as either (i) pro-tumoral or (ii) anti-tumoral [6]. Some leukocytes, such as type 2 macrophages and regulatory T-cells (Tregs), are associated with pro-tumoral effects [8,9], whereas type 1 macrophages, effector T-cells, natural killer (NK) cells and dendritic cells (DC) are linked to anti-tumoral effects [10,11]. However, the complex interplay among different simultaneous immune responses and the way that cancer cells can modulate them are not yet fully understood. Large investigations on the bulk gene expression of infiltrating immune cells have been performed that associated different immune cell types with the risk of relapse [12,13]. Higher infiltration of immune cells has been linked to patient outcomes and treatment responses in several studies [8,14–16]. For example, the presence of cytotoxic T-cells (CD8+) has been associated with better survival in estrogen receptor (ER)-negative and ER-positive/human epidermal growth factor receptor 2 (Her2)-positive breast cancer subtypes [14]. Additionally, the categorization of tumors into immunological inflamed (hot) and non-inflamed (cold) cancers has been advocated for certain tumor entities [17,18]. Most studies focus on the evaluation of single immune cell markers or solely investigate the degree of TIL infiltration, most commonly using imaging methods (H&E/IHC/IF staining) for immune cell assessment and subsequent scoring [19,20]. Yet, recent studies have shown that classification based on one marker may be an oversimplification and does not entirely represent the complex nature of the immune response against cancer [21,22]. In the present study, we established the multiplexed assessment of several immune cell markers by DigiWest [23], a multiplexed bead-based Western blot, in fresh-frozen tissue samples.

The semi-quantitative protein expression analysis of primary breast cancer tissue allowed for the detection of infiltrating immune cells and the concomitant monitoring of the activation state of central signaling pathways. The activation of immune cell signaling and the induction of apoptotic processes were observed in highly immune-cell-infiltrated tumor tissue, whereas the activation of PPAR gamma signaling was found in tumors with low-level immune cell infiltration.

2. Materials and Methods

2.1. Patient Cohort

A retrospective cohort of primary unilateral invasive mamma carcinomas from patients who underwent a primary resection was utilized (snap-frozen, $n = 159$, tumor bank University Hospital Tuebingen). Inclusion criteria were hormone-receptor- and/or human epidermal growth factor receptor (Her2)-negative or -positive carcinomas, determined by immunohistochemistry at the Institute of Pathology, University of Tuebingen, Germany, at the time of surgery. Samples were further classified by the occurrence of distant metastases or local relapse within 10 years (poor responder) versus no occurrence of distant metastases, or a local relapse within 10 years or contralateral carcinoma within 5 years of the primary diagnosis (good responder). In general, the exclusion criteria were the occurrence of contralateral mamma carcinomas before the occurrence of distant metastases in the poor-responder subgroup and within 5 years in the good-responder subgroup, as well as the presence of bilateral mamma carcinomas or other malignancies (Figure S1). All patients enrolled neither received any neo-adjuvant treatment nor had any known metastases before surgery.

2.2. Sample Preparation and Assessment of Tumor Content

Layered cuts of each fresh-frozen sample were prepared, and Hematoxylin–Eosin (H&E) staining was performed according to standard protocols for the first and second layers. Between layers, 100 μm of tissue was trimmed, collected and stored at $-80\text{ }^{\circ}\text{C}$. Prior to protein expression analysis, the prepared layered cuts were H&E-stained (see also Figure 1A), and sections 100 μm apart were re-assessed by a pathologist (A.S). The evaluation of these sections revealed that 2.5% ($n = 4$) of the samples were normal tissue, 5.0% ($n = 8$) were ductal carcinoma in situ (DCIS), and 1.9% ($n = 3$) mostly contained necrotic tissue. In addition, 90.6% ($n = 144$) were classified as invasive ductal carcinoma (IDC) (see also Figure 1B). Yet, 2.5% ($n = 4$) showed a tumor content of app. 5–10%, and 27.7% ($n = 44$) showed a tumor content in between 15% and 45%. Of all samples, 60.4% ($n = 96$) showed a tumor content of 50% or higher (up to 95%) (see also Figure 1B). Samples with $\geq 50\%$ tumor content were selected for further analysis ($n = 84$), and intermediate sections from the generated layered cuts were used for protein preparation. In addition, $n = 10$ samples classified as normal tissue or with low tumor content ($>10\%$) were assigned to the baseline control group. Samples were lysed by incubating the collected tissue at $95\text{ }^{\circ}\text{C}$ for 10 min in lysis buffer (4% LDS, 50 mM DTT) (Figure S2).

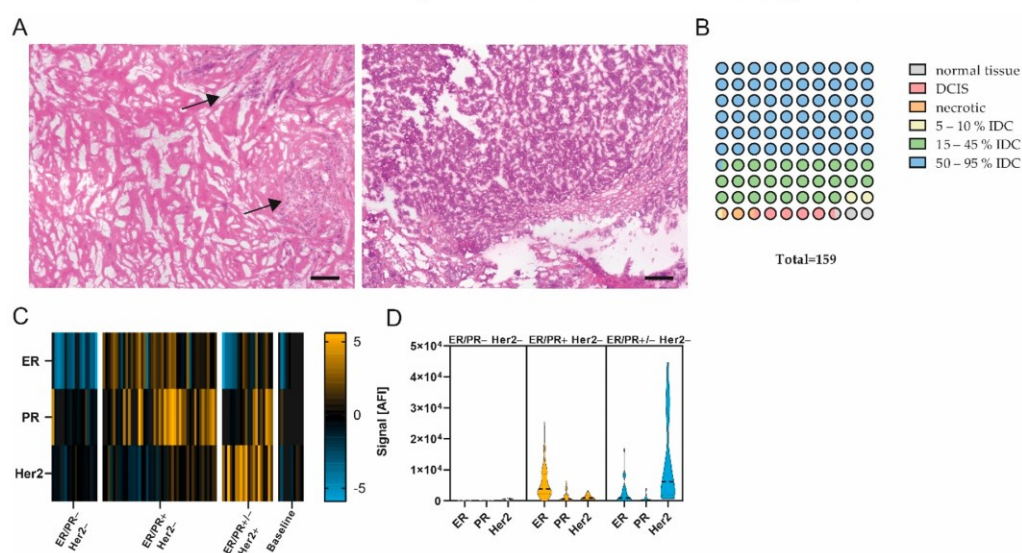


Figure 1. Pathological examination and quality assessment of selected samples. (A) Representative images of H&E-stained breast carcinomas. (Left) App. 20% tumor content. (Right) App. 90% tumor content. Scale bar, 200 μm . Black arrows, tumor area. (B) Pathological classification of entire sample set (1 circle = 1%). $n = 159$. (C) Heatmap showing ER, PR and Her2 protein expression in ER/PR+ Her2- ($n = 18$), ER/PR+ Her2+ ($n = 45$), ER/PR+/- Her2+ ($n = 20$) and baseline ($n = 10$) subgroup; data are median-centered and \log_2 -transformed. Yellow indicates higher expression; blue indicates lower protein expression. (D) Violin plots of ER, PR and Her2 expression in ER/PR+ Her2-, ER/PR+ Her2+ and ER/PR+/- Her2+ subgroups.

To confirm the tumor content of the enrolled sample set, the abundances of the proliferation marker Ki-67 and general carcinoma markers Cytokeratin 8/18, Cytokeratin 8 (pS23) and Cytokeratin 6 were assessed by DigiWest analysis (see below). The expression of these markers was found to be significantly different between the tumor sample set and baseline sample sets, revealing a high tumor content in the analysis of the former sample set (Figure S3A).

2.3. Compliance of Receptor Status

To review the compliance of the prepared samples with the pathological evaluation, the expression levels of the hormone receptors estrogen receptor (ER) and progesterone receptor (PR) and human Her2 were analyzed, and the resulting signals were compared to the pathological receptor status. A significant difference ($p < 0.05$, Mann–Whitney U test) in the signal was found between samples pathologically classified as receptor-positive and receptor-negative or the baseline group. Samples were categorized into three groups by referencing the pathological receptor status. In ER/PR– Her2– samples ($n = 18$), low or no expression of ER/PR or Her2 was observed. The analysis of ER/PR+ Her2– samples ($n = 45$) showed the increased expression of ER and a slight increase in expression in PR but not in Her2, whereas ER/PR+/- Her2+ samples ($n = 20$) displayed a significant increase in Her2 expression compared to the other groups (see also Figure 1C,D; $p < 0.05$, Mann–Whitney U test). We concluded that the DigiWest measurement of hormone receptors and Her2 expression is comparable to the classical pathological assessment of receptor status in the present cohort.

2.4. Immunohistochemical Staining

Immunohistochemical staining was performed on 5 μm formalin-fixed paraffin-embedded sections. After de-paraffinization, epitope retrieval was performed at 95 °C for 20 min in the appropriate antigen retrieval buffer. BLOXXALL-Blocking solution (Vector Laboratories, Burlingame, CA, USA) was added for 10 min. After washing in PBS, the sections were incubated with blocking buffer (PBS, 0.25% Triton-X-100, 10% goat serum, 4 drops/mL streptavidin (Vector Laboratories)). Primary antibody diluted in dilution buffer (PBS, 1%BSA, Biotin (Vector Laboratories)) was added and incubated in a humidified chamber. Rabbit (rb) anti-CD8 α (#85336, clone D8A8Y, Cell Signaling Technology (CST), Leiden, Netherlands, 1:100 dilution), rb anti-CD11c (#45581, clone D3V1E, CST, 1:400 dilution), rb anti-CD68 (#76437, MultiMab, CST, 1:200 dilution) and rb anti-CD16 (ab24622, clone EPR14336, Abcam, 1:400 dilution) antibodies were used for staining. The appropriate biotin-conjugated secondary antibody (Jackson Immuno Research, Cambridge, UK) diluted in PBS/1%BSA was added for 30 min. After subsequent washing in PBST, slides were incubated with streptavidin-labeled horseradish peroxidase. Peroxidase activity was developed with Novolink 3,3'-Diaminobenzidine (Leicabiosystems, Nußloch, Germany). Slides were counterstained with Hematoxylin QS (Vector Laboratories).

Staining for PR, PPAR γ and PPAR γ -pS112 was performed using a DAKO Autostainer Link 48 (Dako, Jena, Germany), and antigen retrieval was performed using a DAKO PT Link (Dako) according to the manufacturer's recommendations. For staining with mouse anti-PR antibody (IR06861, clone PgR636, Dako), slides were incubated in FLEX TRS HIGH pH buffer (K8004, Dako) at 85 °C for 20 min, followed by primary antibody incubation for 20 min and incubation with a mouse linker for 30 min. Subsequently, slides were incubated with a universal secondary antibody (EnVision FLEX/HRP, K8000, Dako) for 15 min. For staining with rb anti-PPAR γ (#2435, clone C26H12, CST, dilution 1:100) and rb anti-PPAR γ -pS112 (orb5574, Biorbyt, dilution 1:400), slides were incubated in FLEX TRS LOW pH buffer (K8005, Dako) at 85 °C for 20 min, followed by primary antibody incubation for 30 min and universal secondary antibody incubation for 20 min. For detection, the EnVision detection system (K500711-2, Dako) was used.

Whole-slide images were taken utilizing an Axio Scan Z.1 (Zeiss, Oberkochen, Germany). For the evaluation of staining intensity, five representative sections of each slide were used, and the mean intensity of DAB staining in positive pixel² was calculated utilizing ZenBlue software 3.1 (Zeiss).

2.5. Multiplex Protein Profiling Via DigiWest

DigiWest was performed as described previously [23]. Briefly, the NuPAGE system (Life Technologies, Carlsbad, CA, USA) with a 4–12% Bis-Tris gel was used for gel electrophoresis and Western blotting onto PVDF membranes. After washing with PBST,

proteins were biotinylated by adding 50 μ M NHS-PEG12-Biotin in PBST for 1 h to the membrane. After washing in PBST, membranes were dried overnight. Each Western blot lane was cut into 96 strips of 0.5 mm each. Strips of one Western blot lane were sorted into a 96-well plate (Greiner Bio-One, Frickenhausen, Germany) according to their molecular weights. Protein elution was performed using 10 μ L of elution buffer (8 M Urea and 1% Triton-X100 in 100 mM Tris-HCl pH 9.5). Neutravidin-coated MagPlex beads (Luminex, Austin, TX, USA) of a distinct color ID were added to the proteins of a distinct molecular weight fraction, and coupling was performed overnight. Leftover binding sites were blocked by adding 500 μ M deactivated NHS-PEG12-Biotin for 1 h. To reconstruct the original Western blot lane, the beads were pooled, for which the color IDs represent the molecular weight fraction of the proteins.

For antibody incubation, 5 μ L of the DigiWest Bead mixes were added to 50 μ L of assay buffer (Blocking Reagent for ELISA (Roche, Rotkreuz, Switzerland) supplemented with 0.2% milk powder, 0.05% Tween-20 and 0.02% sodium azide) in a 96-well plate. Assay buffer was discarded, and 30 μ L of primary antibody diluted in assay buffer was added per well. Primary antibodies were incubated overnight at 15 $^{\circ}$ C on a shaker. Subsequently, they were washed twice with PBST. After washing, 30 μ L of species-specific secondary antibody diluted in assay buffer labeled with phycoerythrin was added, and incubation took place for 1 h at 23 $^{\circ}$ C. Before the readout on a Luminex FlexMAP 3D instrument, the beads were washed twice with PBST.

Analyses and peak integration were performed by utilizing the novel DigiWest-Analyzer software package [24].

2.6. Statistical Analysis

Statistical comparison was performed by using the Mann–Whitney U test (GraphPad Prism version 9.2.0, GraphPad Software, San Diego, CA, USA). A Spearman correlation analysis, hierarchical cluster analysis, Chi-square test, Kaplan–Meier plot and log-rank test were carried out utilizing the DigiWest-Evaluator software package [24]. *p* values of <0.05 were considered statistically significant if not stated differently.

2.7. Pathway Enrichment Analysis

Testing for significantly enriched pathways was performed with an over-representation analysis using Fisher's exact test with subsequent calculation of Storey's Q-values for multiple testing correction. The subsets of analytes that were used for this analysis were defined by applying the Mann–Whitney U test to identify differentially expressed analytes between the good-responder and poor-responder groups. The pathway enrichment pipeline was carried out utilizing the DigiWest-Evaluator software package [24].

3. Results

3.1. Sample Quality Control and DigiWest Protein Expression Analysis

After the initial sample assessment ($n = 159$, Figure 1A,B), samples with a tumor content >50% and a sufficient protein amount ($n = 84$), as well as control samples with 10% or less tumor content ($n = 10$), were selected for extensive protein expression analysis. To identify markers relevant for the differentiation of good and poor responders, we measured 150 proteins and protein variants using DigiWest, mainly focusing on functional signal transduction, i.e., protein phosphorylation (covering 41 phospho-variants). This extensive expression analysis encompassed cell-cycle-control, apoptosis, Jak/Stat, MAPK, Pi3K/Akt, Wnt and autophagic signaling pathways, as well as general tumor and immune cell markers. The DigiWest evaluation of hormone receptor and Her2 receptor expression complied with the pathologically assessed receptor status, confirming the high quality of the selected tumor samples (Figure 1C,D).

To examine the connection between cellular signaling and the responder status, PAN-THER pathway enrichment analysis was conducted for all proteins differentially expressed between good- and poor-responder samples [25,26]. The highest $-\log_2$ Q-value was found

for the Jak/Stat signaling pathway (Figure 2A). Additionally, members of Jak/Stat signaling and several immune cell markers displayed significant differences when comparing the protein expression of good- and poor-responder samples (Mann–Whitney U test, FDR limit 0.1, Figure 2B). Taken together, these results indicate a connection between immune-cell-related signaling pathway activity and patient treatment response.

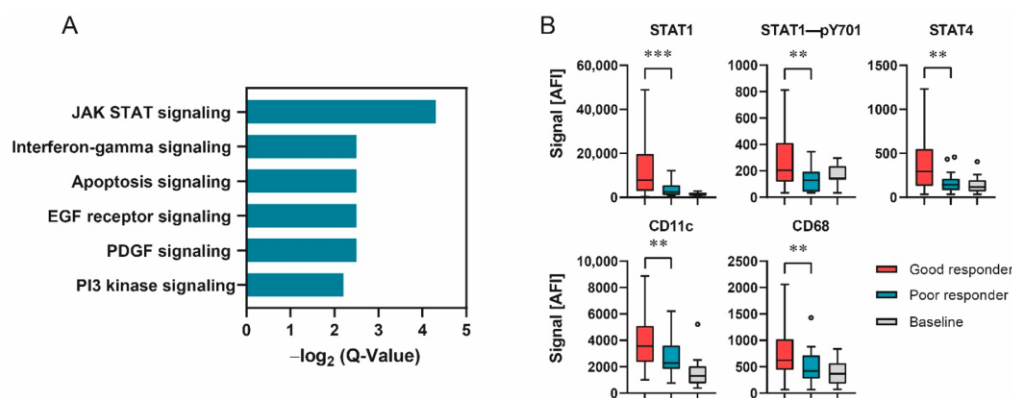


Figure 2. Responder status depended on differences in signal transduction. (A) $-\log_2$ Q-Values of PANTHER pathway analysis as bar graphs. (B) Protein expression of selected analytes displaying significant differences in expression between responder groups. Data shown as box–whisker plots for good-responder ($n = 58$), poor-responder ($n = 21$) and baseline ($n = 10$) subgroups. *** $p < 0.001$, ** $p < 0.01$. Mann–Whitney U test.

3.2. Patient Stratification Based on Immune Cell Infiltration Analysis by DigiWest

The degree and type of tumor infiltration by immune cells have become a novel and promising stratification factor for evaluating patient outcomes. Therefore, we evaluated the subset of measured immune cell markers in more detail. A correlation analysis of CD8 α , CD4, CD68, CD11c, CD16, CD56, CD25 and CD163 protein expression was performed. CD8 α , CD68, CD11c and CD16 displayed the highest correlation (Spearman's $r < 0.55$, Figure 3A, Table S1), suggesting the co-occurrence of represented immune cells.

Unsupervised hierarchical cluster linkage analysis of CD8 α (a common marker for cytotoxic T-cells), CD16 (a common marker for cytotoxic natural killer (NK) cells), CD11c (a marker for dendritic cells) and CD68 (a general marker for macrophages) revealed two distinct sample groups with different levels of immune marker expression (Euclidean distance, complete linkage, Figure 3B,C). The group with higher immune cell marker expression ($n = 27$) is referred to as “hot tumors”, whereas the group with lower immune cell marker expression ($n = 57$) is referred to as “cold tumors”.

Subsequently, CD8 α , CD68, CD11c and CD16 were immunohistochemically stained on matched FFPE sections, when available (Figures 3D and S4). Concomitantly, a significant difference in mean pixel intensity between hot and cold tumor samples categorized by DigiWest was detected (Figure 3E; Mann–Whitney U test, $p < 0.05$).

When comparing various clinical variables, such as the type of surgery, age and, most notably, the receptor status (ER, PR or Her2), we did not observe any difference between hot and cold breast carcinomas. Importantly, the responder status was the only clinical variable significantly enriched within the hot tumor group (Figure 3F; Table 1; $p < 0.05$, chi-square test).

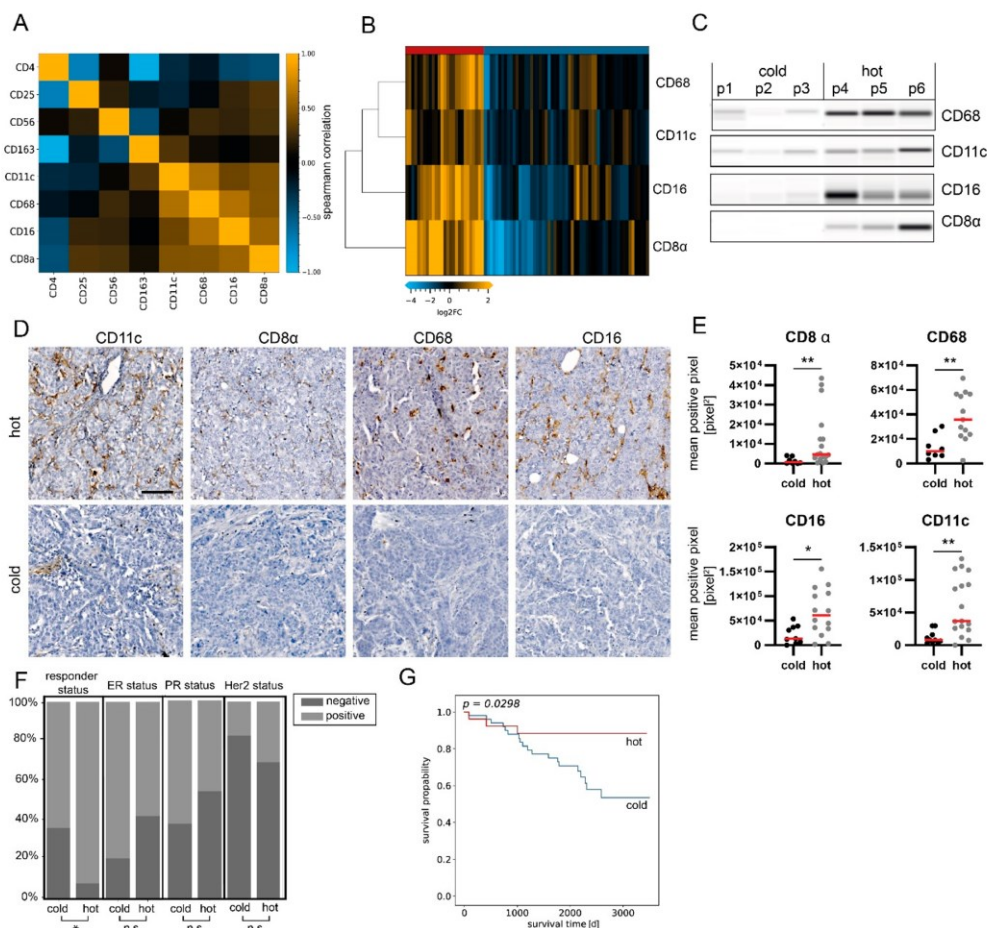


Figure 3. Sample stratification based on immune marker assessment. **(A)** Correlation plot (Spearman's correlation) of immune cell marker expression in the analysis sample set. The highest correlation was found for CD8 α , CD11c, CD68 and CD16 ($r > 0.55$). $n = 84$. **(B)** Heatmap showing protein expression levels of CD8 α , CD11c, CD68 and CD16. Hierarchical clustering of analytes and samples with Euclidean distance and complete linkage. Data are normalized to total protein, centered on median of all samples and log₂-transformed. **(C)** Representative Western blot mimics of CD8 α , CD11c, CD68 and CD16 (grayscale maps generated from DigiWest data). For graphical representation, background-subtracted raw data from representative hot and cold samples were used. $n = 3$. The uncropped blots are shown in Supplementary File S1. **(D)** Representative images of CD11c, CD8, CD68 and CD16 immunohistochemical staining in hot and cold samples. Scale bar, 50 μ m. **(E)** Mean positive pixel values of 5 representative 10 \times sections per available FFPE sample for hot and cold carcinomas classified by DigiWest. CD8 α : cold $n = 8$, hot $n = 17$; CD68: cold $n = 7$, hot $n = 13$; CD16: cold = 9, hot $n = 14$; CD11c: cold $n = 10$, hot $n = 17$. Mann–Whitney U test, ** $p < 0.01$; * $p < 0.05$. **(F)** Distributions of responder, ER, PR and Her2 statuses as percentages, stratified by infiltration status. Chi-square-test, * $p < 0.05$; ns indicates no significant difference. **(G)** Kaplan–Meier analyses of event-free survival in patients stratified by infiltration status. $p = 0.0298$, log-rank test.

Table 1. Patient and tumor characteristics of all samples included in the analysis sample set, stratified by responder and immune infiltration status, as indicated by DigiWest. *p*: Chi-Square or Wilcoxon rank-sum test between the two groups.

Characteristic	Overall (n = 84)		Poor Responder (n = 21)		Good Responder (n = 58)		<i>p</i>	Cold (n = 57)		Hot (n = 27)		<i>p</i>
	No. of Patients	%	No. of Patients	%	No. of Patients	%		No. of Patients	%	No. of Patients	%	
Follow-up, years												0.7
Median (range)	6.1 (0.2–9.9)		6.3 (0.2–9.9)		6.2 (0.3–9.6)		0.49	6.3 (0.2–9.9)		6.2 (0.9–9.4)		
Age at surgery, years												0.4
Median (range)	61 (30–85)		66 (41–85)		58 (84–30)		0.13	60 (31–85)		62 (30–84)		
Tumor size (cm)												0.3
<2	23	27.4	4	19.0	17	29.3		14	24.6	8	29.6	
2–5	55	65.5	13	61.9	39	67.2		37	64.9	19	70.4	
>5	6	7.1	4	19.0	2	3.4		6	10.5	0	0	
Nodal status												0.4
Negative	47	56.0	10	47.6	35	60.34		29	50.9	18	66.7	
Positive	36	42.9	11	52.4	22	37.93		27	47.4	9	33.3	
Unknown	1	1.2	0	0.0	1	1.72		1	1.8	0	0	
Hormone receptor status												0.2
ER-positive	24	28.6	15	71.4	42	72.4	0.84	44	77.2	16	59.3	
ER-negative	60	71.4	6	28.6	16	27.6		13	22.8	11	40.7	
PR-positive	38	45.2	12	57.1	33	56.9	0.81	34	59.6	12	44.4	0.3
PR-negative	46	54.8	9	42.9	25	43.1		23	40.4	15	55.6	
HER2 status												0.5
Positive	20	23.8	4	19.0	14	24.1		11	19.3	8	29.6	
Negative	63	75.0	17	81.0	43	74.1		45	78.9	18	66.7	
Unknown	1	1.2	0	0.0	1	1.7		1	1.8	1	3.7	
Type of surgery												0.4
BCS	47	56.0	12	57.1	34	58.6	0.27	34	59.6	13	48.1	
SSM	1	1.2	1	4.8	0	0.0		1	1.8	0	0	
Ablatio	16	19.0	3	14.3	10	17.2		5	8.8	5	18.5	
Mastectomy	10	11.9	5	23.8	5	8.6		2	3.5	0	0	
Quadrantectomy	2	2.4	0	0.0	1	1.7		10	17.5	5	18.5	
Segmental resection	1	1.2	0	0.0	1	1.7		0	0	1	3.7	
Mastopexy	5	6.0	0	0.0	5	8.6		3	5.3	2	7.4	
NSM	1	1.2	0	0.0	1	1.7		1	1.8	0	0	
Unknown	1	1.2	0	0.0	1	1.7		1	1.8	0	0	
Responder status												0.02
Poor responder	21	25.0	-	-	-	-		19	33.3	2	7	
Good responder	58	69.0	-	-	-	-		34	59.6	24	89	
Unknown	5	6.0	-	-	-	-		4	7.0	1	4	

Tumor infiltration with immune cells is generally associated with patient outcomes and event-free survival (EFS, time from definitive surgery until disease recurrence/metastases or death from any cause). Therefore, we reviewed the difference in clinical outcomes after primary surgery in the present cohort. The group classified as “hot tumors” indeed had a significantly better outcome when evaluating 10-year EFS (Figure 3G; $p = 0.03$, log-rank test). By comparing EFS between hot and cold tumor samples in subgroups categorized through pathological hormone and Her2 receptor statuses, a significant difference was found in ER+ and PR+ samples; yet, more strongly infiltrated samples displayed a tendency toward better EFS (Figure S5). Univariate Cox regression confirmed that the immune cell infiltration status was a prognostic factor of the clinical outcome ($p = 0.04$).

3.3. Focused Protein Expression Analysis of Hot and Cold Breast Carcinomas

Next, we performed a detailed analysis to identify differential protein expression in breast carcinomas classified as hot or cold tumors. We allocated the samples to the hot or cold tumor group by assessing immune cell markers as described above and comparing protein expression levels. $n = 30$ analytes displayed a significant difference in expression (Mann–Whitney U test; Benjamini–Hochberg FDR; corrected $p < 0.05$) and a log2 fold change of at least $+2/3$ or $-2/3$ (Figure 4A,B,D; see Table 2 for all significantly differentially expressed proteins; Figure S6).

Table 2. Protein analytes displaying significantly different expression between hot and cold breast tumor samples (Mann–Whitney U test; Benjamini–Hochberg FDR; corrected $p < 0.05$).

Analyte	Uncorrected p Value	Corrected p Value	log2 Fold
PR	0.002	0.007	−1.8
SRC-3—pT24	<0.001	0.001	−1
FoxP3	0.001	0.005	−1
E2F-4	0.003	0.011	−0.9
PPAR gamma—pS112	0.009	0.025	−0.9
VE-cadherin	0.005	0.015	−0.8
Cytokeratin 8/18	0.016	0.040	−0.6
Glycogen Synthase—pS641	0.014	0.036	−0.6
PTEN	0.001	0.003	−0.6
PDK1	0.001	0.003	−0.6
PTEN—pS380	0.017	0.041	−0.6
mTOR	0.016	0.040	−0.5
Dvl2	0.016	0.040	−0.4
MAD2L1	0.001	0.005	0.3
E2F-1	0.006	0.018	0.3
p70 S6 kinase—pT389	0.008	0.024	0.3
Erk1/2	0.011	0.030	0.3
IKK alpha	0.013	0.035	0.3
p38 MAPK—pT180/Y182	0.008	0.023	0.4
PD-L1	0.002	0.007	0.4
A-Raf	0.002	0.007	0.4
TSG101	0.007	0.020	0.4
NF-kB p65—pS468	0.002	0.006	0.4
PD-L1	<0.001	0.001	0.5

Table 2. Cont.

Analyte	Uncorrected <i>p</i> Value	Corrected <i>p</i> Value	log2 Fold
NF-kB p105/p50 [50 kDa]	0.001	0.003	0.5
CD25	0.001	0.003	0.5
c-Raf—pS259	0.002	0.006	0.5
PI3-kinase p85	0.003	0.009	0.5
CD56	<0.001	0.001	0.5
p38 MAPK	0.001	0.003	0.5
GSK3 beta	0.001	0.003	0.5
RUNX2	<0.001	0.000	0.5
p53—pS37	0.001	0.003	0.5
STAT 5 alpha	<0.001	0.002	0.5
MEK2	<0.001	0.001	0.6
Caspase 3	<0.001	0.001	0.6
Src—pY527	0.008	0.024	0.6
Caspase 9 [47 kDa]	<0.001	<0.001	0.6
Histone H3	<0.001	<0.001	0.6
CDK2	0.002	0.007	0.6
Mcl-1	<0.001	0.001	0.7
CD163	0.001	0.005	0.7
Bax	<0.001	<0.001	0.7
CDK1	<0.001	0.001	0.7
FoxC1	<0.001	<0.001	0.8
Src	<0.001	0.001	0.8
c-Met	<0.001	0.002	0.8
CD11c	<0.001	<0.001	0.8
Caspase 9 [35 kDa]	<0.001	<0.001	0.9
MOB1—pT35	0.001	0.003	0.9
Cyclin B1	<0.001	<0.001	0.9
FLOWER (C9orf7)	0.009	0.025	0.9
PD1	<0.001	<0.001	1
IDH1	<0.001	0.001	1
p53—pS20	<0.001	<0.001	1.2
CD68	<0.001	<0.001	1.2
STAT 1—pT701	<0.001	<0.001	1.4
STAT 4	<0.001	<0.001	1.6
Jak 2	<0.001	<0.001	1.6
CD16	<0.001	<0.001	1.6
STAT 1	<0.001	<0.001	1.7
Histone H3—pS10	0.001	0.004	1.7
Caspase 6 [15 kDa]	<0.001	<0.001	1.9
CD8a	<0.001	<0.001	2.5

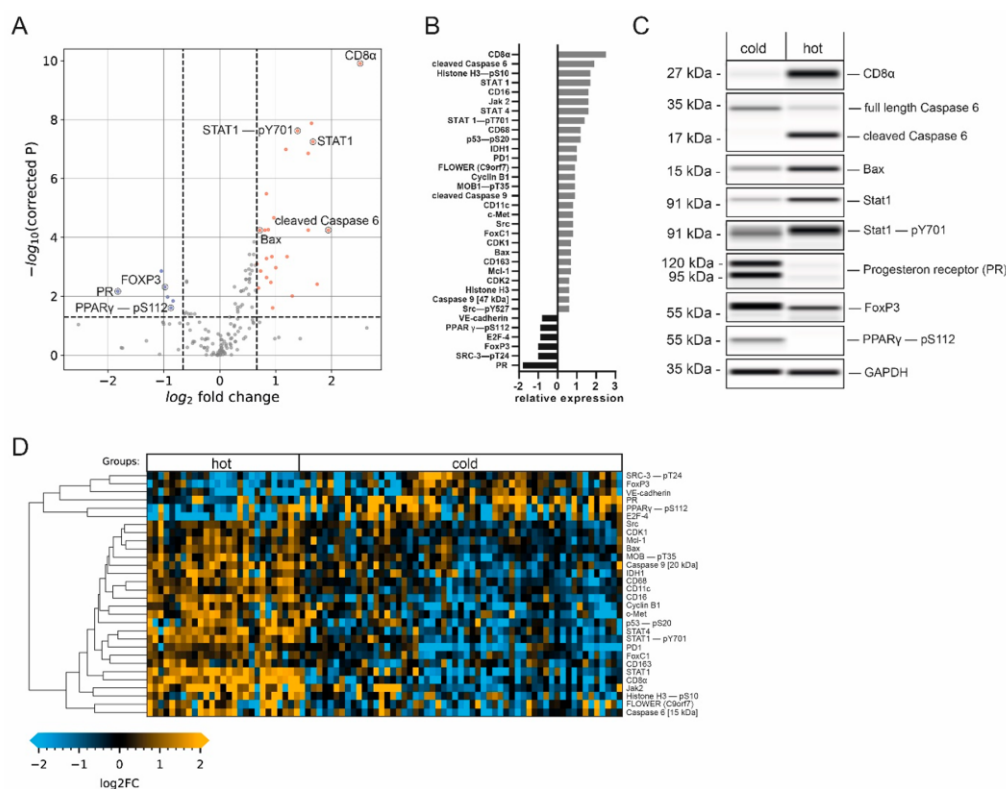


Figure 4. Immune-cell-infiltration-dependent changes in protein expression. (A) Volcano plot ($-\log_{10}$ -corrected p -value versus \log_2 fold change) depicting differences in protein expression between hot ($n = 27$) and cold ($n = 57$) samples. Data from 150 proteins and protein variants were analyzed. Wilcoxon rank-sum test with Benjamini–Hochberg multiple testing correction; the horizontal dashed line indicates a p -value of 0.05; the vertical dashed line indicates a \log_2 fold change of at least 2/3. Blue and red dots indicate analytes with at least a 2/3-fold difference in median expression and a p -value below 0.05. (B) Bar graphs of \log_2 -transformed ratios calculated from the mean protein expression in samples with high and low infiltration. Analytes are sorted from the largest positive change to the largest negative change. (C) Western blot mimics of selected analytes from two representative patients (grayscale maps generated from DigiWest data). For graphical representation, background-subtracted raw data were used. The uncropped blots are shown in Supplementary File S1. (D) Heatmap of analytes with significantly different expression between hot and cold samples displaying a fold change greater than 2/3. Hierarchical clustering of analytes using Euclidean distance and complete linkage.

This data analysis revealed an increase in the expression levels of members of the Jak/Stat pathway in the hot tumor subgroup. STAT4, a known mediator of the IL-12 response [27], as well as STAT1, known to be essential for interferon- α (IFN- α) and IFN- γ responses, and its active phospho-variant (Tyr701) [28] were significantly elevated in hot tumors (Figure 4C), indicating the activation of this pathway. Furthermore, Janus tyrosine kinase 2 (Jak2), an important cytokine receptor [29], displayed 3.0-fold elevated expression (\log_2 fold change of 1.6) in hot tumors. The programmed cell death 1 protein (PD-1), which is known to be an important regulator of immune cell activity [30], was also enriched in this group. Thus, higher immunosurveillance in the hot carcinoma group is characterized by increased expression levels of additional immune cell markers and important members for immune-relevant signaling pathways, supporting the previously established tumor groups.

The expression of CD56, used for the identification of NK cells [31], and IL-2R α /CD25, characteristic of regulatory T-cells (Tregs) [32], was also increased in this subgroup. Interestingly, the transcription factor Foxp3, which is a common marker for Tregs broadly linked to immunosuppression and tumor protection [33,34], showed significantly increased expression in the cold tumor subgroup (Figure 4C). Looking in detail, our data also showed that CD163, a marker for M2-type tumor-associated macrophages (TAMs), displayed moderately elevated expression levels (0.7-fold log₂ increase) in the hot tumor group. While the presence of M2-type macrophages has been linked to tumor progression [35], we interpret this detectable increase as a general indication of higher immune cell activity in this group.

3.4. Hot Tumor Samples Show Increased Proliferative Activity and a More Competitive Phenotype

The expression levels of the proto-oncogene tyrosine kinase Src and the calcium channel flower homolog (FLOWER) were found to be increased in hot tumor samples. Src plays a critical role in multiple cellular processes, including proliferation and invasion, and can be a driver of uncontrolled cell growth [36]. The expression of FLOWER, a cellular fitness sensor, has been associated with a competitive growth advantage of cancer cells [37,38]. In addition, the hepatocyte growth factor receptor (c-Met), which is instrumental in increased cell growth and associated with aggressive cancer phenotypes [39,40], was highly expressed in samples with higher immune cell infiltration. Additionally, the transcription factor forkhead box C1 (FoxC1), which is linked to breast cancer invasiveness [41,42], was highly expressed in samples assigned to the hot tumor subgroup. The expression of vascular endothelial cadherin (VE-cadherin), which is important for the adhesion of cancer cells to the endothelium [43], was decreased as compared to the cold tumor group. An increase in vascular permeability by reducing the amount of VE-cadherin via endocytosis has been observed in response to inflammatory activity; this mechanism facilitates immune cell infiltration [44]. Thus, decreased levels of VE-cadherin may be indicative of generally higher immune cell infiltration. Taken together, these results indicate a more competitive phenotype in hot tumor samples.

Additionally, significant promotion of the cell cycle was found in the hot tumor subgroup, as indicated by the higher expression of the important regulatory proteins Cyclin B1 and cyclin-dependent kinase 1 (CDK1), responsible for G2/M-phase progression [45]. This was accompanied by an increase in the phosphorylation of the mitosis marker Histone H3 at Serine 10 [46], as well as a significant decrease in the expression of the cell growth repressor E2F-4 [47].

In conclusion, it is conceivable that the higher expression of proliferative and competitive signaling proteins facilitates the immune recognition of breast cancer cells and therefore leads to higher rates of immune cell infiltration.

3.5. Elevated Immune Cell Infiltration Induces Expression of Tumor-Suppressive Markers and Apoptotic Activity

Our data also indicate that hot tumor samples show a significant increase in the expression of several tumor suppressors. The phosphorylation of the tumor suppressor p53 at Serine 20, which enhances p53 activity, leading to cell-cycle arrest or apoptosis [48], was detected, and a 1.2-fold increase in phosphorylation was observed. In addition, increased expression of isocitrate-dehydrogenase 1 (IDH1), another suppressor of tumorigenesis [49], and of phosphorylated and activated MOB1 (pT35), a member of the Hippo pathway [50], was observed in hot tumor samples.

Consequently, this subgroup displayed an increase in apoptotic activity, indicated by the enriched expression of several pro-apoptotic proteins. These include the initiator cysteine aspartic acid protease 9 (caspase 9), serving as an amplifier of the apoptotic response [51], and caspase 6 (one of the major executioner caspases). Both promote apoptosis in its cleaved and active forms [52]. Crucially, we observed the upregulation of the cleaved caspase 9 fragment at 35 kDa as well as the cleaved caspase 6 fragment at 15 kDa (Figure 4C), but not of the full-length proteins in the hot tumor subgroup. Similarly, the expression of

the pro-apoptotic factor Bax [53] was significantly enriched in samples with higher immune infiltration. Interestingly, the anti-apoptotic Bcl-2 family member Mcl-1, which antagonizes pro-apoptotic Bcl-2 proteins [54], showed a similar trend. These results suggest that higher immune cell infiltration leads to more apoptotic and tumor-suppressive signaling.

3.6. Cold Breast Tumors Show Increased Expression of Immunosuppressive Factors

Our data revealed that the luminal tumor co-marker progesterone receptor (PR), which is linked to an immunosuppressive tumor microenvironment [55,56], displayed a decrease in expression at the highest significance as compared to the cold subgroup (Figure 4B,C). Another contemplated immunomodulation factor is the PPAR γ /RXR α pathway, which regulates cell proliferation and inflammation [57]. It has been implied that the expression of peroxisome proliferator-activated receptor γ (PPAR γ), a key modulator of this pathway, correlates with suppressed immunosurveillance [58–60]. Interestingly, a positive correlation was found between phosphorylated PPAR γ (pS112) and PR (Figure 5B, Pearson's $r = 0.45$, $p < 0.0001$), indicating the co-expression of both factors by cold carcinomas.

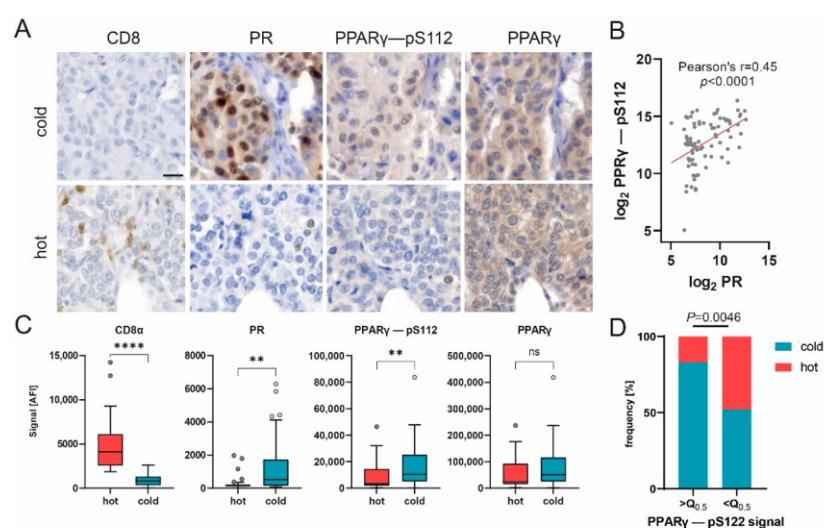


Figure 5. PPAR γ phosphorylation correlates with PR expression and may impair immune infiltration. (A) Representative images of CD8, PR, PPAR γ -pS112 and PPAR γ immunohistochemical staining in hot and cold carcinomas. Scale bar, 20 μ m. (B) Scatter plot of log₂-transformed DigiWest signal for PPAR γ -pS112 and PR. Pearson correlation, $r = 0.45$, $p < 0.0001$. (C) Box plots showing protein expression for CD8 α , PR, PPAR γ -pS112 and PPAR γ in cold ($n = 57$), hot ($n = 27$) and baseline ($n = 10$) samples. Mann–Whitney U test, ** $p < 0.01$, **** $p < 0.0001$; ns indicates no significant difference. (D) Distribution of hot and cold statuses in carcinoma samples with PPAR γ -pS112 expression higher or lower than median expression. $n = 42$. Q0.5 = 7004 AFI. Fisher's exact test, $p = 0.0046$.

Additionally, our results show that the expression of the phosphorylated variant of PPAR γ (pS112), but not the total protein variant, was significantly upregulated in cold tumor samples, whereas CD8 expression displayed the opposite trend (Figures 4C and 5C). Immunohistochemical staining of representative samples verified the predominant expression of PPAR γ (pS112) and PR by cancer cells in cold tumor samples (Figure 5A). Concomitantly, the percentage of samples classified as cold tumors was found to be significantly enriched in samples with an elevated (greater than the median) PPAR γ -pS112 signal (Figure 5D, Fisher's exact test, $p = 0.0046$). Hence, our data suggest that PPAR γ phosphorylation might be involved in a mechanism governing immune cell repulsion in breast cancer.

4. Discussion

Mutational changes in cellular signaling that trigger cell growth are key events in the transformation process that lead to the formation of tumor cells. The targeted analysis of central signaling pathways helps to track the effects of such mutations and can be used to functionally classify tumors by subtype. The DigiWest methodology employed here is capable of achieving this on a much broader scale compared to classical immunohistological approaches, and the knowledge generated by characterizing the activity of central signaling pathways can be utilized to identify novel targets for therapeutic intervention [61].

Here, we used a well-characterized collection of 160 archived breast cancer tissues for targeted protein profiling and aimed to concomitantly detect (i) signaling proteins and their activated variants and (ii) immune cell markers that define the tumor microenvironment. As a result, we were able to screen for aberrations in intra- and extracellular communication and to assign an immune status to each individual tumor tissue. This cohort was chosen since patient-specific follow-up data for all samples were available and could be integrated into the analysis of the correlation between protein expression levels, immune status and tumor recurrence. Yet, a detailed analysis of the prepared tissue sections revealed that the tumor content in a significant fraction of the archived tissues was lower than 50% (75/159, corresponding to 47%). Since only samples with more than 50% tumor content were analyzed, the number of patient samples was reduced to 84. Therefore, some care has to be taken when interpreting the obtained results.

Immune cell infiltration of breast cancer tissue and stroma is linked to a better prognosis [6]. On the contrary, non-immune-infiltrated tumors show no or a low response to current immune therapy [17]. To survey for the presence of infiltrating immune cells in cancer tissue, we measured central immune cell markers (CD8a, CD11c, CD16 and CD68) simultaneously and categorized the present cohort into highly infiltrated (“hot”) tumor and lowly infiltrated (“cold”) tumor samples. The assessment of patient outcome data revealed a significant difference in event-free survival in favor of the highly immune-cell-infiltrated group. Significantly, higher amounts of PD-1 and additional immune cell markers were detected in these samples, indicating higher immunosurveillance. Conversely, the specific Treg cell marker FoxP3, necessary for immune-suppressive activity and immunological tolerance [62–64], was found to be enriched in cold breast tumors. This indicates that in this cohort, higher expression of FoxP3+ cells leads to the retention of immune cell infiltration within the tumor tissue and, consequently, poorer patient outcomes.

At the same time, we show that highly immune-cell-infiltrated tumor samples display elevated immunological signaling activity, as was indicated by the upregulation of regulatory proteins Jak2, STAT4 and STAT1, including its activating phosphorylation at Tyrosine 701. These crucial members of the Jak/Stat pathway are important for the cytokine response and constitute key regulators of the immune system [65,66].

In a recent study, high apoptotic activity in breast cancer tissue was shown to be associated with the high infiltration of immune cells. Based on mRNA expression data, the authors hypothesized that increased apoptosis is associated with immune cell killing [67]. Here, we report that in hot breast cancer tissue, central apoptotic marker proteins such as the cleaved version of the initiator caspase 9, the cleaved effector caspase 6 and Bax were up-regulated. Increased levels of p53 phosphorylated at Ser20 and Histone H3 phosphorylated at Ser10 in these tumors indicate the likely involvement of DNA damage [48].

Phosphorylated PPAR γ (pS112) was present in higher amounts in samples with lower immune cell infiltration. Besides its common function in adipogenesis and lipid metabolism [68], PPAR γ has been linked to worse outcomes in breast cancer patients [69,70], as well as the evasion of immunosurveillance and the impairment of CD8 T-cell infiltration in muscle-invasive bladder cancer [71]. Our data suggest that higher PPAR γ phosphorylation impairs immune cell infiltration in breast cancer, ultimately worsening patient outcomes. Therefore, we hypothesize that PPAR γ phosphorylation may be involved in an immunosurveillance evasion mechanism employed by breast cancer cells. Hence, PPAR γ and its phosphorylated form (pS112) may serve as potential markers for patient stratifica-

tion or as a target for therapeutic intervention. However, additional research is required to elucidate this question further.

The application of DigiWest technology enabled us to review the receptor status, immune cell infiltration and protein expression of approx. 150 proteins and protein variants in parallel from minimal amounts of fresh-frozen breast cancer biopsies, demonstrating the unique potential held by this approach.

5. Conclusions

In the present study, we investigated cellular signaling and immune cell infiltration in a cohort of 84 breast patients not under a neoadjuvant treatment scheme. Tumor resections were analyzed for the expression of cellular signaling molecules and immune cell markers by semi-quantitatively measuring more than 150 proteins employing DigiWest technology. Based on the obtained expression profiles, the primary tumor tissues were categorized into immunological cold or hot tissues (presence of CD8 α , CD11c, CD16 and CD68); the impact of immune cell infiltration on event-free survival was established. This differential expression analysis showed that hot tumor samples displayed higher levels of immunological signaling as well as high apoptotic activity. Elevated immunological signaling was indicated by the activation of Jak/STAT signaling, which was seen at different points of the signaling cascade. Notably, the phosphorylation of PPAR γ at Serine 112 was found to be predominant in immunologically cold tumors, indicating its involvement in an immune surveillance evasion mechanism in breast cancer.

These distinct differences in the tumor microenvironment and in intracellular signaling in the tumor cells point to the modulation of intracellular signaling only in tumors that do not show invasion by immune cells. Further knowledge on the underlying mechanism will be useful for identifying patients that show a high probability of relapse, ultimately improving diagnosis, treatment and patient outcomes.

Supplementary Materials: The following supporting information can be downloaded at: <https://www.mdpi.com/article/10.3390/cancers14184542/s1>, Figure S1: Study flowchart; Figure S2: Schematic depiction of study workflow; Figure S3: Tumor marker and receptor expression in baseline samples versus tumor samples; Figure S4: Overview of IHC staining of immune cells; Figure S5: Influence of infiltrating immune cells on event-free survival in hormone-receptor- and Her2-positive/negative tumors; Figure S6: Differences in protein expression between hot and cold tumors; Table S1: Correlation values for all measured immune cell markers; Supplementary File S1: Full pictures of the Western blots.

Author Contributions: Conceptualization, F.R., A.K. and M.F.T.; methodology, F.R. and M.F.T.; formal analysis F.R., N.K. and M.F.T.; establishment of original pathological diagnosis and receptor profile and review of the adequacy of tumor cell content, A.S. (Annette Staebler); investigation, F.R., S.J. and N.A.; data curation F.R., N.K. and M.F.T.; writing—original draft preparation F.R., A.S. (Aaron Stahl), N.K. and M.F.T.; writing—review and editing, C.S., A.H., M.H. and K.S.-L.; material support, A.K.; supervision, M.F.T., S.Y.B. and K.S.-L.; project administration, C.S. All authors have read and agreed to the published version of the manuscript.

Funding: This work received financial support from the State Ministry of Baden-Wuerttemberg for Economic Affairs, Labour and Tourism (PRIMO project number: 3-4332.62-HSG/84).

Institutional Review Board Statement: The study was conducted in accordance with the Declaration of Helsinki and approved by the Ethics Committee of the Medical Faculty of Tuebingen University (788/2018BO2, 15 November 2018).

Informed Consent Statement: The use of retrospective human samples was ethically approved (788/2018BO2) by the ethics commission at the Medical Faculty of Tuebingen University.

Data Availability Statement: The data that support the findings of this study are available from the corresponding authors upon reasonable request.

Conflicts of Interest: The authors declare no conflict of interest.

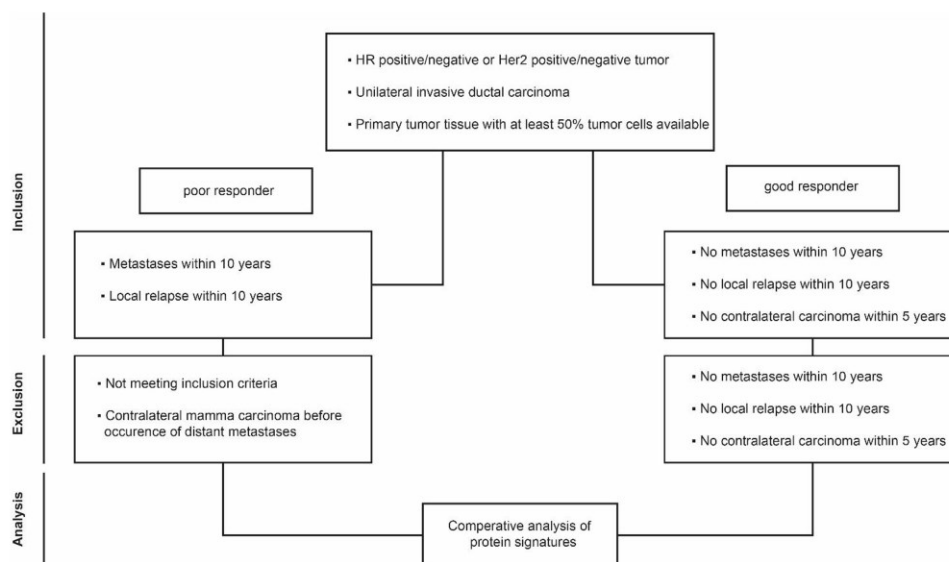
References

1. Sung, H.; Ferlay, J.; Siegel, R.L.; Laversanne, M.; Soerjomataram, I.; Jemal, A.; Bray, F. Global cancer statistics 2020: Globocan estimates of incidence and mortality worldwide for 36 cancers in 185 countries. *CA Cancer J. Clin.* **2021**, *71*, 209–249. [[CrossRef](#)] [[PubMed](#)]
2. Smolarz, B.; Nowak, A.Z.; Romanowicz, H. Breast cancer-epidemiology, classification, pathogenesis and treatment (review of literature). *Cancers* **2022**, *14*, 2569. [[CrossRef](#)] [[PubMed](#)]
3. Binnewies, M.; Roberts, E.W.; Kersten, K.; Chan, V.; Fearon, D.F.; Merad, M.; Coussens, L.M.; Gabrilovich, D.I.; Ostrand-Rosenberg, S.; Hedrick, C.C.; et al. Understanding the tumor immune microenvironment (time) for effective therapy. *Nat. Med.* **2018**, *24*, 541–550. [[CrossRef](#)] [[PubMed](#)]
4. Hewitt, K.; Son, J.; Glencer, A.; Borowsky, A.D.; Cooperberg, M.R.; Esserman, L.J. The evolution of our understanding of the biology of cancer is the key to avoiding overdiagnosis and overtreatment. *Cancer Epidemiol. Biomark. Prev.* **2020**, *29*, 2463–2474. [[CrossRef](#)]
5. Mair, F.; Erickson, J.R.; Frutoso, M.; Konecny, A.J.; Greene, E.; Voillet, V.; Maurice, N.J.; Rongvaux, A.; Dixon, D.; Barber, B.; et al. Extricating human tumour immune alterations from tissue inflammation. *Nature* **2022**, *605*, 728–735. [[CrossRef](#)]
6. Salgado, R.; Denkert, C.; Demaria, S.; Sirtaine, N.; Klauschen, F.; Pruneri, G.; Wienert, S.; Van den Eynden, G.; Baehner, F.L.; Penault-Llorca, F.; et al. The evaluation of tumor-infiltrating lymphocytes (tils) in breast cancer: Recommendations by an international tils working group 2014. *Ann. Oncol.* **2015**, *26*, 259–271. [[CrossRef](#)]
7. Ingold Heppner, B.; Loibl, S.; Denkert, C. Tumor-infiltrating lymphocytes: A promising biomarker in breast cancer. *Breast Care* **2016**, *11*, 96–100. [[CrossRef](#)]
8. Darvishian, F.; Wu, Y.; Ozerdem, U.; Chun, J.; Adams, S.; Guth, A.; Axelrod, D.; Shapiro, R.; Troxel, A.B.; Schnabel, F.; et al. Macrophage density is an adverse prognosticator for ipsilateral recurrence in ductal carcinoma in situ. *Breast* **2022**, *64*, 35–40. [[CrossRef](#)]
9. Shitara, K.; Nishikawa, H. Regulatory t cells: A potential target in cancer immunotherapy. *Ann. N. Y. Acad. Sci.* **2018**, *1417*, 104–115. [[CrossRef](#)]
10. Vitale, I.; Shema, E.; Loi, S.; Galluzzi, L. Intratumoral heterogeneity in cancer progression and response to immunotherapy. *Nat. Med.* **2021**, *27*, 212–224. [[CrossRef](#)]
11. Fridman, W.H.; Pages, F.; Sautes-Fridman, C.; Galon, J. The immune contexture in human tumours: Impact on clinical outcome. *Nat. Rev. Cancer* **2012**, *12*, 298–306. [[CrossRef](#)] [[PubMed](#)]
12. Ali, H.R.; Chlon, L.; Pharoah, P.D.; Markowitz, F.; Caldas, C. Patterns of immune infiltration in breast cancer and their clinical implications: A gene-expression-based retrospective study. *PLoS Med.* **2016**, *13*, e1002194. [[CrossRef](#)] [[PubMed](#)]
13. Aran, D.; Hu, Z.; Butte, A.J. Xcell: Digitally portraying the tissue cellular heterogeneity landscape. *Genome Biol.* **2017**, *18*, 220. [[CrossRef](#)]
14. Ali, H.R.; Provenzano, E.; Dawson, S.J.; Blows, F.M.; Liu, B.; Shah, M.; Earl, H.M.; Poole, C.J.; Hiller, L.; Dunn, J.A.; et al. Association between CD8+ t-cell infiltration and breast cancer survival in 12,439 patients. *Ann. Oncol.* **2014**, *25*, 1536–1543. [[CrossRef](#)] [[PubMed](#)]
15. Nelson, M.A.; Ngamcherdtrakul, W.; Luoh, S.W.; Yantasee, W. Prognostic and therapeutic role of tumor-infiltrating lymphocyte subtypes in breast cancer. *Cancer Metastasis Rev.* **2021**, *40*, 519–536. [[CrossRef](#)]
16. Szeitz, B.; Pipek, O.; Kulka, J.; Szundi, C.; Rusz, O.; Tokes, T.; Szasz, A.M.; Kovacs, K.A.; Pesti, A.; Ben Arie, T.B.; et al. Investigating the prognostic relevance of tumor immune microenvironment and immune gene assembly in breast carcinoma subtypes. *Cancers* **2022**, *14*, 1942. [[CrossRef](#)]
17. Galon, J.; Bruni, D. Approaches to treat immune hot, altered and cold tumours with combination immunotherapies. *Nat. Rev. Drug Discov* **2019**, *18*, 197–218. [[CrossRef](#)]
18. Chen, D.S.; Mellman, I. Elements of cancer immunity and the cancer-immune set point. *Nature* **2017**, *541*, 321–330. [[CrossRef](#)]
19. Hendry, S.; Salgado, R.; Gevaert, T.; Russell, P.A.; John, T.; Thapa, B.; Christie, M.; van de Vijver, K.; Estrada, M.V.; Gonzalez-Ericsson, P.I.; et al. Assessing tumor-infiltrating lymphocytes in solid tumors: A practical review for pathologists and proposal for a standardized method from the international immunooncology biomarkers working group: Part 1: Assessing the host immune response, tils in invasive breast carcinoma and ductal carcinoma in situ, metastatic tumor deposits and areas for further research. *Adv. Anat. Pathol.* **2017**, *24*, 235–251. [[CrossRef](#)]
20. Locy, H.; Verhulst, S.; Cools, W.; Waelput, W.; Brock, S.; Cras, L.; Schiettecatte, A.; Jonckheere, J.; van Grunsven, L.A.; Vanhoeij, M.; et al. Assessing tumor-infiltrating lymphocytes in breast cancer: A proposal for combining immunohistochemistry and gene expression analysis to refine scoring. *Front. Immunol.* **2022**, *13*, 794175. [[CrossRef](#)]
21. Backman, M.; La Fleur, L.; Kurppa, P.; Djureinovic, D.; Elfving, H.; Brunnstrom, H.; Mattsson, J.S.M.; Lindberg, A.; Ponten, V.; Eltahir, M.; et al. Infiltration of nk and plasma cells is associated with a distinct immune subset in non-small cell lung cancer. *J. Pathol.* **2021**, *255*, 243–256. [[CrossRef](#)] [[PubMed](#)]
22. Li, J.; Byrne, K.T.; Yan, F.; Yamazoe, T.; Chen, Z.; Baslan, T.; Richman, L.P.; Lin, J.H.; Sun, Y.H.; Rech, A.J.; et al. Tumor cell-intrinsic factors underlie heterogeneity of immune cell infiltration and response to immunotherapy. *Immunity* **2018**, *49*, 178–193.e177. [[CrossRef](#)] [[PubMed](#)]
23. Treindl, F.; Ruprecht, B.; Beiter, Y.; Schultz, S.; Dottinger, A.; Staebler, A.; Joos, T.O.; Kling, S.; Poetz, O.; Fehm, T.; et al. A bead-based western for high-throughput cellular signal transduction analyses. *Nat. Commun.* **2016**, *7*, 12852. [[CrossRef](#)] [[PubMed](#)]

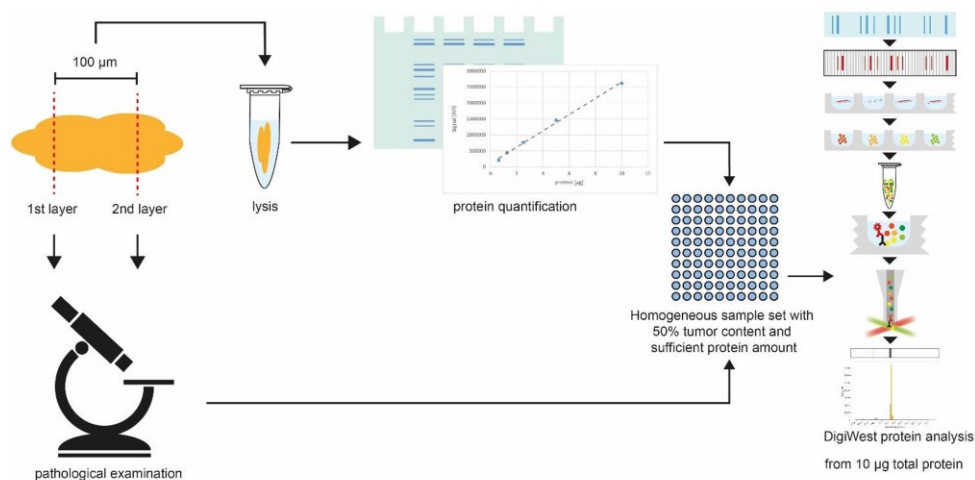
24. Kersten, N. A software pipeline for fast and interpretable evaluation of high-content protein profile analyses. In *Intelligent Systems and Production Engineering (ISPE)*; FZI Research Center for Information Technology: Karlsruhe, Germany, 2022; unpublished manuscript.
25. Mi, H.; Ebert, D.; Muruganujan, A.; Mills, C.; Albou, L.P.; Mushayamaha, T.; Thomas, P.D. Panther version 16: A revised family classification, tree-based classification tool, enhancer regions and extensive api. *Nucleic Acids Res.* **2021**, *49*, D394–D403. [[CrossRef](#)] [[PubMed](#)]
26. Mi, H.; Thomas, P. Panther pathway: An ontology-based pathway database coupled with data analysis tools. *Methods Mol. Biol.* **2009**, *563*, 123–140. [[CrossRef](#)]
27. Thierfelder, W.E.; van Deursen, J.M.; Yamamoto, K.; Tripp, R.A.; Sarawar, S.R.; Carson, R.T.; Sangster, M.Y.; Vignali, D.A.; Doherty, P.C.; Grosveld, G.C.; et al. Requirement for stat4 in interleukin-12-mediated responses of natural killer and t cells. *Nature* **1996**, *382*, 171–174. [[CrossRef](#)]
28. Ihle, J.N.; Withuhn, B.A.; Quelle, F.W.; Yamamoto, K.; Thierfelder, W.E.; Kreider, B.; Silvennoinen, O. Signaling by the cytokine receptor superfamily: Jaks and stats. *Trends Biochem. Sci.* **1994**, *19*, 222–227. [[CrossRef](#)]
29. Leonard, W.J.; O’Shea, J.J. Jaks and stats: Biological implications. *Ann. Rev. Immunol.* **1998**, *16*, 293–322. [[CrossRef](#)]
30. Nishimura, H.; Nose, M.; Hiai, H.; Minato, N.; Honjo, T. Development of lupus-like autoimmune diseases by disruption of the pd-1 gene encoding an itim motif-carrying immunoreceptor. *Immunity* **1999**, *11*, 141–151. [[CrossRef](#)]
31. Robertson, M.J.; Ritz, J. Biology and clinical relevance of human natural killer cells. *Blood* **1990**, *76*, 2421–2438. [[CrossRef](#)]
32. Fehervari, Z.; Yamaguchi, T.; Sakaguchi, S. The dichotomous role of il-2: Tolerance versus immunity. *Trends Immunol.* **2006**, *27*, 109–111. [[CrossRef](#)]
33. Ochs, H.D.; Gambineri, E.; Torgerson, T.R. Ipex, foxp3 and regulatory t-cells: A model for autoimmunity. *Immunol. Res.* **2007**, *38*, 112–121. [[CrossRef](#)] [[PubMed](#)]
34. Mercer, F.; Unutmaz, D. The biology of foxp3: A key player in immune suppression during infections, autoimmune diseases and cancer. *Adv. Exp. Med. Biol.* **2009**, *665*, 47–59. [[CrossRef](#)] [[PubMed](#)]
35. Komohara, Y.; Jinushi, M.; Takeya, M. Clinical significance of macrophage heterogeneity in human malignant tumors. *Cancer Sci.* **2014**, *105*, 1–8. [[CrossRef](#)] [[PubMed](#)]
36. Thomas, S.M.; Brugge, J.S. Cellular functions regulated by src family kinases. *Ann. Rev. Cell Dev. Biol.* **1997**, *13*, 513–609. [[CrossRef](#)]
37. Madan, E.; Pelham, C.J.; Nagane, M.; Parker, T.M.; Canas-Marques, R.; Fazio, K.; Shaik, K.; Yuan, Y.; Henriques, V.; Galzerano, A.; et al. Flower isoforms promote competitive growth in cancer. *Nature* **2019**, *572*, 260–264. [[CrossRef](#)]
38. Madan, E.; Gogna, R.; Moreno, E. Cell competition in development: Information from flies and vertebrates. *Curr. Opin. Cell Biol.* **2018**, *55*, 150–157. [[CrossRef](#)]
39. Sattler, M.; Salgia, R. The met axis as a therapeutic target. *Update Cancer Ther.* **2009**, *3*, 109–118. [[CrossRef](#)] [[PubMed](#)]
40. Eder, J.P.; Vande Woude, G.F.; Boerner, S.A.; LoRusso, P.M. Novel therapeutic inhibitors of the c-met signaling pathway in cancer. *Clin. Cancer Res.* **2009**, *15*, 2207–2214. [[CrossRef](#)]
41. Benayoun, B.A.; Caburet, S.; Veitia, R.A. Forkhead transcription factors: Key players in health and disease. *Trends Genet.* **2011**, *27*, 224–232. [[CrossRef](#)]
42. Dejeux, E.; Ronneberg, J.A.; Solvang, H.; Bukholm, I.; Geisler, S.; Aas, T.; Gut, I.G.; Borresen-Dale, A.L.; Lonning, P.E.; Kristensen, V.N.; et al. DNA methylation profiling in doxorubicin treated primary locally advanced breast tumours identifies novel genes associated with survival and treatment response. *Mol. Cancer* **2010**, *9*, 68. [[CrossRef](#)] [[PubMed](#)]
43. Brock, T.; Boudriot, E.; Klawitter, A.; Grosser, M.; Nguyen, T.T.P.; Giebe, S.; Klapproth, E.; Temme, A.; El-Armouche, A.; Breier, G. The influence of ve-cadherin on adhesion and incorporation of breast cancer cells into vascular endothelium. *Int. J. Mol. Sci.* **2021**, *22*, 6049. [[CrossRef](#)] [[PubMed](#)]
44. Welsh, M. Perspectives on vascular regulation of mechanisms controlling selective immune cell function in the tumor immune response. *Int. J. Mol. Sci.* **2022**, *23*, 2313. [[CrossRef](#)] [[PubMed](#)]
45. Wang, Z.; Fan, M.; Candas, D.; Zhang, T.Q.; Qin, L.; Eldridge, A.; Wachsmann-Hogiu, S.; Ahmed, K.M.; Chromy, B.A.; Nantajit, D.; et al. Cyclin b1/cdk1 coordinates mitochondrial respiration for cell-cycle g2/m progression. *Dev. Cell* **2014**, *29*, 217–232. [[CrossRef](#)] [[PubMed](#)]
46. Hans, F.; Dimitrov, S. Histone h3 phosphorylation and cell division. *Oncogene* **2001**, *20*, 3021–3027. [[CrossRef](#)] [[PubMed](#)]
47. Hsu, J.; Sage, J. Novel functions for the transcription factor e2f4 in development and disease. *Cell Cycle* **2016**, *15*, 3183–3190. [[CrossRef](#)]
48. Hirao, A.; Kong, Y.Y.; Matsuoka, S.; Wakeham, A.; Ruland, J.; Yoshida, H.; Liu, D.; Elledge, S.J.; Mak, T.W. DNA damage-induced activation of p53 by the checkpoint kinase chk2. *Science* **2000**, *287*, 1824–1827. [[CrossRef](#)]
49. Zhao, S.; Lin, Y.; Xu, W.; Jiang, W.; Zha, Z.; Wang, P.; Yu, W.; Li, Z.; Gong, L.; Peng, Y.; et al. Glioma-derived mutations in idh1 dominantly inhibit idh1 catalytic activity and induce hif-1alpha. *Science* **2009**, *324*, 261–265. [[CrossRef](#)]
50. Zeng, Q.; Hong, W. The emerging role of the hippo pathway in cell contact inhibition, organ size control, and cancer development in mammals. *Cancer Cell* **2008**, *13*, 188–192. [[CrossRef](#)]
51. Zou, H.; Li, Y.; Liu, X.; Wang, X. An apaf-1.Cytochrome c multimeric complex is a functional apoptosome that activates procaspase-9. *J. Biol. Chem.* **1999**, *274*, 11549–11556. [[CrossRef](#)]

52. Slee, E.A.; Harte, M.T.; Kluck, R.M.; Wolf, B.B.; Casiano, C.A.; Newmeyer, D.D.; Wang, H.G.; Reed, J.C.; Nicholson, D.W.; Alnemri, E.S.; et al. Ordering the cytochrome c-initiated caspase cascade: Hierarchical activation of caspases-2, -3, -6, -7, -8, and -10 in a caspase-9-dependent manner. *J. Cell Biol.* **1999**, *144*, 281–292. [[CrossRef](#)] [[PubMed](#)]
53. Wei, M.C.; Zong, W.X.; Cheng, E.H.; Lindsten, T.; Panoutsakopoulou, V.; Ross, A.J.; Roth, K.A.; MacGregor, G.R.; Thompson, C.B.; Korsmeyer, S.J. Proapoptotic bax and bak: A requisite gateway to mitochondrial dysfunction and death. *Science* **2001**, *292*, 727–730. [[CrossRef](#)] [[PubMed](#)]
54. Sato, T.; Hanada, M.; Bodrug, S.; Irie, S.; Iwama, N.; Boise, L.H.; Thompson, C.B.; Golemis, E.; Fong, L.; Wang, H.G.; et al. Interactions among members of the bcl-2 protein family analyzed with a yeast two-hybrid system. *Proc. Nat. Acad. Sci. USA* **1994**, *91*, 9238–9242. [[CrossRef](#)] [[PubMed](#)]
55. Walter, K.R.; Balko, J.M.; Hagan, C.R. Progesterone receptor promotes degradation of stat2 to inhibit the interferon response in breast cancer. *Oncimmunology* **2020**, *9*, 1758547. [[CrossRef](#)] [[PubMed](#)]
56. Anurag, M.; Zhu, M.; Huang, C.; Vasaikar, S.; Wang, J.; Hoog, J.; Burugu, S.; Gao, D.; Suman, V.; Zhang, X.H.; et al. Immune checkpoint profiles in luminal b breast cancer (alliance). *J. Natl. Cancer Inst.* **2020**, *112*, 737–746. [[CrossRef](#)]
57. Murphy, G.J.; Holder, J.C. Ppar-gamma agonists: Therapeutic role in diabetes, inflammation and cancer. *Trends Pharmacol. Sci.* **2000**, *21*, 469–474. [[CrossRef](#)]
58. Sweis, R.F.; Spranger, S.; Bao, R.; Paner, G.P.; Stadler, W.M.; Steinberg, G.; Gajewski, T.F. Molecular drivers of the non-t-cell-inflamed tumor microenvironment in urothelial bladder cancer. *Cancer Immunol. Res.* **2016**, *4*, 563–568. [[CrossRef](#)]
59. Kardos, J.; Chai, S.; Mose, L.E.; Selitsky, S.R.; Krishnan, B.; Saito, R.; Iglesia, M.D.; Milowsky, M.I.; Parker, J.S.; Kim, W.Y.; et al. Claudin-low bladder tumors are immune infiltrated and actively immune suppressed. *JCI Insight* **2016**, *1*, e85902. [[CrossRef](#)]
60. Glass, C.K.; Saijo, K. Nuclear receptor transrepression pathways that regulate inflammation in macrophages and t cells. *Nat. Rev. Immunol.* **2010**, *10*, 365–376. [[CrossRef](#)]
61. Kissel, M.; Berndt, S.; Fiebig, L.; Kling, S.; Ji, Q.; Gu, Q.; Lang, T.; Hafner, F.T.; Teufel, M.; Zopf, D. Antitumor effects of regorafenib and sorafenib in preclinical models of hepatocellular carcinoma. *Oncotarget* **2017**, *8*, 107096–107108. [[CrossRef](#)]
62. Fontenot, J.D.; Gavin, M.A.; Rudensky, A.Y. Foxp3 programs the development and function of cd4+cd25+ regulatory t cells. *Nat. Immunol.* **2003**, *4*, 330–336. [[CrossRef](#)] [[PubMed](#)]
63. Brunkow, M.E.; Jeffery, E.W.; Hjerrild, K.A.; Paepker, B.; Clark, L.B.; Yasayko, S.A.; Wilkinson, J.E.; Galas, D.; Ziegler, S.F.; Ramsdell, F. Disruption of a new forkhead/winged-helix protein, scurf, results in the fatal lymphoproliferative disorder of the scurfy mouse. *Nat. Genet.* **2001**, *27*, 68–73. [[CrossRef](#)] [[PubMed](#)]
64. Khattri, R.; Cox, T.; Yasayko, S.A.; Ramsdell, F. An essential role for scurf in cd4+cd25+ t regulatory cells. *Nat. Immunol.* **2003**, *4*, 337–342. [[CrossRef](#)] [[PubMed](#)]
65. Seif, F.; Khoshmirsafa, M.; Aazami, H.; Mohsenzadegan, M.; Sedighi, G.; Bahar, M. The role of jak-stat signaling pathway and its regulators in the fate of t helper cells. *Cell Commun. Signal* **2017**, *15*, 23. [[CrossRef](#)]
66. Liongue, C.; O'Sullivan, L.A.; Trengove, M.C.; Ward, A.C. Evolution of jak-stat pathway components: Mechanisms and role in immune system development. *PLoS ONE* **2012**, *7*, e32777. [[CrossRef](#)]
67. Murthy, V.; Oshi, M.; Tokumaru, Y.; Endo, I.; Takabe, K. Increased apoptosis is associated with robust immune cell infiltration and cytolytic activity in breast cancer. *Am. J. Cancer Res.* **2021**, *11*, 3674–3687.
68. Rosen, E.D.; Hsu, C.H.; Wang, X.; Sakai, S.; Freeman, M.W.; Gonzalez, F.J.; Spiegelman, B.M. C/ebpalpha induces adipogenesis through ppargamma: A unified pathway. *Genes Dev.* **2002**, *16*, 22–26. [[CrossRef](#)]
69. Shao, W.; Kopke, M.B.; Vilsmaier, T.; Zati Zehni, A.; Kessler, M.; Sixou, S.; Schneider, M.; Ditsch, N.; Cavailles, V.; Jeschke, U. Cytoplasmic colocalization of rxralpha and ppargamma as an independent negative prognosticator for breast cancer patients. *Cells* **2022**, *11*, 1244. [[CrossRef](#)]
70. Shao, W.; Kuhn, C.; Mayr, D.; Ditsch, N.; Kailuwait, M.; Wolf, V.; Harbeck, N.; Mahner, S.; Jeschke, U.; Cavailles, V.; et al. Cytoplasmic ppargamma is a marker of poor prognosis in patients with cox-1 negative primary breast cancers. *J. Transl. Med.* **2020**, *18*, 94. [[CrossRef](#)]
71. Korpai, M.; Puyang, X.; Jeremy Wu, Z.; Seiler, R.; Furman, C.; Oo, H.Z.; Seiler, M.; Irwin, S.; Subramanian, V.; Julie Joshi, J.; et al. Evasion of immunosurveillance by genomic alterations of ppargamma/rxralpha in bladder cancer. *Nat. Commun.* **2017**, *8*, 103. [[CrossRef](#)]

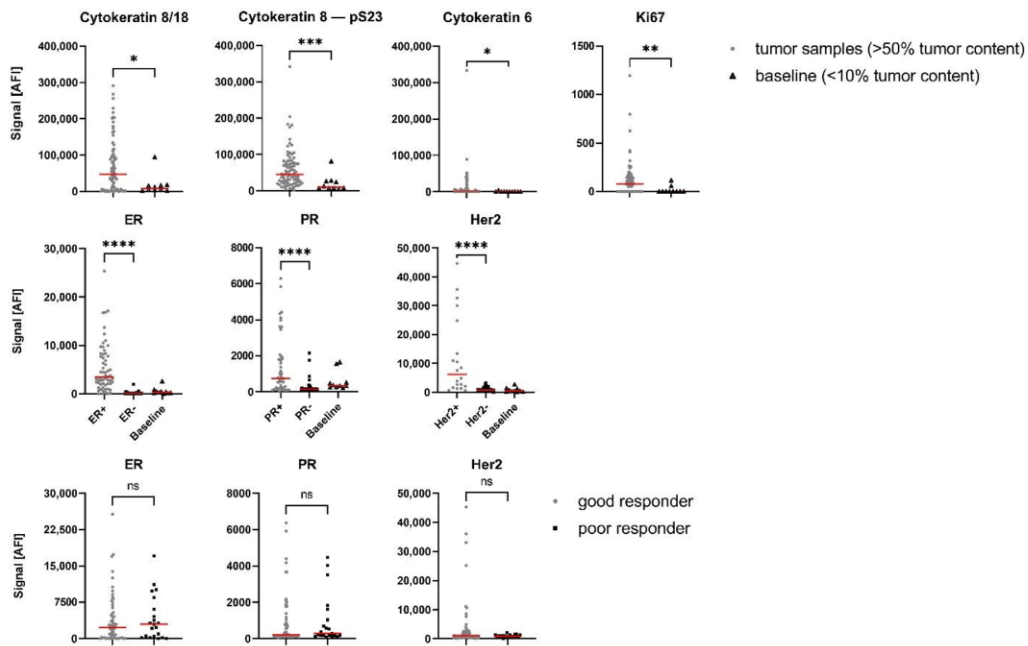
Supplementary Figures



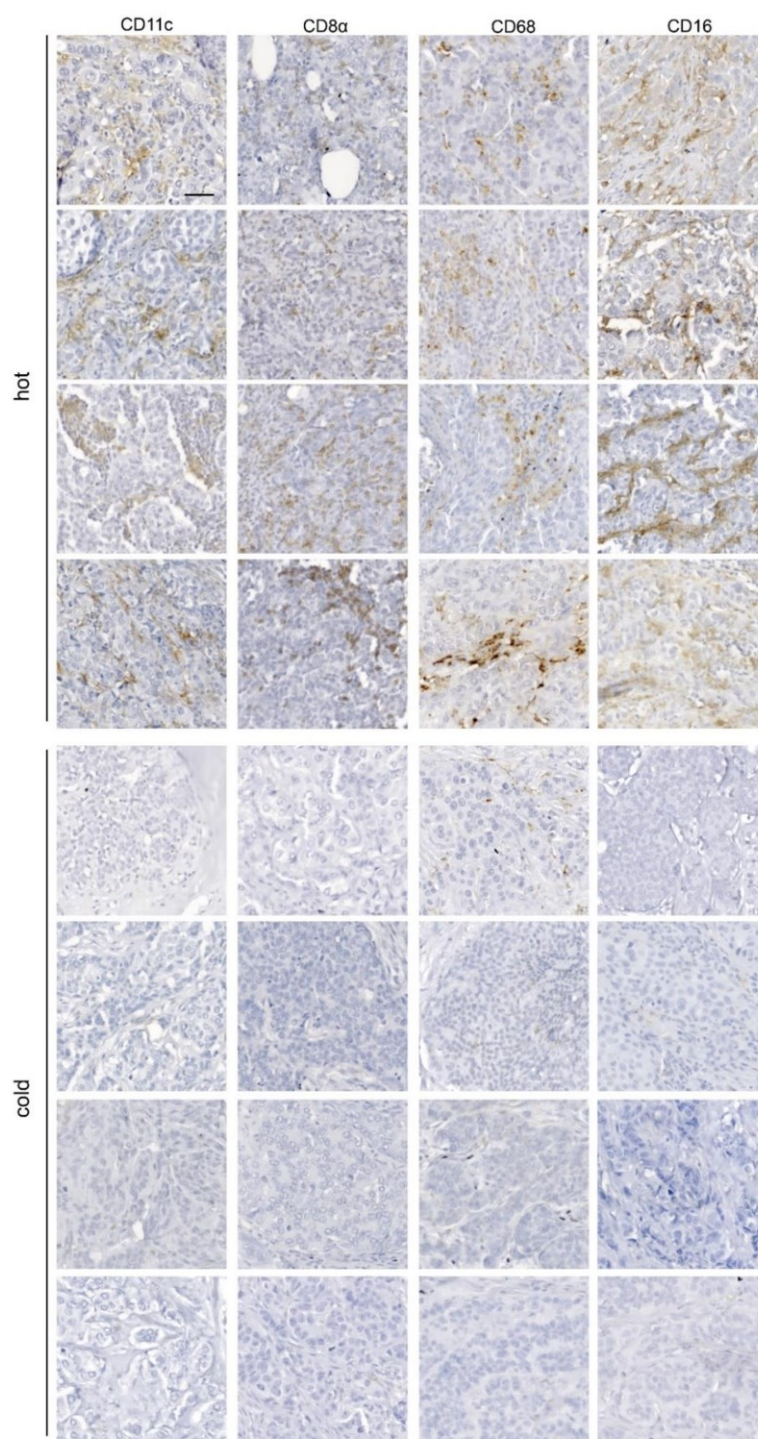
Supplementary Figure S1. Study flowchart.



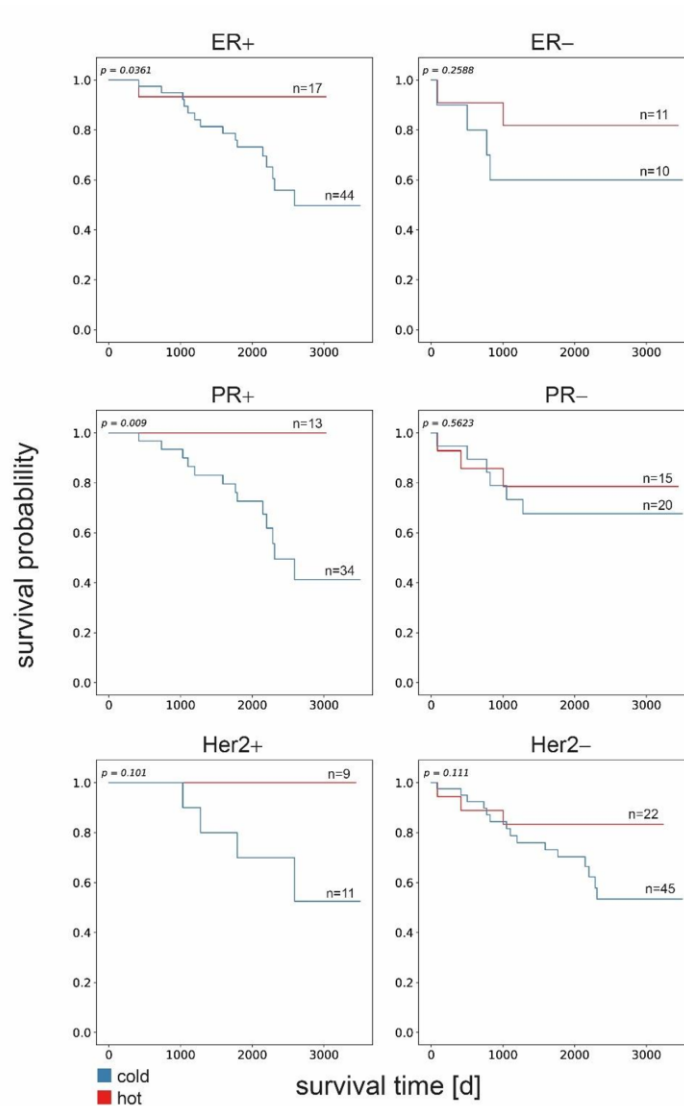
Supplementary Figure S2. Schematic depiction of study workflow. Layered cuts of tumor biopsies were generated, and intermediate tissue (100 µm) was collected. A pathologist assessed tumor content in first and second layer. Collected sample material was lysed and protein quantification was performed. Samples with tumor content of $\geq 50\%$ tumor content and sufficient protein amount were selected for DigiWest analysis.



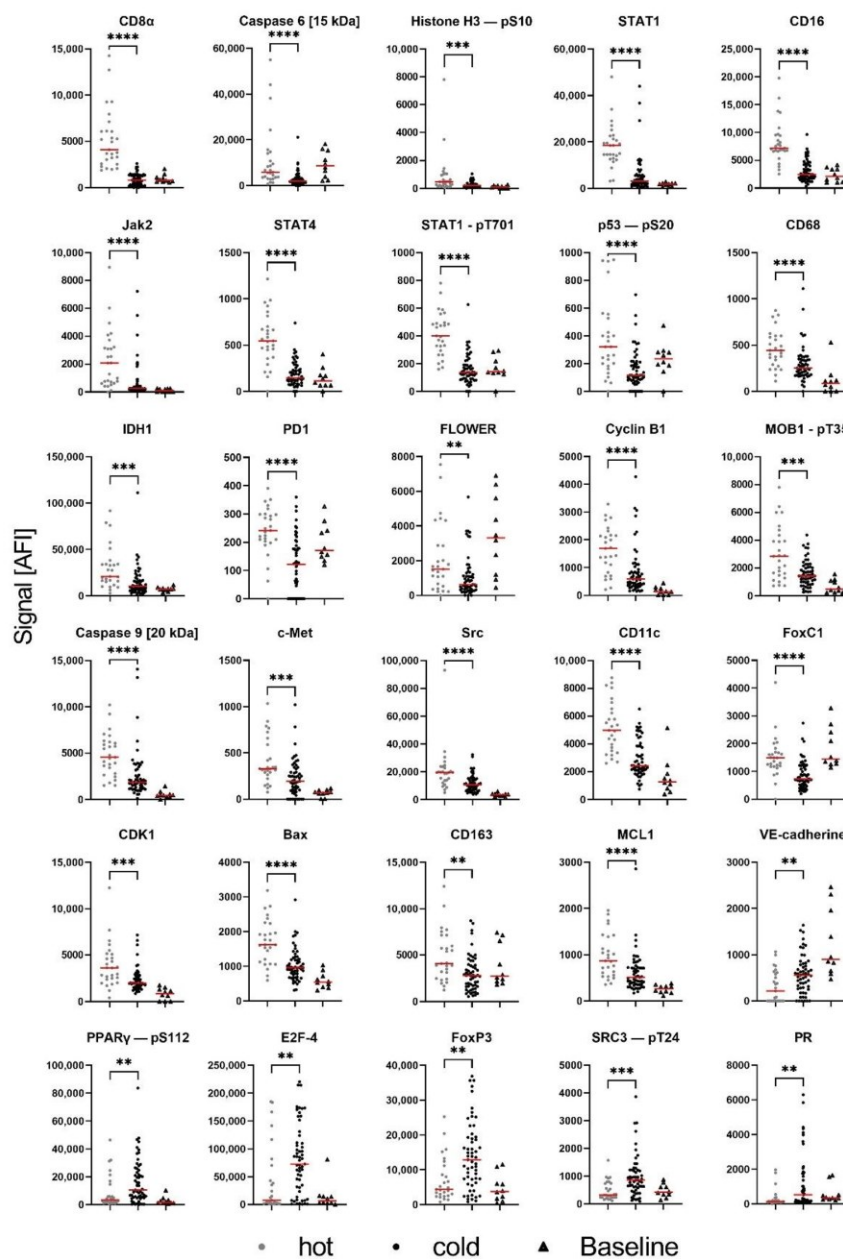
Supplementary Figure S3. Tumor marker and receptor expression in baseline samples versus tumor samples. (A) Cytokeratin 8/18, Cytokeratin 8 – pS23, Cytokeratin 6 and Ki67 expression as scatter plots in samples with $\geq 50\%$ tumor content (Tumor samples, $n=84$) and $\leq 10\%$ tumor content (baseline, $n=10$). (B) Scatter plots showing protein expression of ER, PR and Her2 in respective receptor-positive or negative and baseline subgroup (ER+ $n=60$; ER- $n=24$; PR+ $n=46$; PR- $n=38$; Her2+ $n=20$; Her2- $n=63$) as well as (C) in good ($n=58$) and poor responders ($n=21$). In A, B, C Mann-Whitney-U test, **** $P < 0.0001$; *** $P < 0.001$; ** $P < 0.01$; * $P < 0.05$; ns indicates no significant difference.



Supplementary Figure S4. Overview of IHC staining of immune cells. Representative images of CD11c, CD8, CD68 and CD16 immuno-histochemical staining in hot and cold samples. n=4. Scale bar, 50 μ m.



Supplementary Figure S5. Influence of infiltrating immune cells on event-free survival in hormone receptor and Her2 positive/negative tumors. Kaplan-Meier analysis of event-free survival between hot and cold carcinoma samples in ER, PR and Her2 positive and negative subgroups. A significant difference in EFS was found in ER+ and PR+ subgroup ($P < 0.05$). Log-rank test.

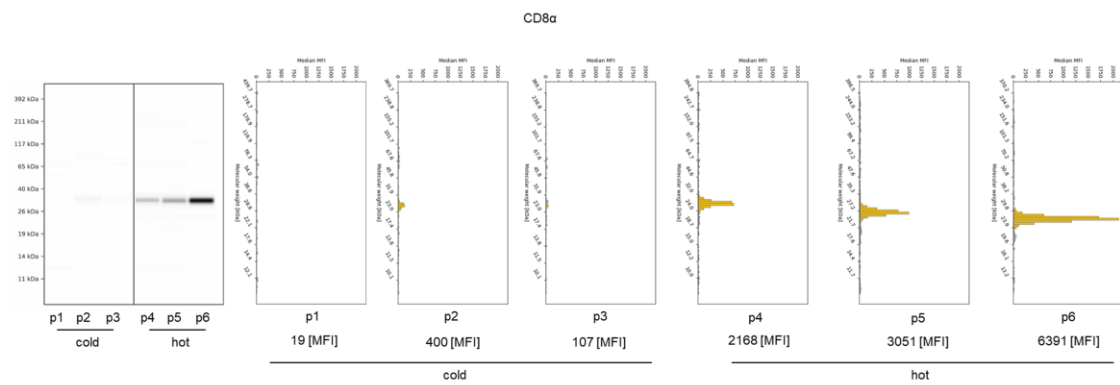


Supplementary Figure S6. Differences in protein expression between hot and cold tumors. Protein expression of 30 analytes for hot (n=27), cold (n=57) and baseline (n=10) subgroup which revealed significant differences in protein expression and a fold change of at least 2/3 between hot and cold samples. Mann-Whitney-U test, ****P<0.0001; ***P<0.001; **P<0.01.

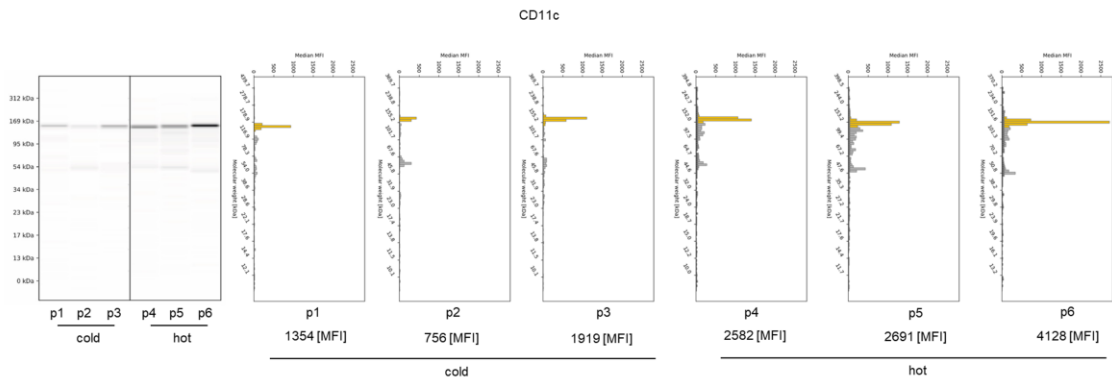
Table S1. Correlation values for all measured immune cell markers. Spearman's correlation.

	CD4	CD25	CD56	CD163	CD11c	CD68	CD16	CD8a
CD4	1	-0.2	0.4	-0.4	0.1	0.2	0	0
CD25	-0.2	1	0.4	0.2	0.1	0.2	0.5	0.5
CD56	0.4	0.4	1	0	0.4	0.5	0.4	0.5
CD163	-0.4	0.2	0	1	0.5	0.4	0.3	0.4
CD11c	0.1	0.1	0.4	0.5	1	0.7	0.6	0.6
CD68	0.2	0.2	0.5	0.4	0.7	1	0.7	0.6
CD16	0	0.5	0.4	0.3	0.6	0.7	1	0.7
CD8a	0	0.5	0.5	0.4	0.6	0.6	0.7	1

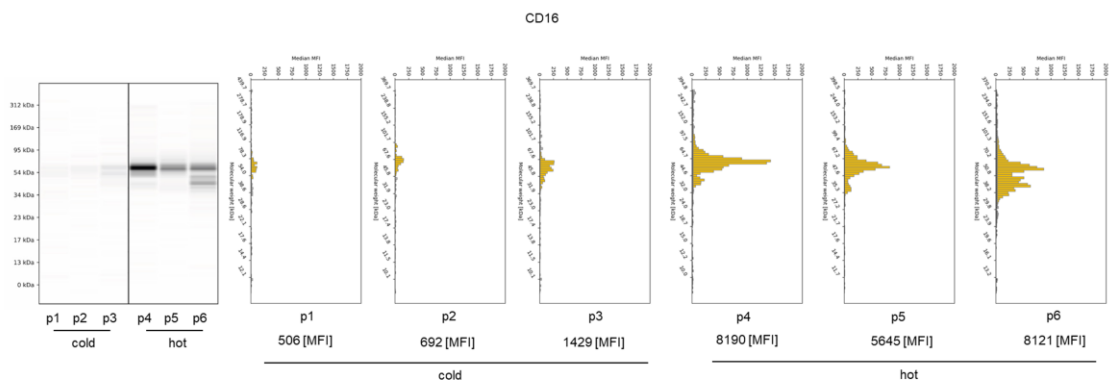
Supporting Material for Figure 3C: Shown are DigiWest data for 3 representative hot and cold patients each. Data is presented as median fluorescence intensities plotted against the molecular weight of the respective protein fraction, resulting raw signals after integration and as resulting digital reconstructed greyscale maps. For more information please see Treindl et al., 2016 (<https://doi.org/10.1038/ncomms12852>).



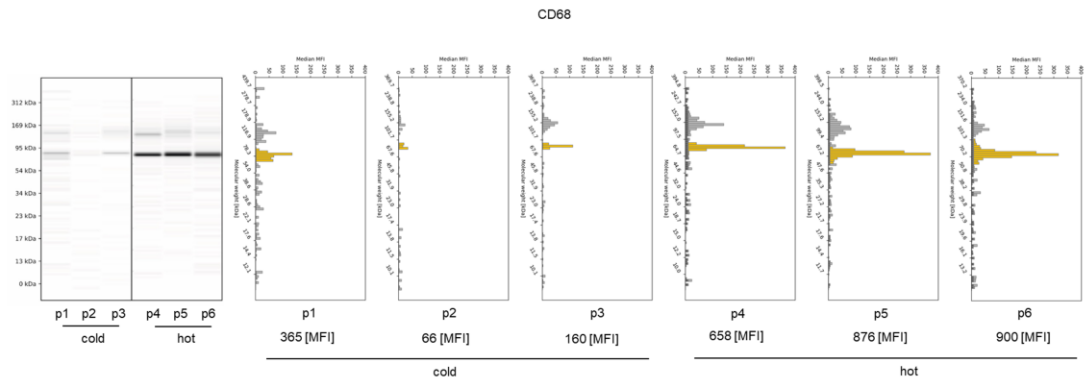
Supporting Material for Ruoff et al., 1/7



Supporting Material for Ruoff et al., 2/7

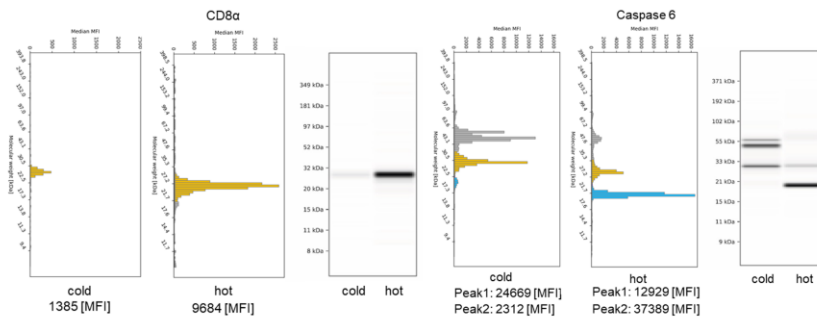


Supporting Material for Ruoff et al., 3/7

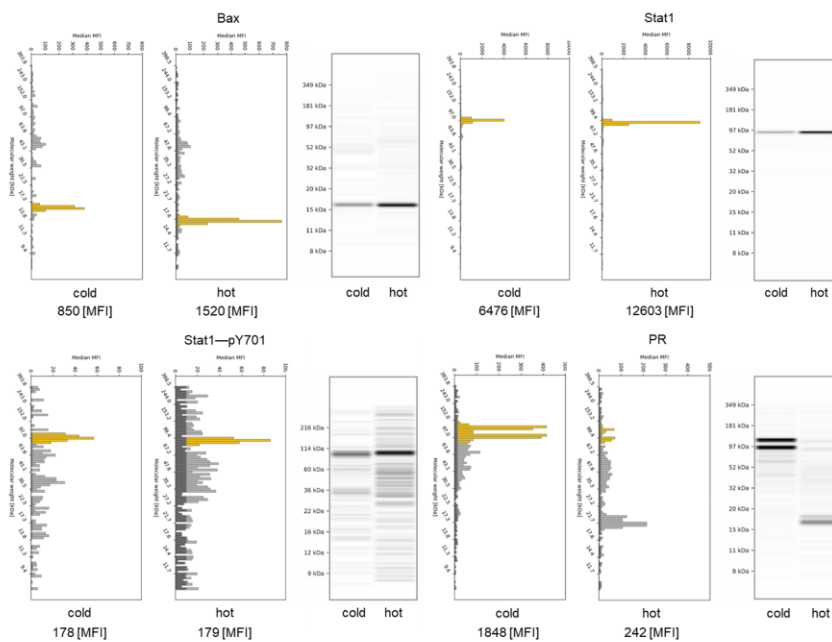


Supporting Material for Ruoff et al., 4/7

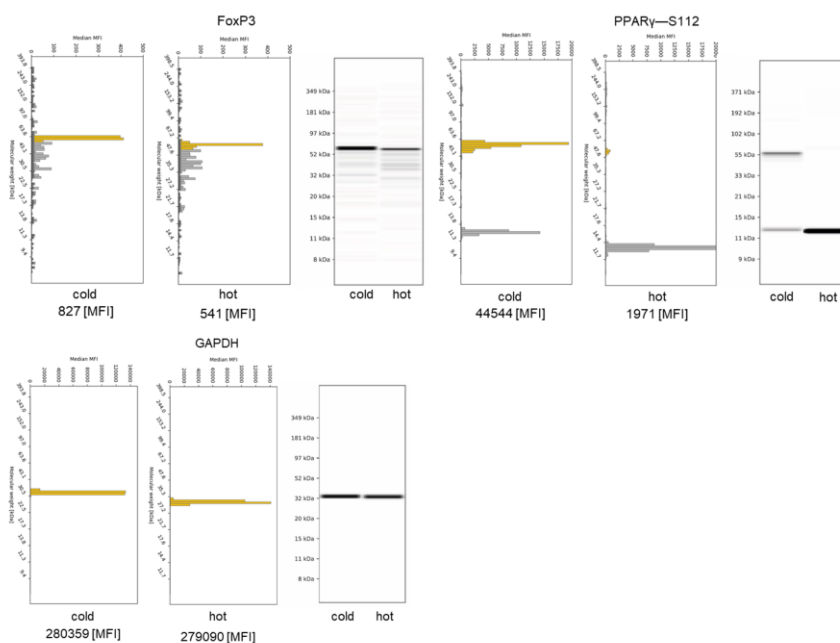
Supporting Material for Figure 4C: Shown are DigiWest data for 2 representative hot and cold patients. Data is presented as median fluorescence intensities plotted against the molecular weight of the respective protein fraction, resulting raw signals after integration and as resulting digital reconstructed greyscale maps. For more information please see Treindl et al., 2016 (<https://doi.org/10.1038/ncomms12852>).



Supporting Material for Ruoff et al., 5/7



Supporting Material for Ruoff et al., 6/7



Supporting Material for Ruoff et al., 7/7